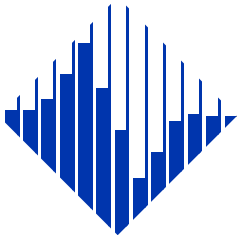

PACIFIC EARTHQUAKE ENGINEERING
RESEARCH CENTER

Shear-Flexure Interaction Modeling for Reinforced Concrete Structural Walls and Columns under Reversed Cyclic Loading

Kristijan Kolozvari
Department of Civil and Environmental Engineering
California State University, Fullerton

Kutay Orakcal
Department of Civil and Engineering
Bogazici University

John Wallace
Department of Civil and Environmental Engineering
University of California, Los Angeles

PEER Report No. 2015/12
Pacific Earthquake Engineering Research Center
Headquarters at the University of California, Berkeley

December 2015

PEER 2015/12
December 2015

Shear-Flexure Interaction Modeling for Reinforced Concrete Structural Walls and Columns under Reversed Cyclic Loading

Kristijan Kolozvari
Department of Civil and Environmental Engineering
California State University, Fullerton

Kutay Orakcal
Department of Civil Engineering
Bogazici University

John Wallace
Department of Civil and Environmental Engineering
University of California, Los Angeles

PEER Report 2015/12
Pacific Earthquake Engineering Research Center
Headquarters at the University of California, Berkeley

December 2015

ABSTRACT

A novel analytical model that captures interaction between axial/flexural and shear responses in reinforced concrete (RC) walls and columns under reversed-cyclic loading conditions has been developed and implemented in the computational platform OpenSees. The proposed modeling approach incorporates RC panel behavior described with a constitutive fixed-strut-angle panel model into a two-dimensional Multiple-Vertical-Line-Element-Model (*MVLEM*) formulation. The coupling of axial and shear responses is achieved at the macro-fiber (panel) level, which further allows coupling of flexural and shear responses at the model element level. New classes added to the existing OpenSees library include: baseline *MVLEM* element with uncoupled axial/flexural and shear behavior, Shear-Flexure-Interaction *MVLEM* element, two-dimensional material model based on the fixed-strut-angle constitutive RC panel model, uniaxial material model for concrete, and uniaxial material model for steel. Applications of the analytical models to quasi-static analysis of RC walls and columns, with comparisons of the analytical and experimental load-deformation responses, are presented. In addition, a dynamic analysis example for a building wall-frame system using the proposed shear-flexure-interaction model is provided. Response comparisons reveal that the implemented analytical models capture well the experimentally measured behavior of RC structural walls and columns. Based on the comparisons presented, model capabilities are assessed and potential model improvements are identified.

ACKNOWLEDGMENTS

This work was supported by the State of California's Transportation Division - Earthquake Risk Reduction Fund through the Pacific Earthquake Engineering Research Center (PEER) Transportation Systems Research Program. Any opinions, findings, and conclusions expressed herein are those of the authors and do not necessarily reflect those of the sponsors.

The authors wish to thank Leonardo Massone, Associate Professor at the University of Chile, Santiago, and Thien A. Tran, post-doctoral researcher at the University of California, Los Angeles, for their valuable help during the course of this project.

CONTENTS

ABSTRACT ..... **iii**

ACKNOWLEDGMENTS ..... **v**

TABLE OF CONTENTS ..... **vii**

LIST OF TABLES ..... **ix**

LIST OF FIGURES ..... **ix**

1 INTRODUCTION **1**

1.1 General **1**

1.2 Background and Objectives **3**

1.3 Organization **4**

2 DESCRIPTION OF ANALYTICAL MODELS **5**

2.1 Shear-Flexure Interaction Element **5**

2.1.1 Baseline Model: Multiple-Vertical-Line-Element-Model 6

2.1.2 Proposed Model: Shear-Flexure Interaction *MVLEM* 7

2.1.2.1 General Model Description *7*

2.1.2.2 Model Element DOFs *9*

2.1.2.3 Element Stiffness Matrix *10*

2.1.2.4 Element Force Vector *12*

2.1.2.5 Element Mass Matrix *12*

2.1.2.6 Global System Matrices *13*

2.2 Constitutive Reinforced Concrete Panel Behavior **15**

2.2.1 Fixed-Strut-Angle-Model (FSAM) 15

2.2.2 Shear Resisting Mechanisms across Cracks 18

2.3 Uniaxial Concrete Constitutive Behavior **20**

2.4 Reınforcıng Steel Uniaxial Constitutive Behavior **25**

2.5 OpenSees Implementation **30**

3 EXAMPLES **33**

3.1 Cyclic Analysis of Reinforced Concrete Columns **33**

3.2 Cyclic Analysis of Reinforced Concrete Walls **38**

3.2.1 Simulation of Flexural Behavior using MVLEM Element 38

3.2.2 Simulation of Shear-Flexural Behavior of a Medium-Rise RC Wall Specimen under Cyclic Loading using the *SFI-MVLEM* Model. 41

3.3 Dynamic Analysis of a Reinforced Concrete Building Wall-Frame System 48

3.3.1 Building Geometry.....48

3.3.2 Design Approach 49

3.3.3 Analytical Modeling 50

3.3.3.1 Model Description 50
3.3.3.2 Material Calibration.....51
3.3.3.3 Ground-Motion Record.....52

3.3.4 Dynamic Analysis Results 53

3.3.4.1 Dynamic Properties 53
3.3.4.2 Time-History Responses.....54
3.3.4.3 Maximum Global Responses over Wall Height 54
3.3.4.4 Bottom Wall Element Responses.....55
3.3.4.5 Single RC Panel Responses 56

4 SUMMARY AND CONCLUSIONS 61

REFERENCES.....63

APPENDIX A USER MANUALS.....67

APPENDIX B INPUT FILES: CYCLIC ANALYSIS OF REINFORCED CONCRETE WALL AND COLUMN SPECIMENS 79

APPENDIX C INPUT FILES: DYNAMIC ANALYSIS OF WALL–FRAME BUILDING SYSTEM.....101

LIST OF TABLES

Table 2.1 Links to OpenSees Wiki pages for implemented models. 31

Table 3.1 Properties of considered column test specimens. 34

Table 3.2 Concrete material parameters. 52

LIST OF FIGURES

Figure 2.1 *MVLEM* element: (a) model element formulation; and (b) rotations and displacements. 7

Figure 2.2 Uncoupled shear and flexural deformations [Orakcal et al. 2004]. 7

Figure 2.3 Implementation of RC panel behavior into *MVLEM*: (a) original *MVLEM*; (b) RC panel element; and (c) *SFI-MVLEM*. 8

Figure 2.4 *SFI-MVLEM* element; DOFs. 10

Figure 2.5 Panel stresses and tributary areas. 11

Figure 2.6 Element deformations of the *MVLEM* element [Vulcano et al. 1988]. 11

Figure 2.7 Sample model assembly: (a) complete model with DOFs; (b) element stiffness matrix and force vector (c) global stiffness matrix; and (d) global force vector. 14

Figure 2.8 Behavior of uncracked concrete in the FSAM: (a) strain field, (b) principal strains; (c) principal stresses in concrete; and (d) concrete stresses. 16

Figure 2.9 Behavior of concrete after formation of the first crack: (a) strain field; (b) concrete strut strains; (c) concrete strut stresses; and (d) concrete stresses. 16

Figure 2.10 Behavior of concrete after formation of the second crack: (a) strain field; (b) concrete strut strains; (c) concrete strut stresses, and (d) concrete stresses. 17

Figure 2.11 Behavior of reinforcing steel in the FSAM; (a) strain field; (b) stress–strain model; (c) dowel action model; and (d) steel stresses. 18

Figure 2.12 Superposition of concrete and steel stresses to obtain resultant (smeared) stresses in concrete: (a) concrete stresses; (b) steel stresses; and (c) resultant stress field. 18

Figure 2.13 Mechanisms in the FSAM for shear-stress transfer across cracks: (a) shear aggregate interlock model; and (b) dowel action model. 20

Figure 2.14 Hysteretic constitutive model for concrete by Chang and Mander [1994]. 20

Figure 2.15 Compression and tension envelope curves. 21

Figure 2.16 Hysteretic properties of the model. 22

Figure 2.17 Unloading from the compression envelope curve. 22

Figure 2.18 Effect of plastic stiffness upon unloading from tension envelope (E_{pl}^{+}) on crack closure. 23
Figure 2.19 Numerical instabilities in the model formulation. 24
Figure 2.20 Sample concrete stress–strain behavior. 25
Figure 2.21 Constitutive model for steel [Menegotto and Pinto 1973]. 26
Figure 2.22 Degradation of cyclic curvature. 26
Figure 2.23 Sensitivity of the stress–strain relationship to cyclic curvature parameters. 27
Figure 2.24 Stress shift due to isotropic strain hardening. 27
Figure 2.25 Comparing the degradation of cyclic curvature in the pre-yielding region for *Steel02* and *SteelMPF*. 28
Figure 2.26 Comparing the stress overshooting upon reloading from low-amplitude unloading for *Steel02* and *SteelMPF*. 29
Figure 2.27 OpenSees implementation of *SFI-MVLEM* model. 30

Figure 3.1 Reinforcement and model discretization of: (a) Specimen #2 [Priestley and Benzoni 1996]; and (b) Specimen 2CLH18 [Lynn et al. 1996]. 36
Figure 3.2 Measured and predicted lateral load versus top displacement response: (a) Specimen S1 [McDaniel 1997]; (b) Specimen H/D(3)-T/M(0.0)/1.32% [Shanmugam 2009]; (c) Specimen Column #2 [Priestley and Benzoni 1997]; and (d) Specimen 2CLH18 [Lynn et al. 1996]. 37
Figure 3.3 Geometry and discretization of wall Specimen RW2. 39
Figure 3.4 Experimental and analytical load versus flexural deformation relationships. 39
Figure 3.5 Sensitivity to material modeling parameters of (a) concrete and (b) steel. 40
Figure 3.6 Analytical strain histories at outermost and central wall fibers. 40
Figure 3.7 Analytically predicted stress–strain relationships at wall outermost fiber: (a) concrete and (b) steel. 41
Figure 3.8 Model discretization: (a) plan view and (b) cross section. 43
Figure 3.9 Wall responses: (a) lateral load versus top displacement behavior, and (b) cracking patterns. 43
Figure 3.10 Load versus deformation behavior for (a) shear and (b) flexure. 44
Figure 3.11 Model element responses: (a) force versus total deformation; (b) force versus flexural deformation; (c) force versus shear deformation; and (d) moment versus curvature. 45
Figure 3.12 Reinforced concrete panel resultant stress versus strain responses: (a) considered RC panel; (b) axial-horizontal; (c) axial-vertical; and (d) shear. 46

Figure 3.13 Predicted stress–strain behavior for concrete: (a) Strut 1 and (b) Strut 2. 47
Figure 3.14 Predicted stress–strain behavior for steel: (a) horizontal (*X*) and (b) vertical (*Y*). 47
Figure 3.15 Building views: (a) plan view; (b) frame elevation; and (c) wall elevation. 48
Figure 3.16 Member cross sections: (a) wall, (b) column, and (c) beam. 50
Figure 3.17 Analytical model of building system: (a) modeling approach and (b) plastic hinge model. 51
Figure 3.18 Ground-motion data: (a) acceleration time history and (b) response spectra. 53
Figure 3.19 Mode shapes: (a) first mode and (b) second mode. 53
Figure 3.20 Building global responses: (a) acceleration; (b) wall top displacement; and (c) wall-base shear force. 54
Figure 3.21 Maximum deformation responses: (a) lateral displacements and (b) interstory drifts. 55
Figure 3.22 Maximum force responses over wall height: (a) shear force and (b) moment. 55
Figure 3.23 Model element responses: (a) lateral load versus total lateral displacement; (b) lateral load versus flexural deformation; (c) lateral load versus shear deformation; and (d) moment versus curvature. 56
Figure 3.24 Panel resultant stress versus strain responses: (a) considered RC panel; (b) axial-horizontal; (c) axial-vertical; and (d) shear. 57
Figure 3.25 Predicted stress–strain behavior for concrete: (a) Strut 1 and (b) Strut 2. 58
Figure 3.26 Predicted stress–strain behavior for steel: (a) horizontal (*X*) and (b) vertical (*Y*). 58
Figure 3.27 Local responses–vertical profiles of maximum: (a) vertical strains and (b) rotations. 59

Figure A.1 Modeling approach: a) MVLEM element, b) MVLEM rotations and displacements. 67
Figure A.2 Modeling approach: (a) SFI_MVLEM element; and (b) RC panel element. 69
Figure A.3 FSAM for converting in-plane strains to smeared stresses on a RC panel element. 70
Figure A.4 Behavior and input/output parameters of the FSAM constitutive model. 72
Figure A.5 Hysteretic constitutive model for concrete by Chang and Mander [1994]. 73
Figure A.6 Compression and tension envelope curves. 74
Figure A.7 Sample oncrete stress–strain behavior. 75

Figure A.8 Constitutive model for steel [Menegotto and Pinto 1973]. 76
Figure A.9 *Steel02* and *SteelMPF* – degradation of cyclic curvature in pre-yielding region. 77
Figure A.10 Comparison of *Steel02* and *SteelMPF*: stress overshooting upon reloading from low-amplitude unloading. 77

1 Introduction

1.1 GENERAL

Reinforced concrete (RC) structural walls and columns are often used as the primary structural elements for resisting earthquake actions in buildings (e.g., core wall systems or wall-frame dual systems) and bridges (e.g., bridge columns). Their role is to provide sufficient lateral strength and stiffness to limit nonlinear behavior and lateral deformations during service level earthquakes, as well as to limit lateral deformations and provide nonlinear deformation capacity (ductility) during design and maximum considered earthquake level shaking. Given the crucial role of RC structural walls and columns in the seismic performance of buildings and bridges, it is essential that analytical models that are capable of capturing important characteristics of nonlinear hysteretic behavior of these structural components are available for design of new structures or evaluation and retrofit of existing structures.

Behavior of RC walls is generally classified according to wall aspect ratio (h_w / l_w), or shear-span-to-depth ratio (M / Vl_w), as either shear-controlled (walls with aspect ratio less than approximately 1.0 to 1.5) or flexure-controlled (aspect ratios greater than 2.5 to 3.0). For walls between these aspect ratios, herein referred to as moderate aspect ratio walls, although flexural yielding is expected, nonlinear shear deformations may be significant and lead to reduced lateral stiffness, strength, and ductility. Experimental results have shown that flexural and shear yielding occur near-simultaneously even when the wall nominal shear strength is as much as twice the shear developed at flexural yielding [Massone and Wallace 2004], suggesting that there is an interaction between nonlinear flexural and shear modes of behavior, commonly referred to as shear-flexure interaction (SFI). This interaction has been observed experimentally even in relatively slender RC walls with aspect ratios of 3.0 [Thomsen and Wallace 1995] and 4.0 [Sayre 2003], with shear deformations contributing approximately by 30% and 10% to lateral displacement at the first story and roof level, respectively [Massone and Wallace 2004].

The degree of interaction could increase for walls with aspect ratios of 1.5 and 2.0, with nonlinear shear deformations constituting as much as 50% and 30% of the wall top displacement, respectively [Tran and Wallace 2012]. The interaction between nonlinear flexural and shear behavior has been also experimentally observed in RC columns (e.g., Saatcioglu and Ozcebe [1989]. Experimental results have shown that the shear and flexural capacities of RC columns could be reduced due to SFI comparing to pure bending case, and that the shear displacements can be significant even when the failure is not governed by shear behavior [Saatcioglu and Ozcebe 1989; Priestley et al. 1996].

Various approaches have been proposed to capture the observed coupling between nonlinear flexural and shear behavior in RC walls and columns [Colotti 1993; Elwood 2002;

Massone et al. 2006 and 2009; Mullapudi and Ayoub 2009; Jiang and Kurama 2010; Xu and Zhang 2010; Beyer et al. 2011; Panagiotou et al. 2011; and Fischinger et al.2012]. The majority of these approaches are based on the use of fiber-type models with interaction incorporated through biaxial representation of concrete behavior (e.g., modified compression field theory; Vecchio and Collins 1986] within each macro-fiber, such as models proposed by Colotti [1993], Massone et al. [2006, 2009], Jiang and Kurama [2010], and Fischinger et al. [2012]. Massone et al. [2006, 2009] provided comparisons of model predictions against experimental results for cantilever walls with aspect ratio (shear-span-to-depth ratio) of 3.0 [Thomsen and Wallace 1995], as well as for squat wall segments with shear-span-to-depth ratio of 0.5 [Massone et al. 2009]. Although the modeling approach used in these studies captured nonlinear shear deformations and the coupling between shear and flexural responses, application of the model was limited to monotonic loading conditions. Jiang and Kurama [2010] provided comparisons between the predictions of their analytical modeling approach and experimental results for a wall specimen with aspect ratio of 2.4 [Oesterle et al. 1979]; however, the comparisons were presented for only lateral-load-versus-top-displacement responses and for tensile strains in boundary longitudinal reinforcement, both of which are not expected to be notably sensitive to SFI for a relatively slender wall [Orakcal and Wallace 2006]. Experimental validation of the analytical model proposed by Mullapudi and Ayoub [2009] and by Mullapudi et al. [2009] was also subject to similar limitations. A methodology based on a strut-and-tie (truss) modeling approach proposed by Panagiotou et al. [2011] has been shown to be a viable method to capture SFI; however, due to overlapping areas of vertical, horizontal, and diagonal concrete struts in the model, achieving accurate displacement responses over a broad range of response amplitudes is a challenge. In addition, strut angles are pre-defined and do not change during the analysis, which may allow for reasonably comparisons with tests on isolated cantilever walls, but does not address variation in strut angles due to changes in axial load for walls with some degree of coupling. The approach proposed by Beyer et al. [2011] determines the degree of interaction from empirical relations derived from test results. Although this approach produces reasonable estimation of the ratio between shear and flexural deformations for walls controlled by flexure—albeit with significant dispersion—the approach is limited due to its reliance on test data.

Analytical approaches that focused on capturing SFI in RC columns can be also found in the literature (e.g., Xu and Zhang [2010] and Elwood [2002]). In the approach proposed by Xu and Zhang [2010], the inelastic response of a column is modeled by use of flexural and shear springs located in the column plastic hinge regions. Behavior of the springs is governed by the flexural and shear backbone curves obtained via segregating the total monotonic backbone curve into flexural and shear deformation components, in order to characterize SFI behavior either experimentally or analytically. Elwood [2002] proposed an indirect approach to link flexural and shear behavior using a limit-state methodology based on results of experimental studies on columns exhibiting flexural yielding followed by shear failure. This model incorporates limit states for shear force and axial load, which are then related to the total lateral displacement. In the shear-force limit case, the total response is bounded by a shear-strength limit curve, where shear strength is reduced at larger displacements. Since the total response is a combination of the flexural and shear components, reaching the shear-limit curve produces degradation in shear strength and flexural unloading. Although these modeling approaches for RC columns captured the behavior of columns reasonably well, the SFI is incorporated indirectly based on pre-defined backbone curves derived primarily from experimental data.

In summary, modeling approaches available in the literature for representing the experimentally-observed SFI behavior are characterized with five significant shortcomings: (1) models are empirical (or semi-empirical) or have cumbersome formulations; (2) models are capable of simulating monotonic responses only; (3) sensitivity of model results to material and modeling parameters have not been studied in detail; (4) models have not been sufficiently validated against global (load-displacement) behavior and local responses (rotations, curvatures, strains) due to lack of detailed experimental data characterized with modest to significant SFI; and (5) models have not been implemented in computational platforms available for public use. Therefore, there is a need for a relatively simple analytical modeling approach that is able to predict important response characteristics of RC walls and columns by incorporating coupling between axial/flexural and shear responses under reversed-cyclic loading conditions. In addition, the model must be validated at both global and local response levels for a range of response amplitudes against detailed data from heavily instrumented tests of wall and column specimens that experienced significant SFI, and implemented into a computational platform available to the broad engineering and research community.

1.2 BACKGROUND AND OBJECTIVES

Given the aforementioned shortcomings, a research project was initiated to develop and implement into the computational platform OpenSees [McKenna et al. 2000], an analytical modeling approach that incorporates the interaction between axial/flexure and shear behavior in RC members, as well as to calibrate and validate the model using experimental data obtained from tests on RC structural walls and columns. The proposed modeling approach involves incorporating a cyclic constitutive RC panel model formulation based on a fixed-crack-angle approach into a fiber-based (multi-spring) model element formulation for simulating the observed coupling between nonlinear axial/flexural and shear responses in RC walls and columns. The coupling of axial and shear responses is accounted for at the RC panel (macro-fiber) level, which further allows coupling of flexural and shear responses at the model element level. The proposed modeling approach was originally developed in Matlab (Math-Works, Inc.) and validated against detailed experimental data obtained for five medium-rise RC wall specimens [Tran and Wallace 2012] that experienced significant SFI [Kolozvari et al. 2015a, b]. Research presented in this report focuses primarily on model implementation into OpenSees and examples of model applications to analysis of RC walls and columns.

In summary, the primary objectives of the study presented in this report are to:

- Implement the new cyclic SFI model, along with the constitutive RC panel model and constitutive material models used in its formulation, into the open-source computational platform developed by the Pacific Earthquake Engineering Research (PEER) Center, OpenSees [McKenna et al. 2000], so that it is available for public use and future development
- Validate the model implemented into OpenSees for RC structural walls and columns
- Develop user manuals and examples
- Provide training and education for engineers and researchers

1.3 ORGANIZATION

This report is divided into four chapters. Chapter 2 provides descriptions of the implemented modeling approaches and constitutive material models, including formulations of the baseline *MVLEM*, the proposed shear-flexure-interaction model (*SFI-MVLEM*), the constitutive RC panel model, and the uniaxial material models for concrete and steel. Chapter 3 provides examples of model applications and presents cyclic analysis results for RC column specimens using the *SFI-MVLEM*, a relatively slender RC wall specimen with flexure-dominated response using the *MVLEM*, a moderately slender structural wall specimen using the *SFI-MVLEM*, as well as a dynamic analysis example for a five-story building wall-frame system using the *SFI-MVLEM*. Summary and conclusions, along with recommendations for future model improvements, are presented in Chapter 4. The report also includes three appendices. Appendix A presents the OpenSees user manual for new model elements and constitutive material models; Appendix B provides complete input files used to obtain the analytical results for selected examples presented in Sections 3.1 and 3.2; and Appendix C provides complete input files used to obtain the analytical results for example presented in Section 3.3.

2 Description of Analytical Models

This chapter provides descriptions of the analytical models implemented into OpenSees [McKenna et al. 2000] within the scope of this research. Implementation of the proposed shear-flexure interaction model element also included implementation of the following baseline or constitutive model elements and material models into OpenSees:

- Multiple-Vertical-Line-Element-Model element (*MVLEM*, Vulcano et al. [1988] and Orakcal et al. [2004]) with uncoupled axial/flexural and shear behavior (baseline model)
- Shear-Flexure-Interaction Multiple-Vertical-Line-Element-Model element (*SFI-MVLEM*, Kolozvari [2013] and Kolozvari et al. [2015 a, b]) with coupled axial/flexural and shear responses under cyclic loading conditions
- Plane-stress constitutive RC panel model developed by Ulugtekin [2010] and extended by Orakcal et al.[2012] and Kolozvari [2013] to incorporate shear aggregate interlock effects and dowel action
- Uniaxial material model for concrete based on the constitutive relationship proposed by Chang and Mander [1994]
- Uniaxial material model for reinforcing steel based on the nonlinear hysteretic model of Menegotto and Pinto [1973] and extended by Filippou et al. [1983] to incorporate isotropic strain hardening effects

2.1 SHEAR-FLEXURE INTERACTION ELEMENT

The proposed analytical model incorporates RC panel behavior into a two-dimensional (2D) macroscopic fiber model to capture the experimentally observed SFI in RC structural walls and columns. The Multiple-Vertical-Line-Element-Model (*MVLEM*) formulation adopted by Orakcal et al.[2004] is chosen as the baseline model for the implementation of a new cyclic SFI model because of its relatively simple formulation, detailed material behavior, numerical stability, efficiency, and reasonably accurate predictions of flexural responses [Orakcal and Wallace 2006]. Behavior of the RC panel elements in the proposed cyclic SFI model is described with a 2D constitutive RC panel model formulation that is based on the so-called Fixed-Strut-Angle-Model (FSAM; Ulugtekin [2010] and Orakcal et al. [2012]), which was developed using the fixed-crack-angle modeling approach (e.g., Pang and Hsu [1996]; Hsu and Zhang [1996]; and Mansour and Hsu [2005]). The coupling of axial and shear responses is achieved at the panel (macro-fiber) level, which further allows coupling of flexural and shear responses at the model

element level. Conceptually, the modeling approach is similar to the one proposed by Massone et al.[2006], which captured monotonic SFI behavior in RC walls by implementing constitutive RC panel behavior described by a rotating-crack-angle modeling approach (Rotating Angle Softened Truss Model, Pang and Hsu [1995] into the *MVLEM* formulation. However, extension of the model by Massone et al. [2006] to capture cyclic responses proved cumbersome due to the formulation of the rotating-crack-angle panel model. An overview of implemented modeling approach is presented here; detailed information can be found in the dissertation by Kolozvari [2013].

2.1.1 Baseline Model: Multiple-Vertical-Line-Element-Model

The baseline Multiple-Vertical-Line-Element-Model (*MVLEM*), originally proposed by Vulcano et al. [1988] and extended by Orakcal et al [2004], is a 2D fiber-based analytical model for simulation of nonlinear responses of RC walls and columns. A structural element is modeled as a stack of *n* model elements shown on Figure 2.1(a), placed upon one another. The flexural response is simulated by a series of uniaxial elements (macro-fibers) connected to rigid beams at the top and bottom levels. The stiffness properties and force-displacement relationships of the uniaxial elements are derived according to cyclic constitutive models for concrete and reinforcing steel, and the tributary areas assigned to each uniaxial element. The relative rotations between top and bottom faces of the model element (curvatures) are concentrated at the center-of-rotation defined for each element at height *ch*. The distribution of wall curvature over the height of each model element is assumed to be uniform, as opposed to a displacement-based fiber model formulation, in which linear distribution of curvature is assumed between element nodes; see Figure 2.1(b). Rotations and resulting transverse displacements are calculated based on wall curvature and derived from section and material properties, corresponding to the bending moment at height *ch* of each element. A value of $c = 0.4$ was recommended by Vulcano et al. [1988] and verified by Orakcal and Wallace [2006] based on comparison of model responses with experimental results. Shear response of the model element is simulated by a horizontal spring placed at the height *ch*, with behavior typically described by nonlinear *ad hoc* force-deformation rules (e.g., an origin-oriented hysteresis model proposed by Kabeyasawa et al. [1983]). Since shear and axial-flexural behaviors are described independently, there is no coupling between these responses in the original *MVLEM*; see Figure 2.2. A user manual describing input and output parameters of the *MVLEM* model element implemented in OpenSees is presented in Appendix A.1.

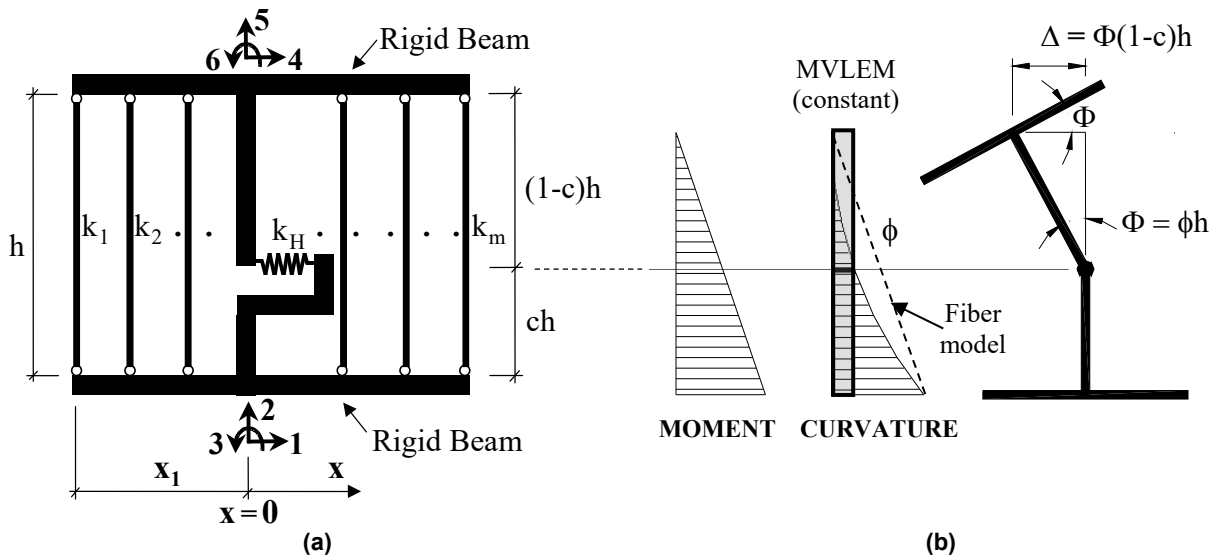

Figure 2.1 ***MVLEM*** **element: (a) model element formulation; and (b) rotations and displacements.**

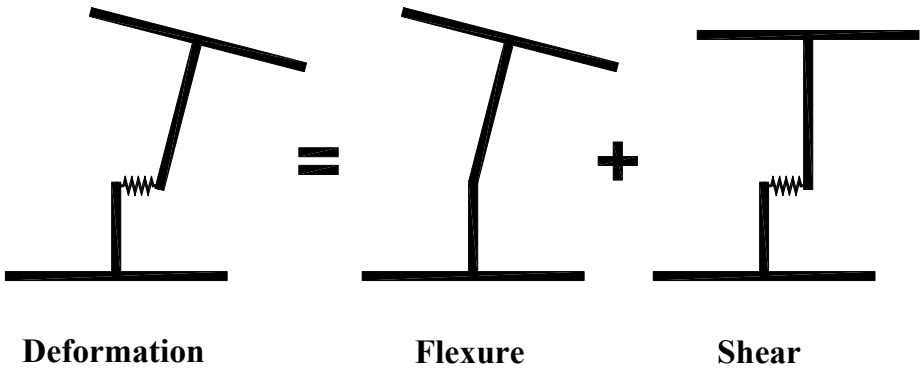

Figure 2.2 **Uncoupled shear and flexural deformations [Orakcal et al. 2004].**

2.1.2 Proposed Model: Shear-Flexure Interaction *MVLEM*

2.1.2.1 General Model Description

The formulation of the proposed *MVLEM* incorporating SFI behavior [*SFI-MVLEM*, Figure 2.3(c)] involves modifying the original formulation of the *MVLEM* with uncoupled shear and flexural responses, as shown in Figure 2.3(a) [Vulcano et al. 1988; Orakcal et al. 2004], by replacing each uniaxial element (macro-fiber) with a RC panel element subjected to membrane actions, as shown on Figure 2.3(b). The behavior of RC panel elements under reversed cyclic loading conditions is described with a constitutive RC panel model based on the so-called Fixed-Strut-Angle-Model (FSAM, Ulugtekin [2010]; Orakcal et al. [2012]). In the implemented modeling approach, the original formulation of FSAM is modified by incorporating shear aggregate interlock behavior in concrete [Orakcal et al. 2012] and dowel action in reinforcement (as described in Section 2.2.2 and Kolozvari [2013]) along inclined cracks of a RC panel to obtain improved model predictions. The RC panel model represents a 2D constitutive

relationship that relates the strain field imposed on a RC panel element (ε_x, ε_y, and γ_{xy}) to the resulting (smeared) stress field on concrete (σ_x, σ_y, and τ_{xy}), as shown in Figure 2.3(b). Thereby, the coupling of axial and shear responses is achieved at the macro-fiber (panel) level, which further incorporates interaction between flexural/axial and shear forces and deformations at the model element level.

The proposed model formulation involves three main assumptions: (a) plane sections remain plane; (b) shear strains are uniformly distributed across the wall cross section; and (c) the resultant of horizontal normal stresses associated with steel and concrete (i.e., horizontal smeared stress in concrete, σ_x) along the length of the wall are equal to zero. Assumptions (a) and (b) are characteristic of the original *MVLEM* formulation, while Assumption (c) is required in the formulation of the *SFI-MVLEM* to satisfy equilibrium of the RC panel elements in the horizontal (x) direction, so that the normal strain in the horizontal direction (ε_x) can be obtained for each panel element. Similar to the original *MVLEM*, flexural response of the model element is captured through axial deformations of the RC panel elements (macro-fibers) in the vertical (y) direction [Figure 2.3(c)], which correspond to deformations of the uniaxial fiber elements in the original *MVLEM* formulation [Figure 2.3(a)], and the relative rotation between the top and bottom faces of the wall element occurs on the central axis of the element at a relative height of *ch;* see Figure 2.3(c). The shear deformation of a *SFI-MVLEM* element also occurs at the relative height *ch*, imposing shear strain (assumed to be uniformly distribution along the wall length) on each RC panel within a *SFI-MVLEM* element. Since the shear deformation of a *SFI-MVLEM* element is captured through shear deformations of its individual panels, the shear spring from the original *MVLEM* formulation [Figure 2.3(a)] is removed in the *SFI-MVLEM* formulation, as shown in Figure 2.3(c). Rotations and resulting lateral displacements are calculated based on the wall curvature and shear deformations coupled at the model element level, derived from section and material properties of RC panel elements, respectively, corresponding to the bending moment and shear force at relative height *ch* of each element. The OpenSees input format and modeling parameters for the *SFI-MVLEM* model element are presented in Appendix A.2.

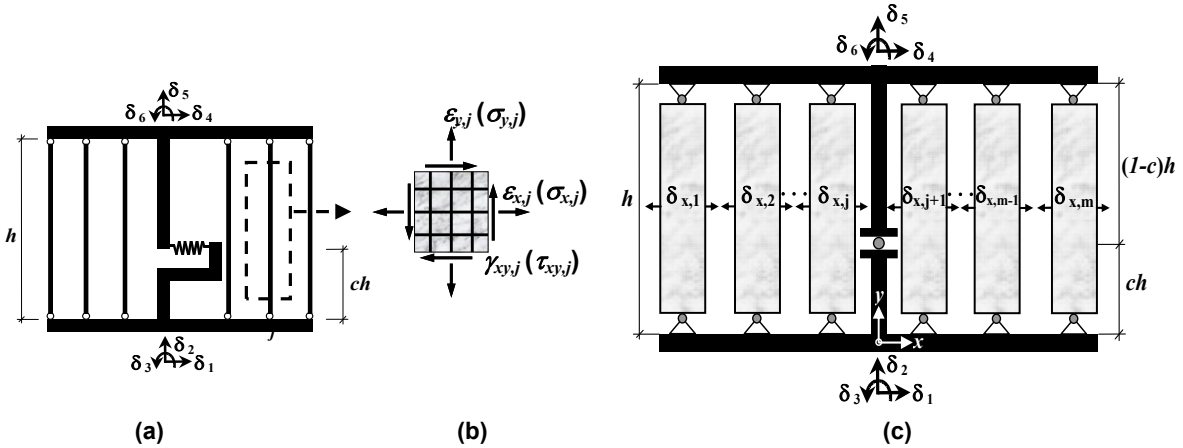

Figure 2.3 Implementation of RC panel behavior into *MVLEM*: (a) original *MVLEM*; (b) RC panel element; and (c) *SFI-MVLEM.*

The assumption of a uniform distribution of shear strains along wall length does not significantly influence the predicted wall behavior in case of slender RC members because lateral displacements are primarily due to flexural deformations. However, using the same assumption for short columns or squat walls may not be reasonable due to the possible presence of different deformation modes (e.g., warping) or load transfer mechanisms (e.g., strut action or contribution of shear deformations). In addition, the relatively small height of the structural member may not be adequate to allow redistribution of stresses concentrated within the proximity of the points of load application or supports (the so-called Saint-Venant's effect). Such effects in the case of short walls and columns can introduce non-uniformity in stresses and strains that may change the observed responses considerably. Furthermore, the assumption of zero resultant horizontal stress (σ_x) within each RC panel element implies that the resultant horizontal normal stresses along the length of a structural member are equal to zero. Although this assumption is consistent with the boundary conditions of the member if no transverse loads are applied over the member height, it may not be realistic for short walls and columns due to the aforementioned effects. Massone et al. [2006] demonstrated that assumptions of zero resultant horizontal stress, uniform shear strain distribution, and that plane-sections-remain-plane are reasonable for cantilever walls with aspect ratios greater than 1.0. Therefore, it is expected that application of the proposed modeling approach is suitable for relatively slender or medium-rise RC walls and columns, with shear-span-to-depth ratios greater than 1.0.

2.1.2.2 Model Element DOFs

Each *SFI-MVLEM* element is characterized with six external degrees-of-freedom located at the center of the top and bottom rigid beams of a model element $\{\delta_N\} = \{\delta_1 \quad \delta_2 \ldots \delta_6\}^T$ (Figure 2.4), which represent horizontal and vertical displacements, and rotations at the top and bottom element nodes. Deformation components at these DOFs are used to calculate the normal strain in the vertical direction $\varepsilon_{y,j}$ and shear strain $\gamma_{xy,j}$ for each RC panel element (macro-fiber), based on the plane-section kinematic assumption and the assumption of uniform distribution of shear stresses along the wall cross section. Normal strain in the horizontal direction on each RC panel element $\varepsilon_{x,j}$, necessary to complete the strain field in each panel, is defined by the use of additional (internal) deformational DOFs defined in the horizontal direction, $\{\delta_x\} = \{\delta_{x,1} \quad \delta_{x,2} \ldots \delta_{x,m}\}^T$, where m is the number of RC panels (macro-fibers) in one model element, as shown on Figure 2.4. The displacement at each degree-of-freedom $\delta_{x,j}$ is equal to deformation (extension) in the horizontal direction $u_{x,j}$ of each panel element ($u_{x,j} = \delta_{x,j}$). These internal deformation DOFs in the horizontal direction on the panel macro-fibers $\{\delta_x\}$ are assumed to be kinematically independent from the six external nodal displacement DOFs at the top and bottom of the element $\{\delta_N\}$. Therefore, the total number of DOFs necessary to describe the deformation of one *SFI-MVLEM* element is increased from six in the original formulation of the *MVLEM* to 6+m.

Let $\{\delta\}$ be the vector representing the displacement components at all 6+m DOFs of the *SFI-MVLEM* element shown on Figure 2.4. The components of vector $\{\delta\}$ can be separated into two sub-vectors: (1) $\{\delta_N\}$, which represents the six nodal DOFs; and (2) $\{\delta_x\}$, which represents the internal DOFs in the horizontal direction for each RC panel element. Hence, displacement vector $\{\delta\}$ can be written as:

$$\{\delta\} = \{\delta_N \quad \delta_x\}^T \tag{2.1}$$

where: $\{\delta_N\} = \{\delta_1 \quad \delta_2 \quad \delta_3 \quad \delta_4 \quad \delta_5 \quad \delta_6\}^T$ and $\{\delta_N\} = \{\delta_{x,1} \quad \delta_{x,2} \ldots \delta_{x,m}\}^T$.

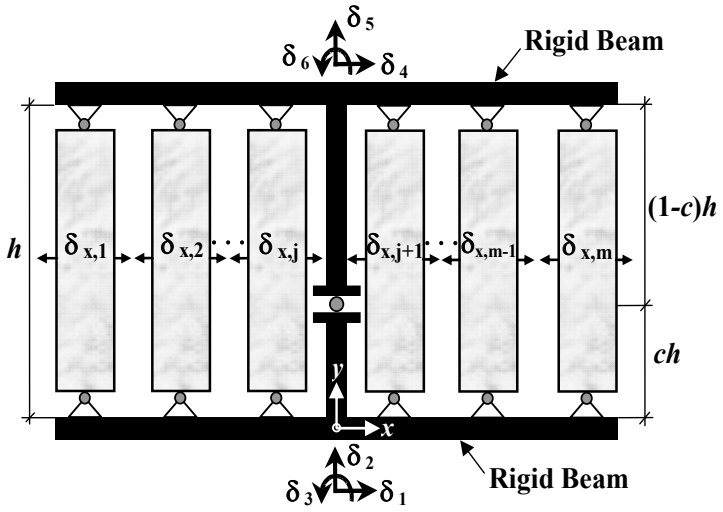

Figure 2.4 ***SFI-MVLEM* element; DOFs.**

2.1.2.3 Element Stiffness Matrix

For any set of displacements imposed on the DOFs of a model element $\{\delta\}$, the strain field acting on each of its RC panels is obtained using geometric transformation, as described by Kolozvari [2013]. The stiffness properties and force-deformation relationships of the panel macro-fibers are then defined according to one of three behavioral stages of the implemented constitutive panel model (as described in Section 2.2), and the tributary areas of concrete and reinforcing steel assigned to each panel macro-fiber. Since the deformation of each RC panel element is described by three strain DOFs ($\varepsilon_{x,j}$, $\varepsilon_{y,j}$, and $\gamma_{xy,j}$), the tangent stiffness properties of a single RC panel element are given by the following 3×3 partial stiffness matrix:

$$\left[K_p\right]_j = \begin{bmatrix} \frac{\partial \sigma_x}{\partial \varepsilon_x} & \frac{\partial \sigma_x}{\partial \varepsilon_y} & \frac{\partial \sigma_x}{\partial \gamma_{xy}} \\ \frac{\partial \sigma_y}{\partial \varepsilon_x} & \frac{\partial \sigma_y}{\partial \varepsilon_y} & \frac{\partial \sigma_y}{\partial \gamma_{xy}} \\ \frac{\partial \tau_{xy}}{\partial \varepsilon_x} & \frac{\partial \tau_{xy}}{\partial \varepsilon_y} & \frac{\partial \tau_{xy}}{\partial \gamma_{xy}} \end{bmatrix}_j \tag{2.2}$$

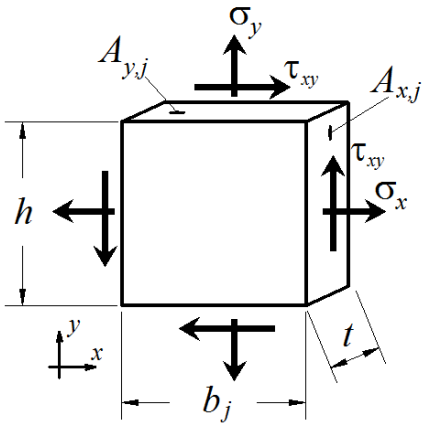

Figure 2.5 Panel stresses and tributary areas.

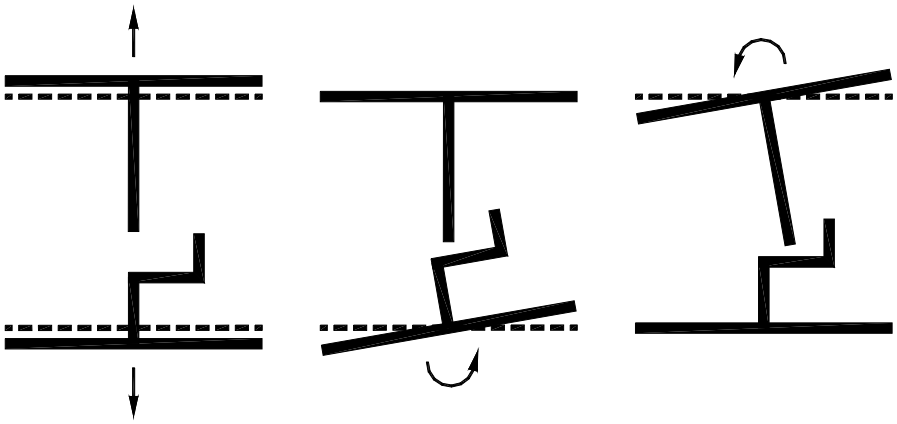

Figure 2.6 Element deformations of the *MVLEM* element [Vulcano et al. 1988].

For any prescribed strain level ($\varepsilon_{x,j}$, $\varepsilon_{y,j}$, and $\gamma_{xy,j}$), the axial stiffness in x and y directions ($k_{x,j}$ and $k_{y,j}$) and the shear stiffness ($k_{H,j}$) of the jth RC panel element are derived based on the panel partial stiffnesses, panel geometry, and tributary areas; see Figure 2.5. The shear stiffness of a *SFI-MVLEM* element for a prescribed shear deformation is calculated as a sum of shear stiffness of all RC panel elements in one model element.

For a specified set of displacement components at the six nodal DOFs of a *SFI-MVLEM* wall element $\{\delta_N\}$ (Figure 2.4), the element stiffness matrix relative to these DOFs $[K_e]_N$ is derived based on geometric transformation of displacements at element DOFs to the element deformations of extension, relative rotation at the bottom, and relative rotation at the top of each wall element; see Figure 2.6 [Orakcal et al. 2004].

Given that the horizontal DOFs at each panel macro-fiber $\{\delta_x\}$ are independent from each other, the element stiffness matrix relative to these DOFs is a diagonal matrix consisting of stiffness in the horizontal direction of each RC panel macro-fiber. The element stiffness matrix is now assembled from element stiffness sub-matrices $[K_e]_N$ and $[K_e]_x$. Since the displacements at the six DOFs $\{\delta_N\}$ and the deformations along the m extensional DOFs $\{\delta_x\}$ are kinematically independent, the element stiffness matrix is a block matrix consisting two sub-matrices $[K_e]_N$ and $[K_e]_x$ given by:

$$[K_e] = \begin{bmatrix} [K_e]_N & [0] \\ [0] & [K_e]_x \end{bmatrix} \tag{2.3}$$

2.1.2.4 Element Force Vector

The internal resisting force vector of a *SFI-MVLEM* element is assembled from the axial forces in the horizontal and vertical directions, and shear forces along the horizontal plane for all of the RC panel elements within one model element, which are calculated based on the resultant panel axial and shear stresses, and corresponding tributary areas; see Figure 2.5. The total shear force in one model element is obtained as the sum of the shear forces on all of the panel elements along the length of the member. Similar to the element stiffness matrix, the resisting (internal) force vector can be written as a combination of two sub-vectors: the force vector relative to the six DOFS $[F_{\text{int},e}]_N$, which is the same as in the original formulation of the *MVLEM* [Orakcal et al. 2004], and the force vector relative to m extensional DOFs $[F_{\text{int},e}]_x$ as:

$$\{F_{\text{int},e}\} = \begin{Bmatrix} \{F_{\text{int},e}\}_N \\ \{F_{\text{int},e}\}_x \end{Bmatrix} \tag{2.4}$$

2.1.2.5 Element Mass Matrix

Similarly to element stiffness matrix, the element mass matrix is divided in two element stiffness sub-matrices $[M_e]_N$ and $[M_e]_x$ as:

$$[M_e] = \begin{bmatrix} [M_e]_N & [0] \\ [0] & [M_e]_x \end{bmatrix} \tag{2.5}$$

Element mass is lumped at top and bottom nodes of each model element (Figure 2.4), and mass equal to one-half of the total element mass is assigned to translational horizontal (δ_1 and δ_4) and vertical (δ_2 and δ_5) DOFs only, whereas rotational masses corresponding to DOFs δ_3 and δ_6 are neglected. Therefore, element mass sub-matrix $[M_e]_N$ takes the following form:

$$[M_e]_N = \begin{bmatrix} M/2 & 0 & 0 & 0 & 0 & 0 \\ 0 & M/2 & 0 & 0 & 0 & 0 \\ 0 & 0 & 0 & 0 & 0 & 0 \\ 0 & 0 & 0 & M/2 & 0 & 0 \\ 0 & 0 & 0 & 0 & M/2 & 0 \\ 0 & 0 & 0 & 0 & 0 & 0 \end{bmatrix} \tag{2.6}$$

where M is the total mass of the model element. In addition, masses corresponding to the m extensional DOFs $\{\delta_x\}$ are all assumed to be equal to zero, thus sub-matrix $[M_e]_x$ becomes a zero matrix, resulting in the following form of the total element mass matrix:

$$[M_e] = \begin{bmatrix} [M_e]_N & [0] \\ \hline [0] & [0] \end{bmatrix} \tag{2.7}$$

2.1.2.6 Global System Matrices

A complete model of a structural element is assembled by stacking *SFI-MVLEM* elements on top of each other, as shown in Figure 2.7(a). The total number of DOFs in the complete model is:

$$N = (3 \cdot n + 3) + m \cdot n \tag{2.8}$$

where n is the number of *SFI-MVLEM* elements in the complete model, and m is the number of RC panel elements per model element. Figure 2.7 illustrates a sample assembly of stiffness matrices and force vectors for the complete model of a structural member from the element stiffness matrices and force vectors for the case where n = 3 and m = 4. The total number of DOFs for this member model according to Equation (2.8) is N = 24.

The global stiffness matrix $[K]$ [Figure 2.7(c)] is a square matrix of dimension $N \times N$, assembled from the element stiffness matrices $[K_e]$; see Figure 2.7(b). As given by Equation (2.3), the element stiffness matrix $[K_e]$ is a block matrix consisting of two sub-matrixes $[K_e]_N$ and $[K_e]_x$ corresponding to the element DOFs $\{\delta_e\}_N$ and $\{\delta_e\}_x$, respectively. The components of the global stiffness matrix $[K]$ that correspond to the nodal DOFs $\{\delta_N\} = \{\delta_1 \ldots \delta_{12}\}$ [Figure 2.7(a)] are grouped in global sub-matrix $[K]_N$, which is assembled from the model element sub-matrices $[K_e]_N$ [Figure 2.7(b)] and located in the upper left corner of the global stiffness matrix $[K]$ [Figure 2.7(c)]. The components of the global stiffness matrix $[K]_x$, corresponding to the $n \times m$ extensional DOFs $\{\delta_x\} = \{\delta_{13} \ldots \delta_{24}\}$ [Figure 2.7(a)] are assembled from diagonal model element sub-matrices $[K_e]_x$ [Figure 2.7(b)] and located in the lower right corner of the global stiffness matrix $[K]$; see Figure 2.7(c).

Global internal (resisting) force vector $\{F_{int}\}$ [Figure 2.7(d)] has dimensions of $N \times 1$ and is assembled from element internal force vectors $\{F_{int,e}\}$ [Figure 2.7(b)]. Each element force vector $\{F_{int,e}\}$ consists of two sub-vectors $\{F_{int}\}_N$ and $\{F_{int}\}_x$ that correspond to DOFs $\{\delta_e\}_N$ and $\{\delta_e\}_x$, respectively. The terms of the nodal force vectors of each model element $\{F_{int,e}\}_N$ are grouped in the global force sub-vector $\{F_{int}\}_N$, and located at the upper part of the global force vector $\{F_{int}\}$ [elements 1 to 12, Figure 2.7(d)], while the terms of the extensional force vectors of each element $\{F_{int,e}\}_x$ [Figure 2.7(b)] are grouped in the global force sub-vector $\{F_{int}\}_x$, and located at lower part of the global internal force vector $\{F_{int}\}$ [elements 13 to 24, Figure 2.7(d)].

n = 3: # of MVLEM-SFI elements

m = 4: # of RC panel elements

N = 24: Total # of DOFs

e = 1, 2, 3

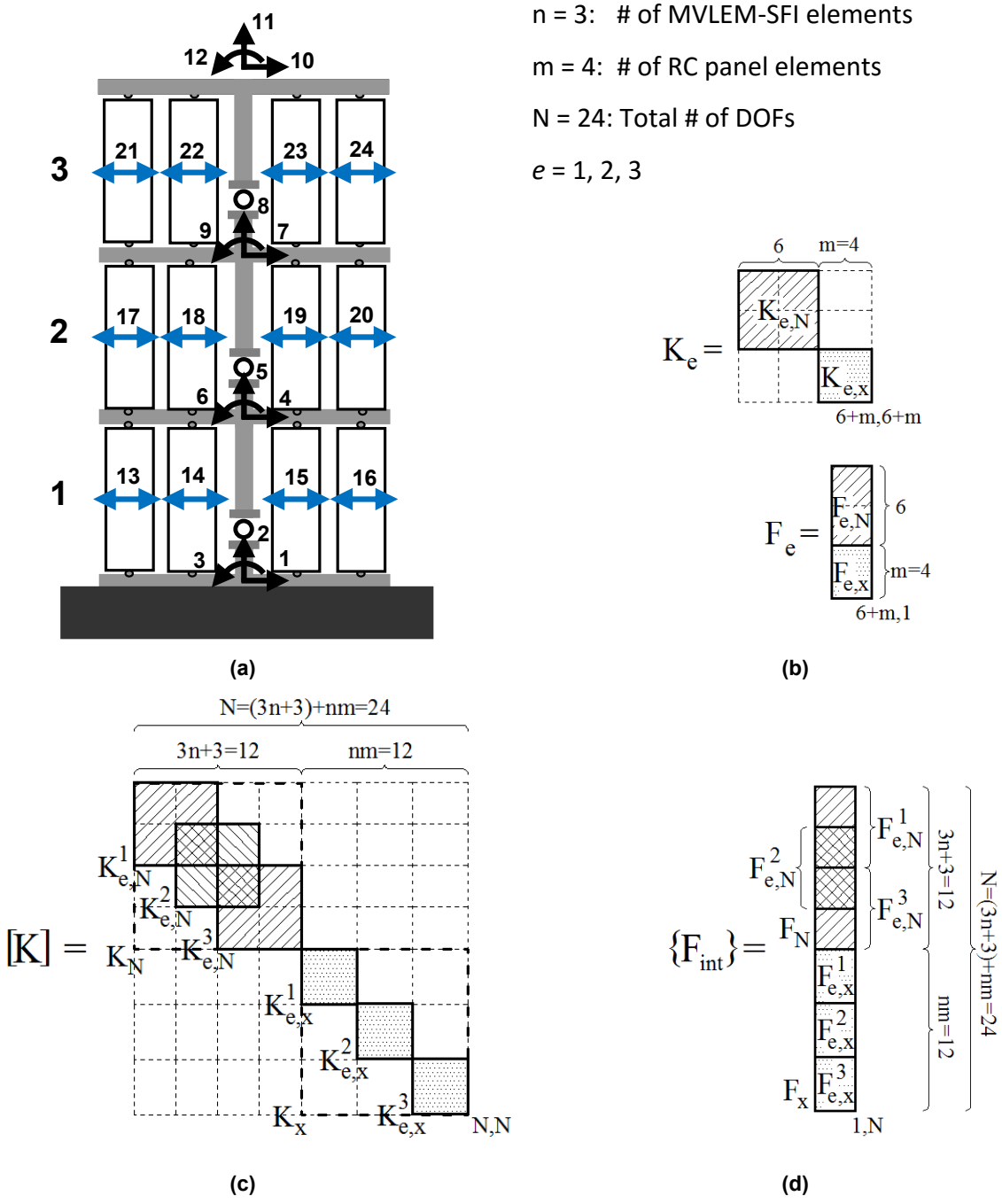

Figure 2.7 **Sample model assembly: (a) complete model with DOFs; (b) element stiffness matrix and force vector (c) global stiffness matrix; and (d) global force vector.**

2.2 CONSTITUTIVE REINFORCED CONCRETE PANEL BEHAVIOR

The constitutive RC panel behavior under generalized reversed-cyclic in-plane membrane actions is described by the Fixed-Strut-Angle-Model (FSAM) proposed originally by Ulugtekin [2010], which was shown to replicate the results of cyclic panel tests available in the literature with reasonable accuracy. Formulation of the FSAM is inspired from the fixed-angle-softened-truss approach introduced by Pang and Hsu [1996] and Hsu and Zhang [1996] for monotonic loading, and extended by Mansour and Hsu [2005] for reversed-cyclic loading conditions. Shear aggregate interlock effects in concrete [Orakcal et al. 2012] and dowel action on longitudinal reinforcement [Kolozvari 2013] are incorporated into the original formulation of the FSAM to improve the predictions of the *SFI-MVLEM*. A conceptual overview of the implemented RC panel model formulation is provided in this section; additional details can be found in Ulugtekin [2010] and Orakcal et al. [2012].

2.2.1 Fixed-Strut-Angle-Model (FSAM)

As described in Section 2.1.2, strains calculated at each load-step/iteration are applied on each of the constitutive RC panel elements (macro-fibers) in the *SFI-MVLEM*. The strain fields acting on concrete and reinforcing steel components of a RC panel element are assumed to be equal to each other, incorporating the assumption of perfect bond between concrete and reinforcing steel bars. Other inherent assumptions in the formulation of the original FSAM [Ulugtekin 2010] are that the directions of principal stress in concrete coincide with the directions of cracks, implying zero shear-stress action along cracks, and therefore, zero shear aggregate interlock, and that dowel action on the reinforcement is equal to zero. Therefore, in the original FSAM, the reinforcing bars develop uniaxial stresses under uniaxial strains in their longitudinal directions, and concrete behavior is based on uniaxial stress–strain relationships applied in biaxial directions with orientations determined by the state of concrete cracking. A modified formulation of the FSAM was implemented in OpenSees as a part of this research, where shear aggregate interlock effects in concrete were incorporated [Orakcal et al. 2012], and a simple model was adopted to account for dowel action on reinforcing steel bars. The improved FSAM formulation was incorporated into the *SFI-MVLEM* for obtaining improved cyclic response predictions for RC walls and columns. Constitutive behavior of concrete in the RC panel model is characterized by three consecutive stages: (a) uncracked concrete, (b) after formation of the first crack, and (c) after formation of the second crack; each of these stages is described in the following paragraphs.

In the formulation of the FSAM, the stress–strain behavior of uncracked concrete is represented with a rotating strut approach (e.g., the Modified Compression Field Theory, [Vecchio and Collins 1986] and the Rotating Angle Strut and Tie Model [Pang and Hsu 1995]). The strain field imposed on concrete is transformed into principal strain directions, which are assumed to coincide with principal stress directions, and uniaxial stress–strain relationships for concrete are applied along the principal strain directions in order to obtain the principal stresses in concrete. The concrete principal stresses are then back-transformed to obtain the concrete stresses in x–y directions, including the shear stress in concrete. At this stage of the behavior, monotonic stress–strain relationships for concrete are used in principal strain (stress) directions, since it is reasonable to assume that concrete behavior follows monotonic stress–strain relationship prior to first cracking under a biaxial state of stress; see Figure 2.8.

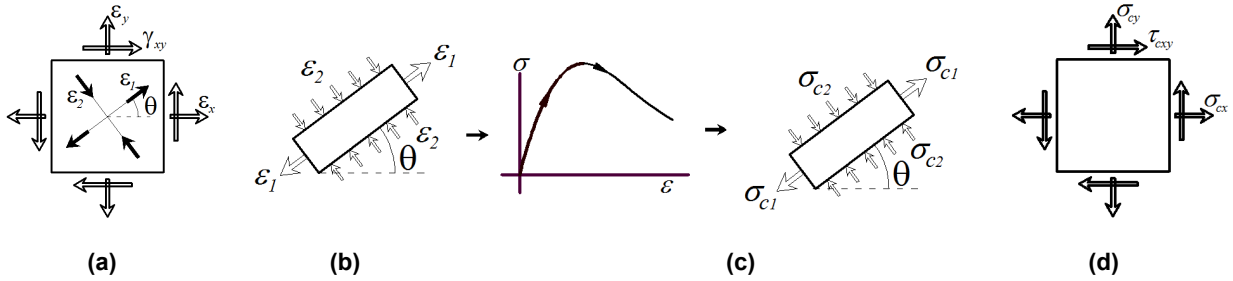

Figure 2.8 **Behavior of uncracked concrete in the FSAM: (a) strain field, (b) principal strains; (c) principal stresses in concrete; and (d) concrete stresses.**

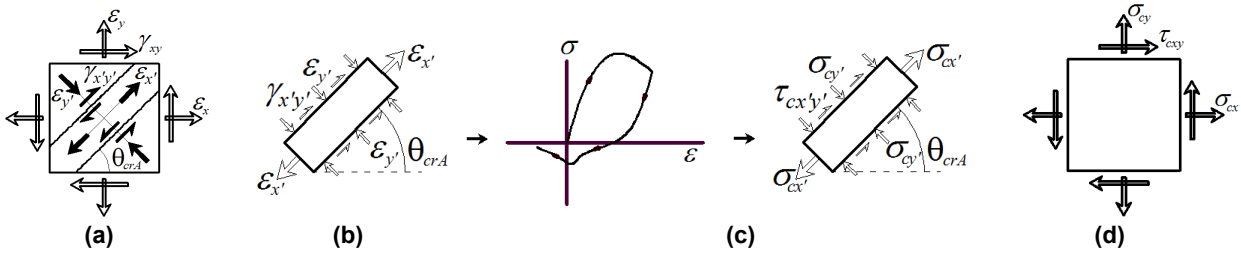

Figure 2.9 **Behavior of concrete after formation of the first crack: (a) strain field; (b) concrete strut strains; (c) concrete strut stresses; and (d) concrete stresses.**

When the value of the principal tensile strain in concrete exceeds the monotonic cracking strain of concrete for the first time, the first crack is formed, and for following loading stages, the principal strain direction corresponding to first cracking in concrete is assigned as the first "fixed strut" direction for the panel. After formation of this first crack, while principal directions of the applied strain field continue to rotate based on the applied strain field, the principal stress directions in concrete are assumed to be along and perpendicular to the first fixed strut direction. This physically implies zero shear aggregate interlock along a crack, which was an inherent assumption of the original model formulation [Ulugtekin 2010]. Since the direction of the first strut is fixed, a uniaxial hysteretic stress–strain relationship for concrete can now be applied in principal stress directions (parallel and perpendicular to the first strut), and history variables in the concrete stress–strain relationship can tracked in the two fixed directions. For calculation of concrete stresses in principal directions, the strain field in concrete is transformed into strain components that are parallel and perpendicular to the first fixed strut direction instead of principal strain directions; see Figure 2.9. As well, the shear strain parallel to the first strut (crack) is used to calculate the shear stress in concrete along the crack, using the shear aggregate interlock model adopted. The concrete stresses on the strut are finally back-transformed into *x*–*y* directions.

The behavior of concrete continues in the form of a single fixed strut mechanism until the formation of the second crack, upon which the second strut will develop. When the strain along the first strut direction first exceeds the cyclic cracking strain (which depends on both the monotonic cracking strain and the plastic strain upon reversal from a compressive stress), the second crack is formed. In case of the zero aggregate interlock assumption (when zero shear stress is assumed along the crack), the second crack has to develop in the perpendicular direction

to the first crack since the first strut direction is a principal stress direction. Although other cracking criteria may be used when shear transfer across cracks is considered in the model, the orthogonal crack assumption remains a simple yet reasonable approach. After formation of this second crack, the second "fixed strut" will develop in the direction of the second crack (in perpendicular direction to the first strut), and for further loading stages, the concrete mechanism consists of two independent struts, working as interchanging compression and tension struts in the two fixed strut directions based on the applied strain field. Since the direction of both struts are fixed, the uniaxial hysteretic stress–strain relationship for concrete can be applied in principal stress directions (parallel to the first and second strut directions), and history variables in the concrete stress–strain relationship can be tracked and stored in the two fixed directions. For calculation of concrete stresses in the two strut directions, the strain field in concrete is transformed into components that are parallel to the first and second fixed strut directions (Figure 2.10). Shear strains parallel to the first and second struts (cracks) are used to calculate the shear stress in concrete along the two cracks, using the shear aggregate interlock model adopted. The concrete stresses on the two struts are finally back-transformed into *x*–*y* directions and superimposed.

The stress field on the reinforcing steel in the FSAM is obtained from the axial strains developing in the reinforcing steel bars in horizontal and vertical directions, using the uniaxial stress–strain relationship adopted for reinforcing steel (e.g., Menegotto and Pinto [1973]). It is assumed that the strain field acting on concrete and reinforcing steel in a RC panel element are identical, implying perfect bond. As well, the shear stress developing perpendicular to the vertical reinforcement is calculated based on a shear strain acting on the RC panel using a linear elastic dowel action model implemented in the FSAM formulation (Figure 2.11) for the cracked stages of RC panel behavior, as described in the following section.

Finally, the stress fields for concrete and reinforcing steel are superimposed (using reinforcement ratios in horizontal and vertical directions), to obtain the resultant (smeared) state of stress in the panel element; see Figure 2.12.

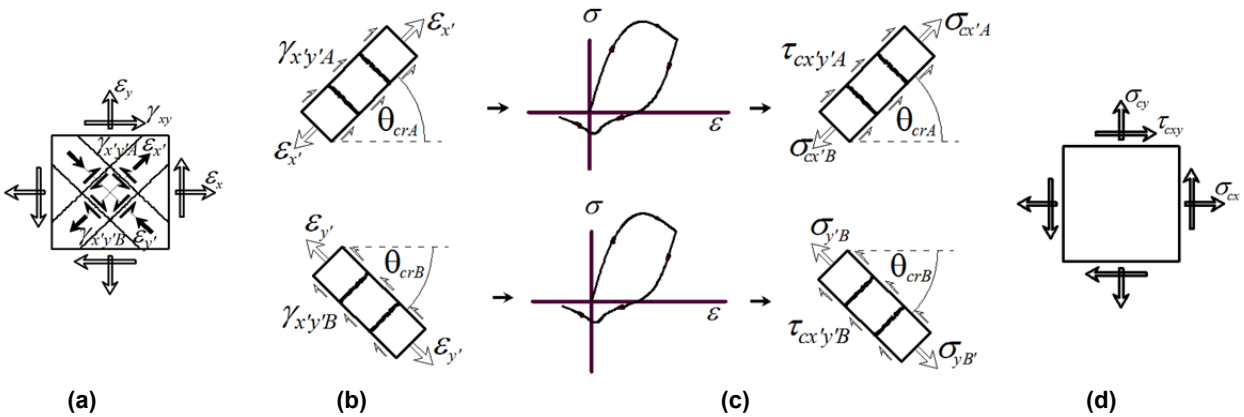

Figure 2.10 **Behavior of concrete after formation of the second crack: (a) strain field; (b) concrete strut strains; (c) concrete strut stresses, and (d) concrete stresses.**

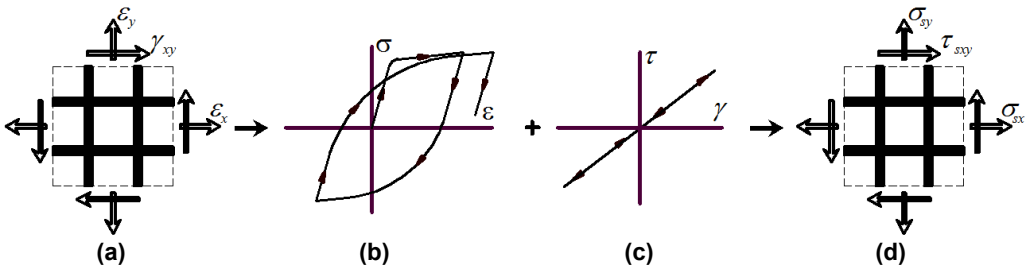

Figure 2.11 **Behavior of reinforcing steel in the FSAM; (a) strain field; (b) stress–strain model; (c) dowel action model; and (d) steel stresses.**

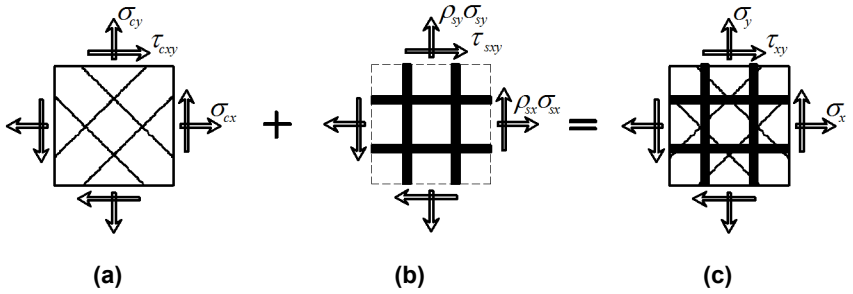

Figure 2.12 **Superposition of concrete and steel stresses to obtain resultant (smeared) stresses in concrete: (a) concrete stresses; (b) steel stresses; and (c) resultant stress field.**

In the implementation of the FSAM, the formulation of the uniaxial Chang and Mander [1994] model for concrete was modified to represent behavioral features of concrete under biaxial loading via inclusion of empirical parameters representing compression softening (described by Vecchio and Collins [1993]) and hysteretic biaxial damage (described by Mansour et al. [2002]). In addition, tension stiffening effects (e.g., described by Belarbi and Hsu, [1994]) need to be considered in calibration of the material parameters. Details of the FSAM are provided by Ulugtekin [2010] and Kolozvari [2013]. A user manual with input and output parameters of the FSAM implemented in OpenSees is presented in Appendix A.3.

2.2.2 Shear Resisting Mechanisms across Cracks

The original formulation of the FSAM described by Ulugtekin [2010] adopted the zero shear aggregate interlock assumption along the cracks. However, formulation of the FSAM allows incorporation of a suitable model for aggregate interlock, which represents the shear stress versus shear (sliding) strain behavior parallel to a crack. In the model formulation implemented here, a simple friction-based constitutive model was adopted [Orakcal et al. 2012], since the zero-aggregate-interlock assumption generally results in overestimation of sliding shear strains along crack surfaces for panels with inclined reinforcement or non–equal reinforcement ratios in the x and y directions. The present model formulation also incorporates a simple linear elastic shear stress versus strain model to represent dowel action on the reinforcing steel bars.

The shear aggregate interlock model implemented in the present FSAM formulation starts with linear loading/unloading behavior, which relates the sliding shear strain along a crack to the shear stress via a simple linear elastic relationship between the sliding shear strain and the

resulting shear stress along the crack surface. However, the shear stress is restrained to zero value when the concrete normal stress perpendicular to the crack is tensile (crack open); it is bounded via the product of a shear friction coefficient η [Figure 2.13(a)]) and the concrete normal stress perpendicular to the crack when the concrete normal stress is compressive (crack closed). The linear unloading/reloading slope of the shear stress versus sliding strain relationship was taken as a fraction of the concrete elastic modulus (a value $0.4E_c$ was adopted, representing the elastic shear modulus of concrete). The shear friction coefficient typically takes values between 0.45 and 1.4, which is based on previous research conducted on transfer of shear force in RC members through the shear-friction mechanism. However, for modeling of individual panel specimens, lower values (e.g., 0.2) were found to provide more accurate results (e.g., see Orakcal et al. [2012]). In OpenSees implementation of the RC panel constitutive material model, an input parameter **nu** (see Appendix A.3) is assigned to the shear-friction coefficient. Results of sensitivity studies of analytical predictions of *SFI-MVLEM* model to variations of the shear-friction coefficient are presented by Kolozvari [2013]. Under constant compressive stress in concrete perpendicular to the crack, this model yields an elasto–plastic aggregate interlock behavior under cyclic loading [Figure 2.13(a)], which is similar to the cyclic stress–strain behavior of reinforcing steel. Note that the "clamping" effect of reinforcing steel bars on the shear aggregate interlock mechanism is not considered in the present formulation of the model.

A simple linear elastic constitutive model [Kolozvari 2013] is also implemented in the formulation of the FSAM for simulating the influence of dowel action on vertical (longitudinal) reinforcing bars in a structural wall or column. The constitutive model relates the shear strain in a panel element with the shear stress developing in the vertical reinforcement (along the horizontal plane of a wall or column) by using an elastic modulus defined as a fraction of the modulus of elasticity for reinforcing steel via dowel stiffness parameter α [Figure 2.13(b)] represented by a FSAM input parameter **alfadow** (see Appendix A.3). While incorporation of this dowel action model in the FSAM greatly enhances the numerical stability and rate of convergence of the *SFI-MVLEM*, analysis results for structural elements may be influenced by selection of parameter **alfadow**, in terms of the level of shear deformations and pinching characteristics of the response [Kolozvari 2013; Kolozvari et al. 2015a].

Overall, with its assumptions and simplifications, the FSAM is a behavioral (macro) model for simulating in-plane behavior of RC panel elements. It can be interpreted as a stress–strain-based strut-and-tie model; however, crack (strut) angles need not be specified as input parameters, and constitutive models for shear aggregate interlock and dowel action can be easily implemented in its formulation. Detailed constitutive models for aggregate interlock and dowel action are available in the literature. The FSAM formulation presented here is flexible for such implementations and further improvement. In addition, the FSAM can be feasibly used to describe the constitutive behavior of four-node quadrilateral membrane elements (e.g., quad element in OpenSees) for finite element (FE) modeling of structural walls. Results of preliminary studies (e.g., Gullu and Orakcal [2014]; Gullu et al. [2014]; and Horoz et al. [2015]) show that FE models constructed using the FSAM capture with reasonable accuracy the lateral load response characteristics of both rectangular and nonrectangular walls with various aspect ratios.

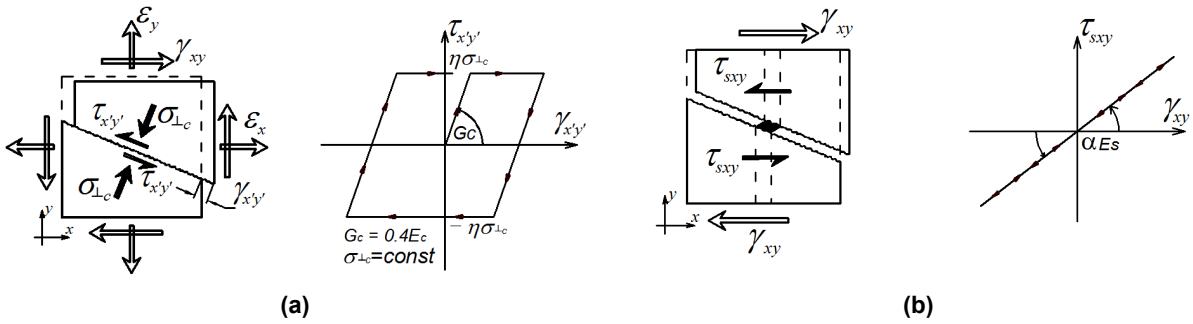

Figure 2.13 **Mechanisms in the FSAM for shear-stress transfer across cracks: (a) shear aggregate interlock model; and (b) dowel action model.**

2.3 UNIAXIAL CONCRETE CONSTITUTIVE BEHAVIOR

The uniaxial constitutive stress–strain relationship for concrete implemented in OpenSees as part of this research is the hysteretic constitutive model developed by Chang and Mander [1994]. The model by Chang and Mander [1994] is a refined, rule-based, generalized, and non-dimensional constitutive model that allows calibration of the monotonic and hysteretic material modeling parameters, and can simulate the hysteretic behavior of confined and unconfined, ordinary and high-strength concrete in both cyclic compression and tension; see Figure 2.14. The model addresses important behavioral features, such as continuous hysteretic behavior under cyclic compression and tension, progressive stiffness degradation associated with smooth unloading and reloading curves at increasing strain values, and gradual crack closure effects.

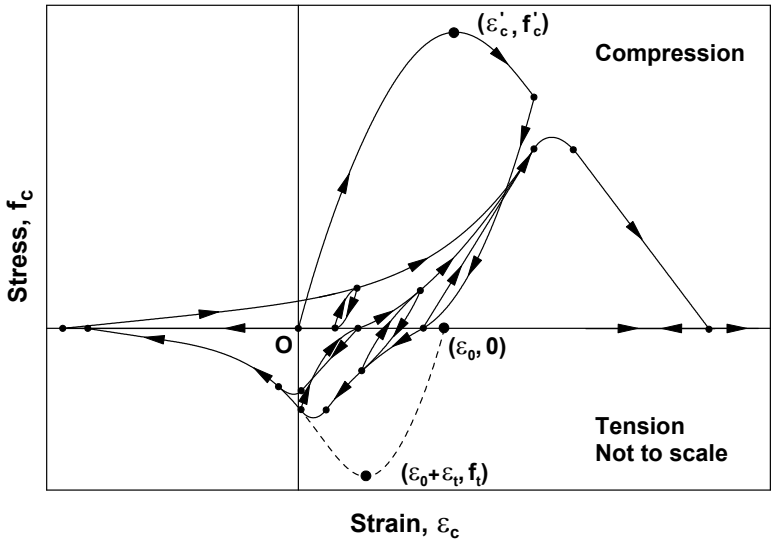

Figure 2.14 **Hysteretic constitutive model for concrete by Chang and Mander [1994].**

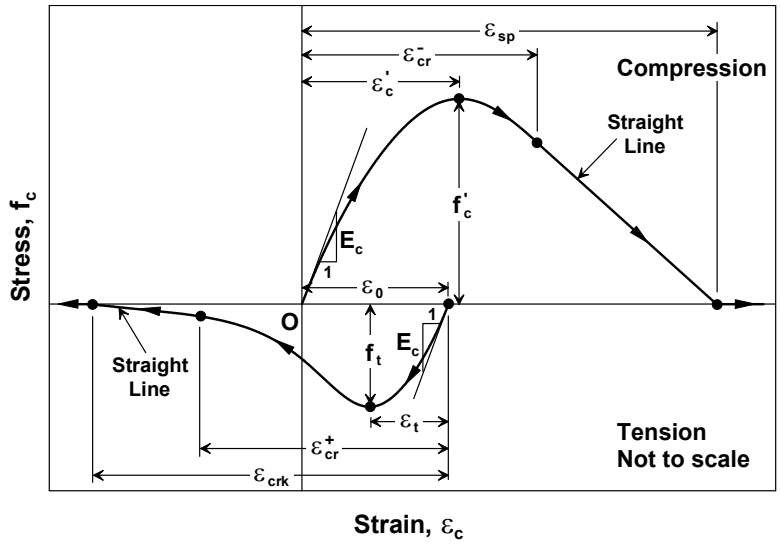

Figure 2.15 Compression and tension envelope curves.

The compression envelope curve of the model by Chang and Mander [1994] is defined by the initial tangent slope E_c, the peak coordinate (ε_c', f_c'), a parameter r from Tsai's [1988] equation defining the shape of the envelope curve, and a parameter ε_{cr}^{-} to define normalized (with respect to ε_c') strain where the envelope curve starts following a straight line until zero compressive stress is reached at the spalling strain, ε_{sp}. These parameters can be controlled based on specific experimental results for a refined calibration of the compression envelope; see Figure 2.15. Chang and Mander [1994] proposed empirical relationships for parameters E_c, ε_c', and r for unconfined concrete with compressive strength f_c', based on review of previous research. Parameters f_c', ε_c', E_c, r, and ε_{cr}^{-} can also be calibrated to represent the stress–strain behavior of confined concrete in compression to follow the constitutive relationships for confined concrete proposed by Mander et al. [1988] or similar constitutive models.

The shape of the tension envelope curve in the model by Chang and Mander [1994] is similar to that of the compression envelope; however, the tension envelope curve is shifted to a new origin that is based on the unloading strain from the compression envelope; see Figure 2.15. In addition, the strain ductility experienced previously on the compression envelope is also reflected on the tension envelope. The parameters associated with the tension envelope curve include the tensile strength of concrete (f_t), the monotonic strain at tensile strength (ε_t), a parameter r from Tsai's [1988] equation defining the shape of the tension envelope curve, and a parameter (ε_{cr}^{+}) to define normalized (with respect to ε_t) strain where the tension envelope curve starts following a straight line until zero tensile stress is reached at a strain of ε_{crk}. These parameters can also be controlled and calibrated based on specific experimental results or empirical relations proposed by other researchers (e.g., Belarbi and Hsu [1994]) to model the behavior of concrete in tension and the tension-stiffening phenomenon. Concrete experiencing tension stiffening can be considered to not have cracked completely; that is, a large value for parameter ε_{cr}^{+} (e.g., 10,000) can be defined. All of these monotonic parameters that define the compression and tension envelopes of concrete stress–strain behavior are implemented as input parameters for the Chang and Mander concrete material model in OpenSees, as presented in Appendix A.4.

In order to define the hysteretic properties of the model, statistical regression analyses were performed by Chang and Mander [1994] on an extensive experimental database. Based on regression analyses, empirical relations were developed for key hysteretic parameters, such as those for secant stiffness (E_{sec}) and plastic stiffness (E_{pl}) upon unloading from, and stress and strain offsets (Δf and $\Delta\varepsilon$) upon return to the compression and tension envelopes; see Figure 2.16. A reversal from the compression envelope curve was done, as shown in Figure 2.17, by calculating the shifted origin (ε_0) of the tension envelope curve and evaluating the unloading strain (ε_{un}^{+}) from the tension envelope curve. Upon each unloading from the compression envelope, the origin of the tension envelope is shifted based on the unloading strain from the compression envelope (ε_{un}^{-}), and the unloading strain from the tension envelope (ε_{un}^{+}) is re-evaluated so that it corresponds to a tension strain ductility equal to a previously-experienced compression strain ductility upon unloading from the compression envelope or a previously-experienced tension strain ductility, whichever is greater.

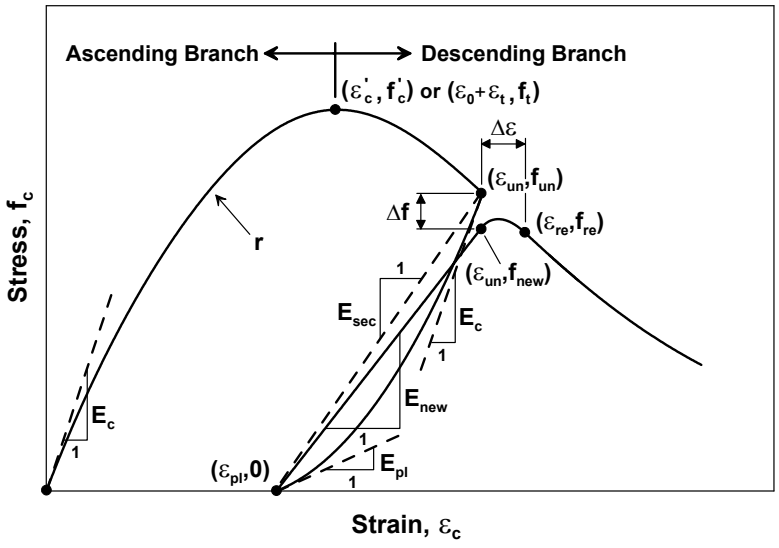

Figure 2.16 Hysteretic properties of the model.

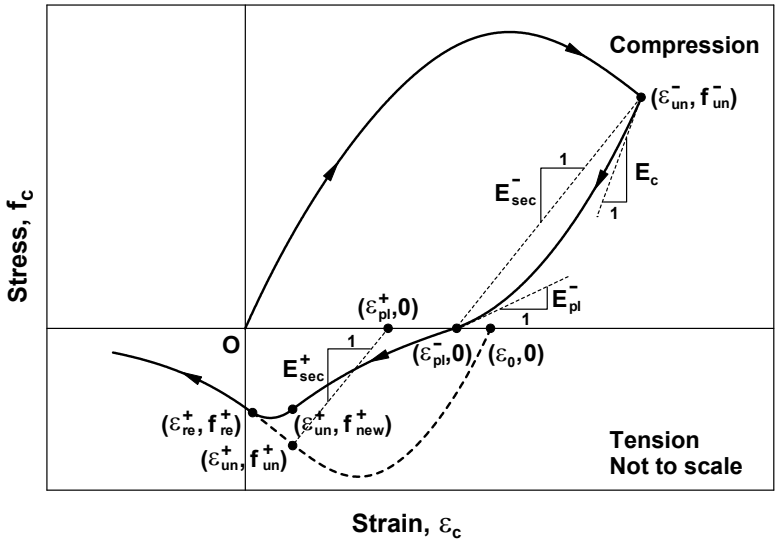

Figure 2.17 Unloading from the compression envelope curve.

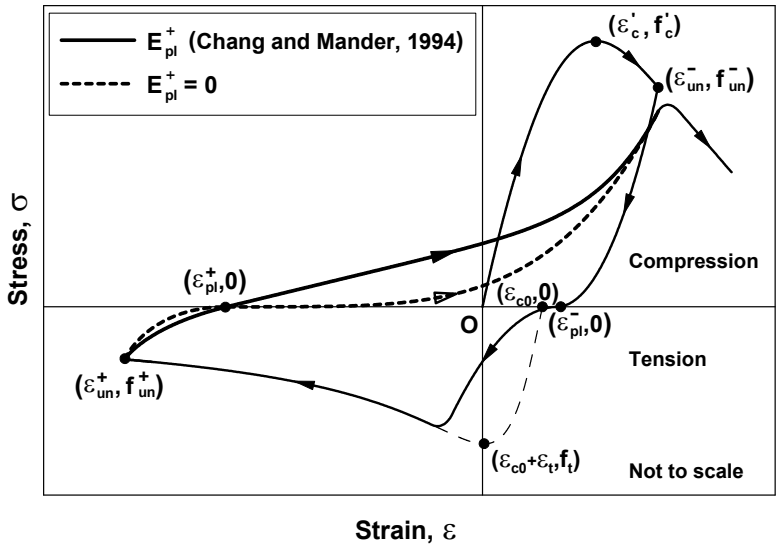

Figure 2.18 Effect of plastic stiffness upon unloading from tension envelope (E_{pl}^{+}) on crack closure.

The hysteretic parameters of the model (E_{sec}, E_{pl}, Δf, and $\Delta\varepsilon$ for compression or tension), presently defined in the code using the empirical equations by Chang and Mander [1994], can also be calibrated based on individual test results or updated upon availability of new experimental data. For example, Figure 2.18 compares sample stress–strain histories generated by the model with the original expression derived by Chang and Mander [1994] for the plastic stiffness for unloading from the tension envelope (E_{pl}^{+}) and an illustrative value of zero. The concrete material model implemented in OpenSees provides the opportunity to define the plastic stiffness for unloading from the tension envelope (E_{pl}^{+}) according to the empirical relationship proposed by Chang and Mander, or a zero value (via "switch" parameter **gap**), as described in Appendix A.4.

In terms of modeling generalized hysteretic behavior, the constitutive model uses smooth "connecting" curves for unloading and reloading between the compression and tension envelope curves, and smooth "transition" curves for partial unloading and reloading between the connecting curves (Figure 2.14). The connecting and transition curves are geometrically defined such that they commence at the prescribed starting point (e.g., ε_{un}, f_{un} in Figure 2.19) with a prescribed initial slope (e.g., E_c), and end up at a prescribed final (target) point (e.g., ε_{pl}, 0) with a prescribed final slope (e.g., E_{pl}). Chang and Mander [1994] proposed additional empirical expressions for determining the position of the target points for the transition curves. Both connecting and transition curves have slope continuity with uniform (constant) sign of curvature (second strain derivative of the curve equation) in between the starting and final points. These features enable capturing the gradual gap closure, which are not considered in the majority of available concrete constitutive models.

The hysteretic rules of the original Chang and Mander [1994] model occasionally yield some minor numerical inconsistencies. For some strain histories, using connecting and transition curves with no change in the sign of the curvature is geometrically incompatible for commencing at a starting point with a prescribed initial slope and ending at a target point with a prescribed ending slope. For such cases, where curves with uniform sign of curvature are geometrically insufficient, a straight line with a secant slope was adopted to represent the connecting or

transition curve between the starting and target points; see Figure 2.19. Another inconsistency in the original model formulation is associated with the value of this secant slope. For a range of values for unloading strain from the tension and compression envelopes (approximately for $\varepsilon_{un}^{+} < \varepsilon_0 + 0.5\varepsilon_t$ and $\varepsilon_{un}^{-} < 0.1\,\varepsilon_c'$ for ordinary strength concrete), using the stress and strain offsets (Δf and $\Delta\varepsilon$) proposed by Chang and Mander [1994], can result in a value for the secant modulus that is larger than the initial tangent modulus E_c; see Figure 2.19. This is physically unlikely and may also lead to convergence problems in the nonlinear solution algorithm. For simplicity, under such conditions (for the aforementioned range of unloading strains), the stress offsets (Δf) in compression and tension were set to zero in the model code. Details are available in the dissertation by Orakcal [2004]. The minor adjustments implemented here do not induce a significant deviation from stress–strain relations generated by the original model formulation, but were necessary in order to ensure its stability and consistency under various arbitrary strain histories.

Apart from these minor numerical inconsistencies, which were remedied in the code, the Chang and Mander [1994] model successfully generates continuous hysteretic stress–strain relationships with slope continuity for confined and unconfined concrete in both compression and tension. Details of the model are available in Chang and Mander [1994]. An example hysteretic stress–strain history generated by the model code is illustrated in Figure 2.20.

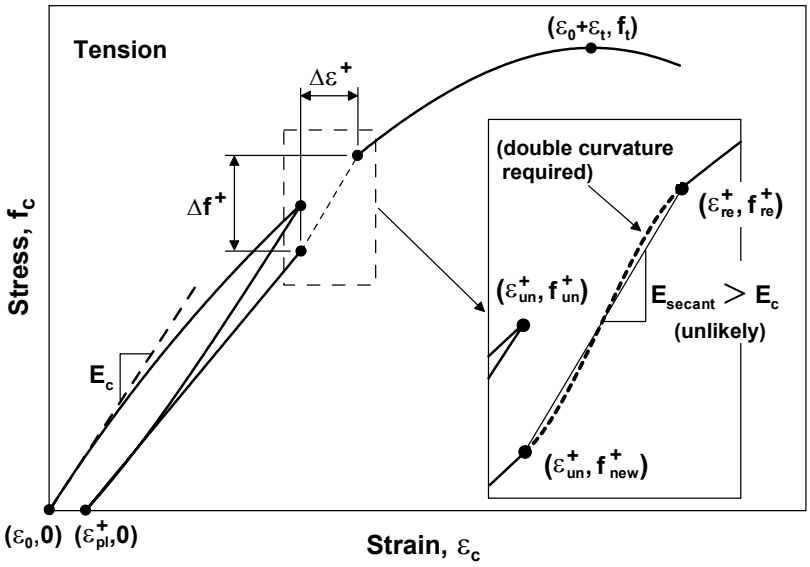

Figure 2.19 Numerical instabilities in the model formulation.

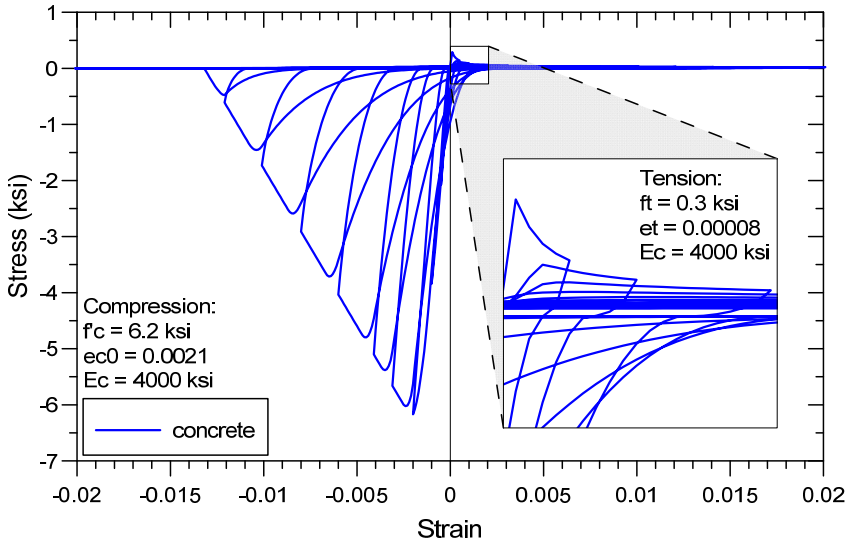

Figure 2.20 Sample concrete stress–strain behavior.

2.4 REINFORCING STEEL UNIAXIAL CONSTITUTIVE BEHAVIOR

The uniaxial constitutive stress–strain relationship for reinforcing steel implemented in OpenSees as a part of this research is the well-known nonlinear hysteretic model of Menegotto and Pinto [1973], as extended by Filippou et al.[1983] to include isotropic strain hardening effects. The relationship is in the form of curved transitions (Figure 2.21), each from a straight-line asymptote with slope E_0 (modulus of elasticity) to another straight-line asymptote with slope $E_1 = bE_0$ (yield modulus), where the parameter b is the strain hardening ratio. The curvature of the transition curve between the two asymptotes is governed by a cyclic curvature parameter R, which permits the Bauschinger effect to be represented. Parameters σ_r and ε_r are the stress and strain at the point of strain reversal, which also forms the origin of the asymptote with slope E_0. Parameters σ_0 and ε_0 are the stress and strain at the point of intersection of the two asymptotes. As indicated in Figure 2.21, the strain and stress pairs $(\varepsilon_r, \sigma_r)$ and $(\varepsilon_0, \sigma_0)$ are updated after each strain reversal.

The curvature parameter R is dependent on the absolute strain difference between the current asymptote intersection point and the previous maximum or minimum strain reversal point (Figure 2.22), depending on whether the current strain is increasing or decreasing, respectively. The absolute strain difference between the current asymptote intersection point and the previous maximum or minimum strain reversal point is represented by the parameter ξ; see Figure 2.22. Parameter ε_0 is the strain at the current intersection point of the two asymptotes; parameter ε_y is the strain at monotonic yield point (Figure 2.21). As shown in Figure 2.22, both ε_m and ε_0 lie on the same asymptote, and ξ is updated following a strain reversal.

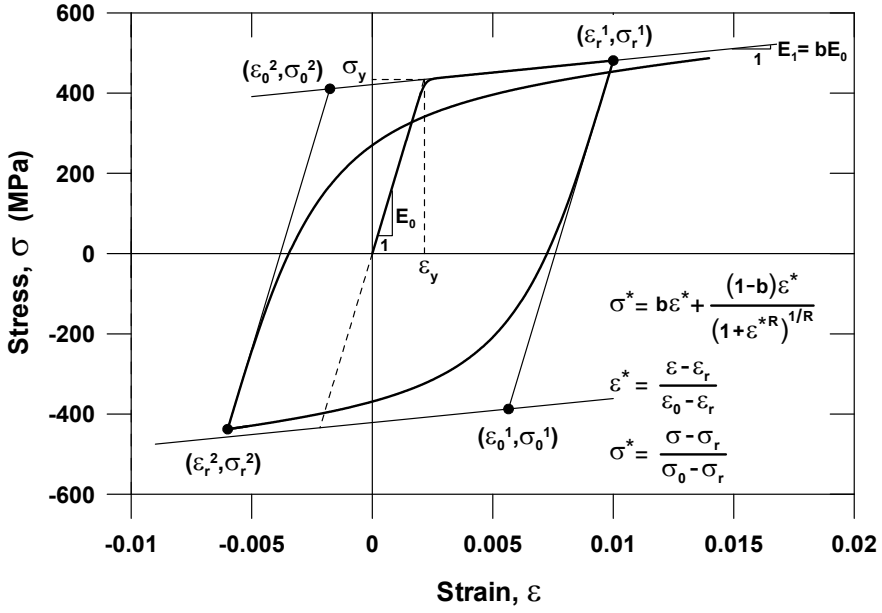

Figure 2.21 Constitutive model for steel [Menegotto and Pinto 1973].

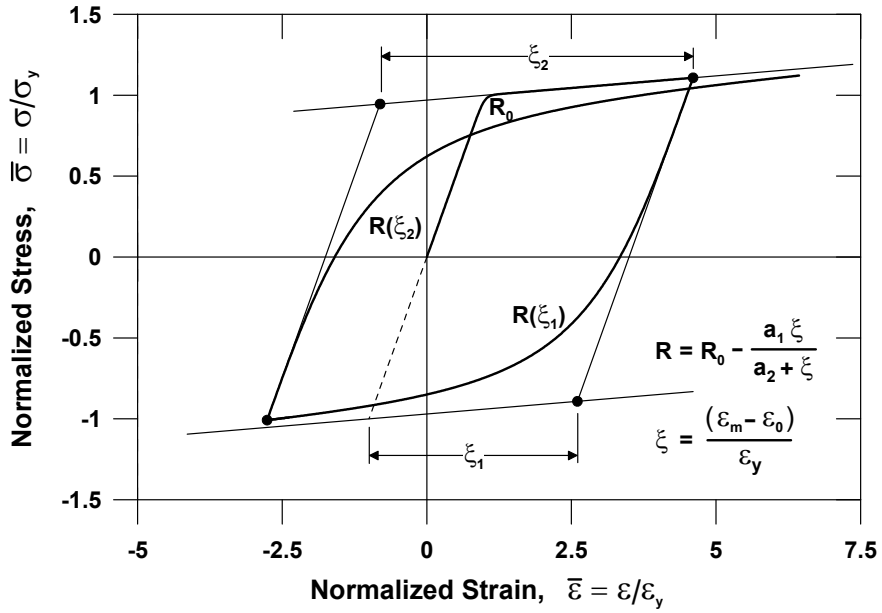

Figure 2.22 Degradation of cyclic curvature.

Figure 2.23 compares the stress–strain histories generated by the constitutive model for two different sets of values for parameters R_0, a_1, and a_2 (accounting for the cyclic degradation of the curvature coefficient R), experimentally calibrated by prior researchers (R_0, a_1, a_2 = 20, 18.5, 0.15 by Menegotto and Pinto [1973]; R_0, a_1, a_2 = 20, 18.5, 0.0015 by Elmorsi et al. [1998]) based on results of cyclic tests on reinforcing bars. The figure reveals how the constitutive model simulates different levels of cyclic degradation of the curvature of the stress–strain relationship, accounting for the Bauschinger effect.

In order to account for isotropic strain hardening to improve the prediction of the strains in reinforcing bars in RC members during crack closure, Filippou et al. [1983] proposed a

modification to the original model by Menegotto and Pinto [1973] by introducing stress shifts to the yield asymptotes in compression and tension. The shift is accomplished by moving the initial (or monotonic) yield asymptote by a stress magnitude, σ_{st}, parallel to its direction (Figure 2.24), based on the maximum plastic strain experienced.

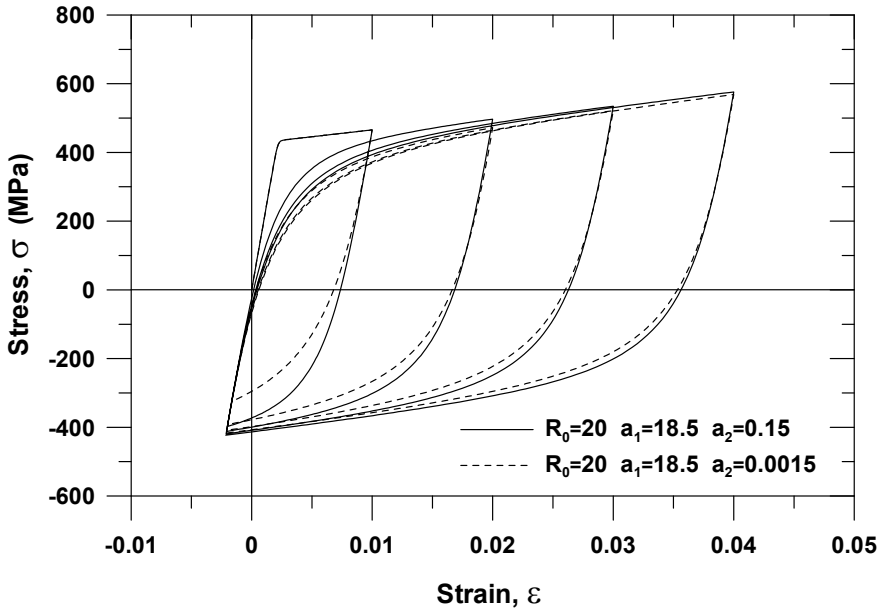

Figure 2.23 Sensitivity of the stress–strain relationship to cyclic curvature parameters.

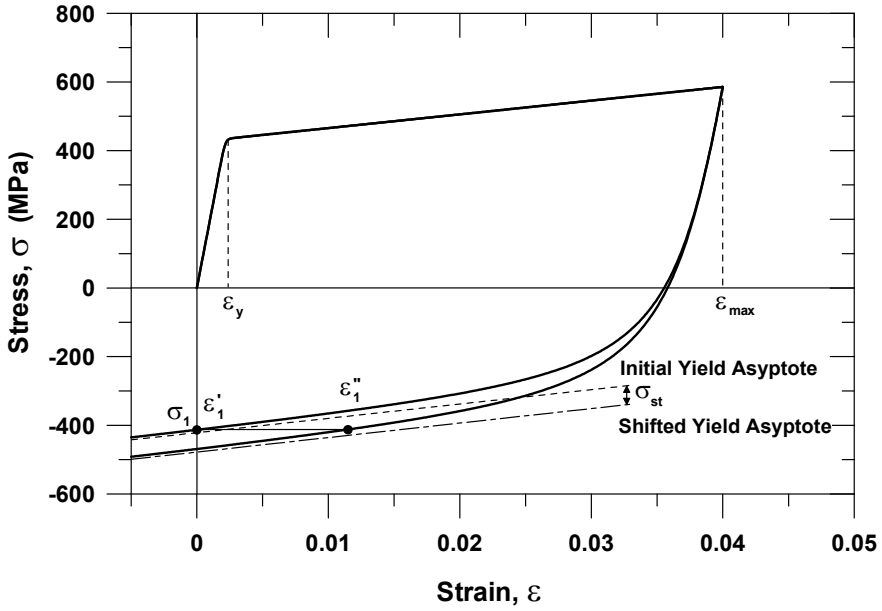

Figure 2.24 Stress shift due to isotropic strain hardening.

Based on test results, Filippou et al. [1983] calibrated the parameter values as follows: $R_0 = 20$, $a_1 = 18.5$, $a_2 = 0.15$, $a_3 = 0.01$, and $a_4 = 7.0$, where the values for the first three parameters were previously suggested by Menegotto and Pinto [1973], and parameters a_3 and a_4 are related to isotropic strain hardening. The modification proposed by Filippou et al. [1983] to the hysteretic model of Menegotto and Pinto was implemented in the present model formulation to account for the isotropic strain hardening effects on reinforcing bars. The isotropic strain hardening parameters can be defined separately for compression and tension, allowing flexibility in description of the hardening behavior. Input parameters for the present model implemented in OpenSees are presented in Appendix A.5.

Although the Menegotto-Pinto [1973] model formulation extended by Filippou et al. [1983] is already available in OpenSees (e.g., *Steel02*), the present model formulation implemented in OpenSees brings several distinctive features compared to the existing models. For example, the implemented model allows definition of different yield stress and strain hardening ratios for compression and tension, which allows consideration of tension stiffening effects on the tensile stress–strain behavior of reinforcing bars embedded in concrete. As well, the implemented model considers degradation of the cyclic curvature parameter *R* for strain reversals in both pre- and post-yielding regions of the hysteretic stress–strain behavior, which may provide more accurate predictions of the yield capacity of RC structural members under cyclic loading (see Section 3.2.1), whereas *Steel02* considers the cyclic curvature degradation after formation of post-yield strains only. Figure 2.25 compares strain–stress relationships obtained using model implemented in this study (*SteelMPF*) and the existing OpenSees model (*Steel02*) for a strain history that includes strain reversals at strain values equal to one-half of the yield strain (i.e., $\varepsilon_r = \pm 0.001 = \varepsilon_y/2$).

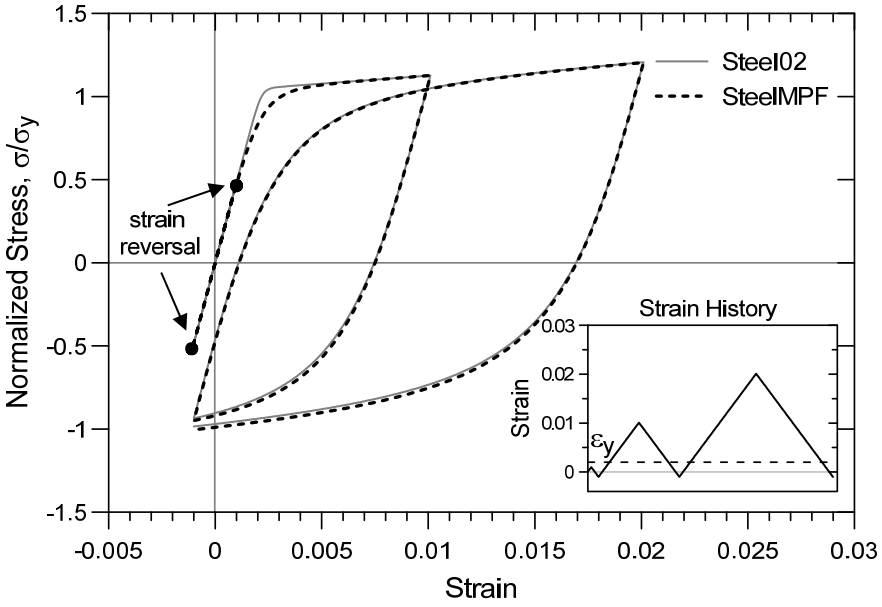

Figure 2.25 Comparing the degradation of cyclic curvature in the pre-yielding region for *Steel02* and *SteelMPF*.

Furthermore, it has been observed from the strain–stress relationships obtained from quasi-static or dynamic analyses using existing steel models in OpenSees (e.g., *Steel02*) that after partial unloading occurs in a model element caused by dynamic loading or stress re-distribution under quasi-static loading due to concrete cracking or crushing, the Menegotto-Pinto formulation produces stress overshooting in the cyclic stress–strain behavior of reinforcing steel. This overshooting effect is not behavioral and causes non-physical hardening in the stress–strain behavior upon reloading from the partial unloading loop. This phenomenon is illustrated in Figure 2.26 for the *Steel02* model in OpenSees. This anomaly results in overestimation of steel stresses predicted by the *Steel02* model upon return from partial unloading, yielding strain–stress curves that may not represent the physical constitutive behavior of reinforcing steel under cyclic loading. This limitation in the Menegotto-Pinto model formulation has also been acknowledged by Filippou et al. [1983] as well as other researchers (e.g., Kunnath et al. [2009]).

The overshooting effect observed in the existing OpenSees material model for reinforcing steel (*Steel02*) has been remedied in the new reinforcing steel constitutive relationship developed and implemented as a part of this study (*SteelMPF*), via manipulating the model formulation so that reloading behavior after partial unloading cannot overshoot the previous loading loop in the cyclic stress–strain behavior. The comparison between strain–stress relationships obtained using the material model implemented in this study (*SteelMPF*) and the existing OpenSees model (*Steel02*) for a strain history that includes low-amplitude unloading followed by reloading is presented in Figure 2.26.

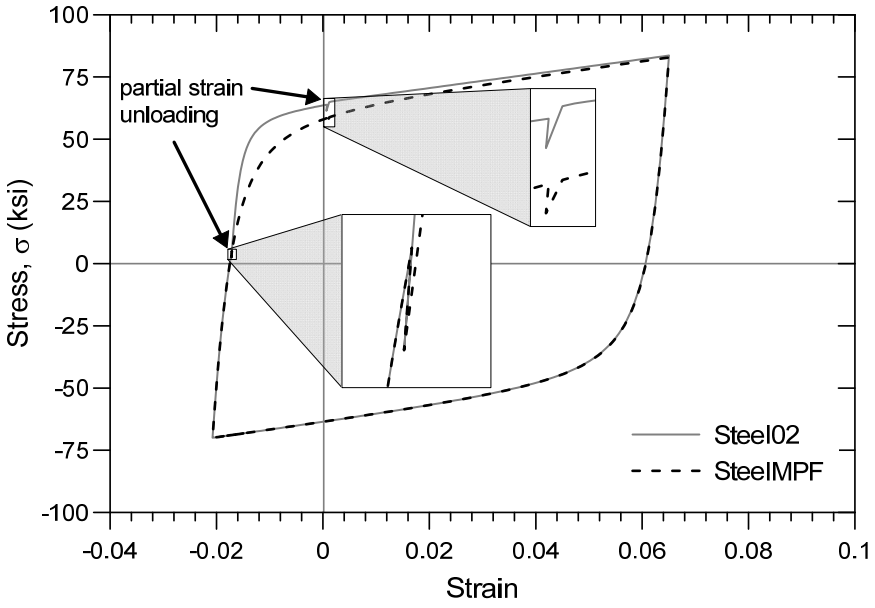

Figure 2.26 Comparing the stress overshooting upon reloading from low-amplitude unloading for *Steel02* and *SteelMPF*.

2.5 OPENSEES IMPLEMENTATION

Analytical model formulations described in this chapter, along with the uniaxial material models for reinforcing steel and concrete and the biaxial constitutive model for RC panel elements, have been implemented into the computational platform OpenSees for nonlinear analysis of RC structural walls and columns. The following new classes were added to the existing OpenSees library, as illustrated in Figure 2.27:

- Element *MVLEM*: macroscopic element with uncoupled flexural and shear behavior
- Element *SFI_MVLEM:* macroscopic element with shear-flexure interaction
- *nDMaterial FSAM*: plane-stress RC panel constitutive behavior
- *uniaxialMaterial ConcreteCM*: uniaxial material model for concrete
- *uniaxialMaterial SteelMPF*: uniaxial material model for steel

Given the research objectives, OpenSees implementation of new model elements and material models included not only development of computer codes, but also generation of detailed user manuals for new OpenSees classes (Appendix A), examples of model applications to analysis of RC structural walls, columns, and building systems (Chapter 3), and corresponding input files used to generate results for selected examples (Appendices B and C). Information regarding the analytical models, user manuals and input files are also available on the OpenSees Wiki page (Table 2.1).

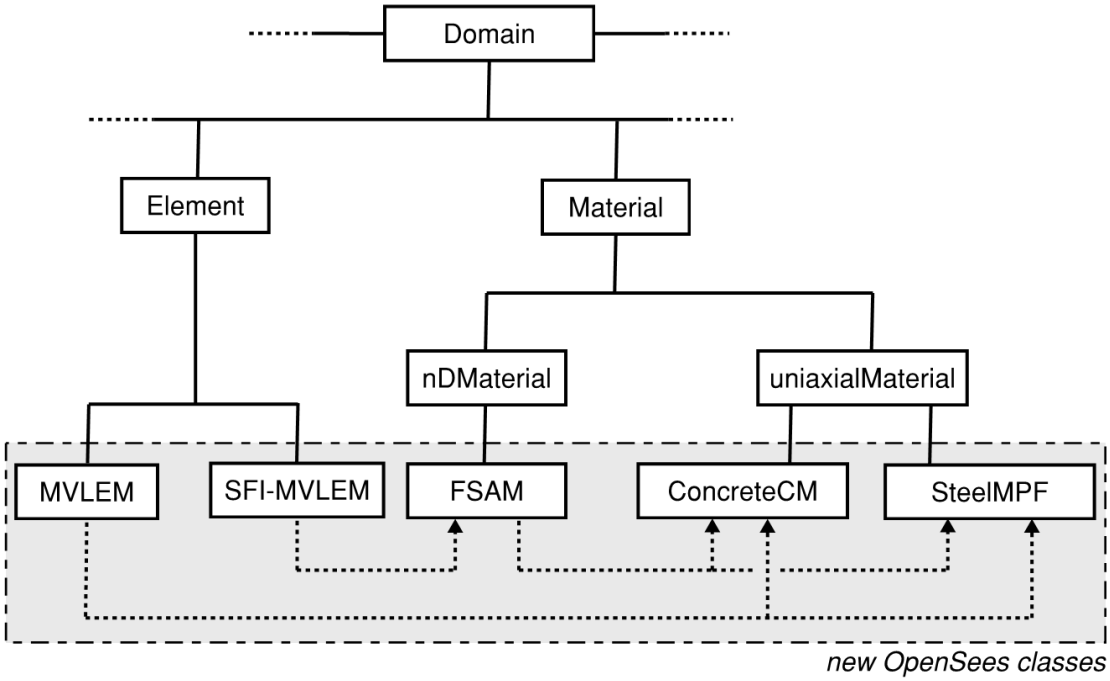

Figure 2.27 OpenSees implementation of *SFI-MVLEM* model.

Table 2.1 Links to OpenSees Wiki pages for implemented models.

OpenSees Class	Link
SteelMPF	http://opensees.berkeley.edu/wiki/index.php/SteelMPF_-_Menegotto_and_Pinto_(1973)_Model_Extended_by_Filippou_et_al._(1983)
ConcreteCM	http://opensees.berkeley.edu/wiki/index.php/ConcreteCM_-_Complete_Concrete_Model_by_Chang_and_Mander_(1994)
FSAM	http://opensees.berkeley.edu/wiki/index.php/FSAM_-_2D_RC_Panel_Constitutive_Behavior
MVLEM	http://opensees.berkeley.edu/wiki/index.php/MVLEM_-_Multiple-Vertical-Line-Element-Model_for_RC_Walls
SFI_MVLEM	http://opensees.berkeley.edu/wiki/index.php/SFI_MVLEM_-_Cyclic_Shear-Flexure_Interaction_Model_for_RC_Walls

3 Examples

This chapter provides examples of applications of the analytical models described in Chapter 2 to displacement-controlled analysis of RC column and wall components, and dynamic analysis of a building system. In particular, Section 3.1 presents applications of the SFI model (*SFI-MVLEM*) to simulation of the cyclic behavior of RC column test specimens with circular and rectangular cross sections, Section 3.2 provides information on applications of the *MVLEM* (uncoupled model) and the SFI-MVLEM to cyclic analysis of RC structural wall specimens. An example that illustrates application of *SFI-MVLEM* to dynamic analysis of a five-story building wall-frame system is provided in Section 3.3. Response comparisons between experimentally measured and analytically predicted load versus deformation responses are presented for all component analyses (Sections 3.1 and 3.2). In addition, Sections 3.2 and 3.3 provide detailed information on the analytically obtained responses at both global (component and model element) and local (RC panel and material) response levels, and references to particular recorders used, to illustrate various output available using the new analytical models implemented in OpenSees.

3.1 CYCLIC ANALYSIS OF REINFORCED CONCRETE COLUMNS

The SFI-MVLEM model implemented in OpenSees was used to simulate the behavior of four RC column specimens selected from the literature [McDaniel 1997; Shanmugam 2009; Priestley and Benzoni 1997; and Lynn et al. 1996] that were tested under constant axial load and a reversed-cyclic lateral displacement history applied at the top. Three of the specimens were scaled models of bridge columns with circular cross sections, and one column specimen represented a building column with a square cross section. Considered test specimens represented a range of column characteristics including shear-span-to-depth ratio (1.5, 2.0, 3.0, and 3.2), horizontal and vertical reinforcing ratios (low to moderate), axial load levels (from 0% to 7% of $A_g f_c'$) and failure modes (flexural, shear, and shear-flexure failure). Important specimen characteristics are summarized in Table 3.1. Three of the four specimens were tested under double curvature, whereas only Specimen #2 (Table 3.1, Shanmugam [2009]) was tested in a single curvature.

Analytical models of column specimens were generated in OpenSees using the *SFI-MVLEM* model elements. The specimens were discretized with a number of model elements along the height of the column (n) such that height-to-width ratio of each model element is approximately between 0.5 and 1.0, and a number of RC macro-fibers along the column cross section (m) based on the number and locations of vertical reinforcing bars.

Figure 3.1 illustrates typical discretization of specimen geometry for a circular column specimen (Specimen #3; Table 3.1, Priestley and Benzoni [1996]) with eight elements along the height (n = 8) and eleven macro-fibers (m = 11) used to represent the column cross section [Figure 3.1(a)], as well as for a rectangular column specimen (2CLH18, Lynn et al. [1996]) with seven elements along the height (n = 7) and seven macro-fibers (m = 7) used to represent the column cross section; see Figure 3.1(b). Discretization of the model for other column specimens considered in this study was performed in a similar manner. The reinforcing ratio in vertical direction for each macro-fiber (RC panel) was obtained based on the areas of vertical reinforcing bars and concrete within the macro-fiber; the reinforcing ratio in horizontal direction was obtained based on the area of transverse reinforcement provided within the model element multiplied by the cosine of the angle between the orientation of the horizontal reinforcement and the direction of loading [e.g., E-W, Figure 3.1(a)]. Uniaxial material models for concrete and reinforcing steel were calibrated to match as-tested material properties. If applicable, concrete compressive strength was increased due to effect of confinement based on provided transverse reinforcement using the confinement model proposed by Mander et al. [1988]. Finally, axial load and lateral displacement history matching test conditions were applied at the top node of the analytical models. For illustration purposes, the input file used to generate the analytical model of specimen H/D(3)-T/M(0.0)/1.32% [Shanmugam 2009] is provided in Appendix B.1; the input files used to perform gravity and lateral analysis are available in Appendices B.4 and B.5, respectively.

Table 3.1 Properties of considered column test specimens.

Spec.	Size (in.)	Height (in.)	Span to depth ratio	Vertical reinf.	Vertical reinf. fatio	Horiz. reinf.	Horiz. reinf. fatio	f_y (ksi)	f'_c (ksi)	Axial load (kips)	Axial load ratio	Failure type
1.	ϕ 24	96	2.0	20 - #5	0.0136	1.6*mm*@4	0.0013	65.8	4.32	4.23	0.002	Shear
2.	ϕ 24	72	3.0	12 - #8	0.0210	#4@2.75	0.0132	65.4	3.74	133	0.070	Flex.
3.	ϕ 24	72	1.5	24 - #4	0.0104	#2@5	0.0017	67.0	4.36	113	0.057	Flex-Sh
4.	18×18	116	3.2	8 - #8	0.0194	#3@18	0.0007	48.0	4.80	113	0.073	Flex-Sh

1. S1, McDaniel [1997]
2. H/D(3)-T/M(0.0)/1.32%, Shanmugam [2009]
3. Column #2, Priestley and Benzoni [1997]
4. 2CLH18, Lynn et al. [1996]

Figure 3.2 compares the experimentally measured and analytically predicted lateral load versus deformation response for the test specimens considered. Note that the analytical model predicts reasonably well the lateral strength under reversed-cyclic loading and the pinching characteristics of the load-deformation response for all four specimens; lateral strength is underestimated by approximately 5% at small and intermediate drift levels for Specimen#2 [Shanmugam 2009] and at most of the drift levels in the positive loading direction for Specimen #3 [Priestley and Benzoni 1997]. Initial stiffness of column Specimens #1 and #3 is captured reasonably well, whereas for Specimens #2 and #4 it is slightly overestimated. Loading and unloading stiffness is reasonably well-predicted by the analytical model for Specimens #1, #2, and #4, whereas the *SFI-MVLEM* model predicts generally higher unloading stiffness than observed in the experimental results for Specimen #3, resulting in modestly larger hysteretic loops and residual displacements (corresponding to zero lateral load) predicted by the model. Although the experimentally measured load-deformation behavior of the specimens is generally predicted reasonably well by the *SFI-MVLEM*, including their lateral load capacity, cyclic stiffness degradation, and pinching characteristics of the response, strength loss observed in the experiments due to flexure, shear-flexure or shear failure was not captured in the analytical results. This model's shortcoming is mainly associated with the inability of the proposed modeling approach to represent strength degradation mechanisms, such as buckling of reinforcing bars observed in specimen tested by Shanmugam [2009], or shear failure, due to the simplified shear-resisting mechanisms across the cracks implemented in the model formulation, which typically leads to overestimation of the column drift capacity. Future studies will focus on model improvements to address these issues.

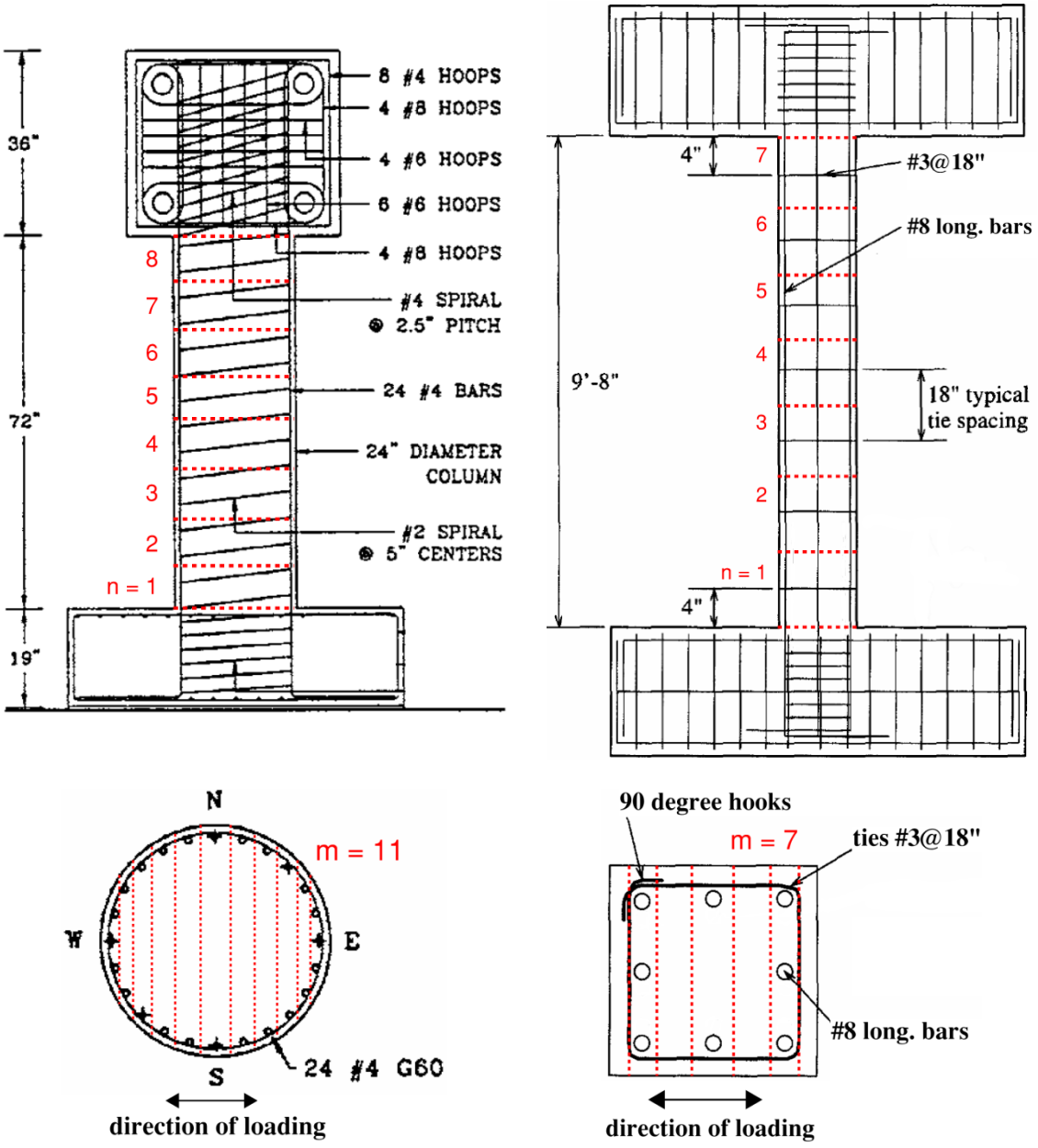

Figure 3.1 **Reinforcement and model discretization of: (a) Specimen #2 [Priestley and Benzoni 1996]; and (b) Specimen 2CLH18 [Lynn et al. 1996].**

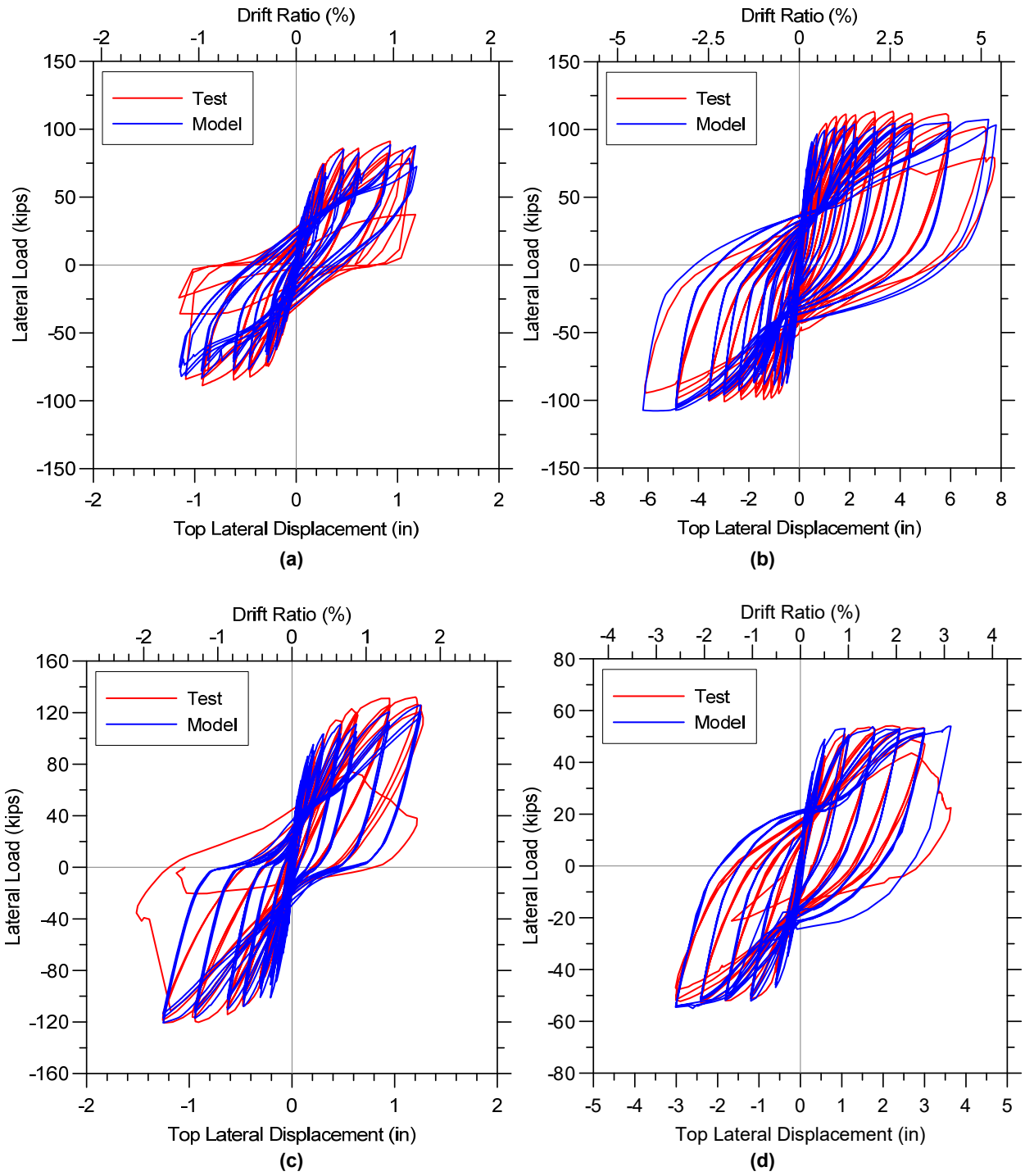

Figure 3.2 **Measured and predicted lateral load versus top displacement response: (a) Specimen S1 [McDaniel 1997]; (b) Specimen H/D(3)-T/M(0.0)/1.32% [Shanmugam 2009]; (c) Specimen Column #2 [Priestley and Benzoni 1997]; and (d) Specimen 2CLH18 [Lynn et al. 1996].**

3.2 CYCLIC ANALYSIS OF REINFORCED CONCRETE WALLS

3.2.1 Simulation of Flexural Behavior using MVLEM Element

Application of the *MVLEM* element to simulate the flexural response of RC walls is illustrated using the wall Specimen RW2 tested by Thomsen and Wallace [1995]. Specimen RW2 was 144 in. tall, 48 in. wide, and 4 in. thick, resulting in aspect ratio of 3.0 (i.e., slender wall). The specimen was subjected to a constant axial load of approximately 7% of wall axial load capacity ($0.07\,A_g f_c'$) and cyclic lateral displacement history applied at the top of the wall. The compressive strength of concrete used for design of the wall specimen was 4.0 ksi; however, concrete compressive strengths at the time of testing ranged from 4.16 ksi to 8.47 ksi, with mean compressive strengths at the base of the wall specimen (0 to 36 in.) of approximately 6.21 ksi. Peak compressive stress was reached for a cylinder compressive strain of approximately 0.002. Longitudinal reinforcement at wall boundaries consisted of eight #3 bars (Grade 60, f_y = 60 ksi), whereas uniformly distributed web reinforcement consisted of two curtains of deformed #2 bars (f_y = 65 ksi), as shown in Figure 3.3. Figure 3.3 also displays model discretization of the RW2 cross section, with eight uniaxial elements defined along the length of the wall. The analytical model was discretized along wall height with 16 *MVLEM* elements with element heights in agreement with instrumentation provided on the specimen to allow for consistent strain comparisons between model and experimental results [Orakcal and Wallace 2006]. The material models for concrete (*ConcreteCM*) and steel (*SteelMPF*) were calibrated to match as-tested material properties. Details on specimen RW2 and the test procedure are provided by Thomsen and Wallace [1995]; detailed information regarding model calibration and experimental validation are presented by Orakcal and Wallace [2006].

Only flexural behavior of the wall was predicted using the *MVLEM*. Therefore, a large shear stiffness was assigned to the model elements, and the experimentally-filtered flexural displacement history was applied at the top of the wall model to compare experimentally measured and analytically predicted flexural responses. Complete input files used to generate the model and perform gravity and lateral (displacement-controlled) analyses are provided in Appendices B.2, B.4, and B.5, respectively.

Figure 3.4 compares the flexural load-deformation responses predicted by the *MVLEM* and measured during the test. As shown in the figure, the analytical model captures reasonably well the experimentally measured wall flexural load-deformation behavior. Cyclic properties of the response, including stiffness degradation, hysteretic shape, plastic (residual) displacements, and pinching behavior are accurately represented in the analytical results; therefore, cyclic characteristics of the implemented stress–strain relationships for steel and concrete are suitable for obtaining accurate global response predictions. The lateral capacity of the wall was predicted very closely for most lateral drift levels. The underestimation of the wall capacity at intermediate drift levels in the negative loading direction (e.g., 0.5 to 1.5% drift) can be attributed to the inability of the yield asymptote in stress–strain model for steel in tension that represents the curved strain-hardening region observed in the stress–strain tests for the #3 longitudinal reinforcing bars, as well as uncertainties in calibration of the cyclic parameters governing the implemented steel stress–strain model (R_0, a_1, and a_2 of *SteelMPF*) and the parameters associated with concrete tensile strength (f_t and ε_t of *ConcreteCM*).

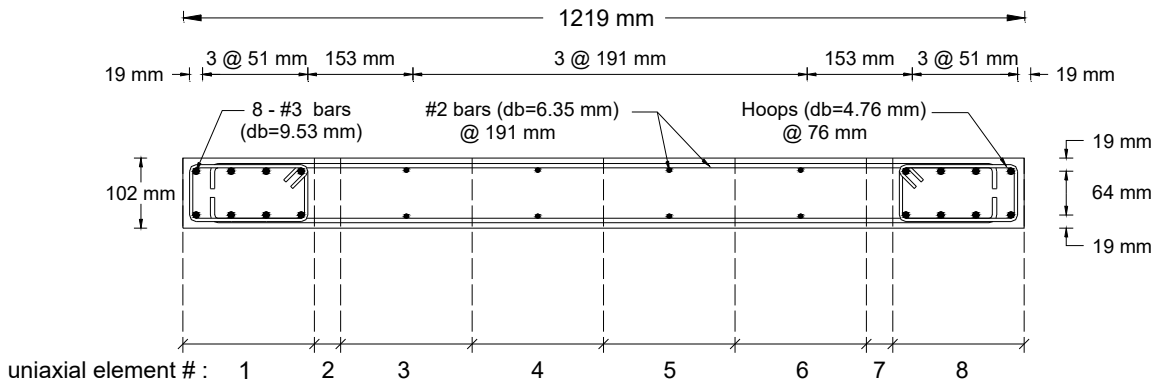

Figure 3.3 Geometry and discretization of wall Specimen RW2.

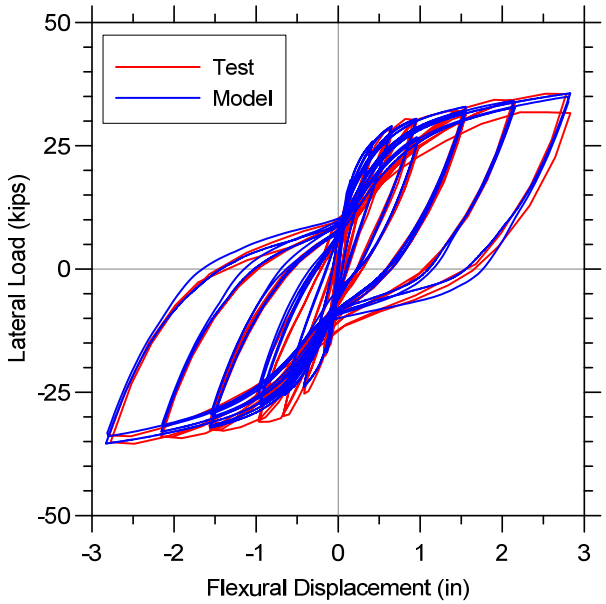

Figure 3.4 Experimental and analytical load versus flexural deformation relationships.

Figure 3.5 illustrates the sensitivity of analytical predictions obtained using the *MVLEM* to the optional gap closure parameter of the *ConcreteCM* model (*-GapClose $gap*, described in Appendix A.1 and Section 2.3), which allows consideration of different intensities of gradual gap closure in concrete [Figure 3.5(a)], as well as selection of the steel material model *SteelMPF* versus *Steel02*; see Figure 3.5(b). Note in Figure 3.5(a) that pinching characteristics of the response are slightly more pronounced when less gradual gap closure versus more gradual gap closure (i.e., *gap*=0 versus *gap*=1) is adopted. Figure 3.5(b) illustrates that the wall yield capacity, as well as pinching characteristics of the behavior predicted by the *MVLEM*, vary slightly when *SteelMPF* versus *Steel02* is used; i.e., using *Steel02* predicts larger yield capacity and more pinching.

For illustration purposes, additional response predictions obtained using the *MVLEM* model are presented in Figure 3.6 and Figure 3.7. Figure 3.6 illustrates analytically predicted

strain histories at the outermost and central wall fibers, whereas concrete and steel strain–stress relationships at the outermost fiber are presented in Figure 3.7. Responses are obtained using *MVLEM* recorders *Fiber_Strain*, *Fiber_Stress_Concrete*, and *Fiber_Stress_Steel* described in *MVLEM* user manual (Appendix A.1).

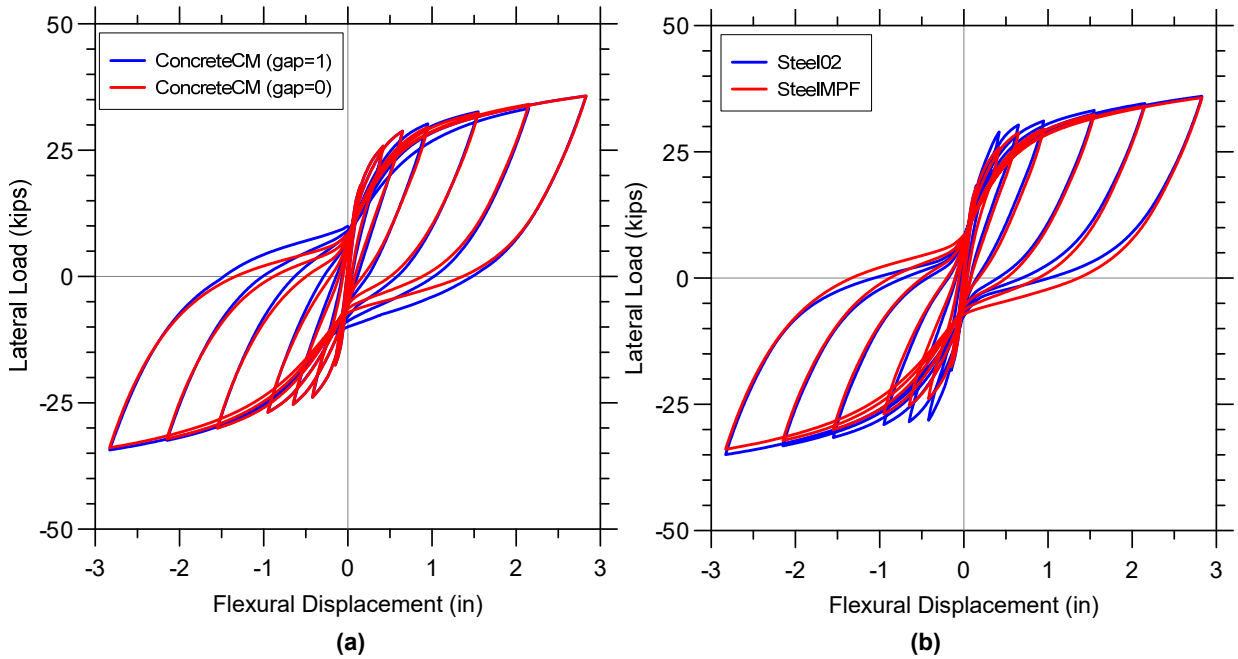

Figure 3.5 Sensitivity to material modeling parameters of (a) concrete and (b) steel.

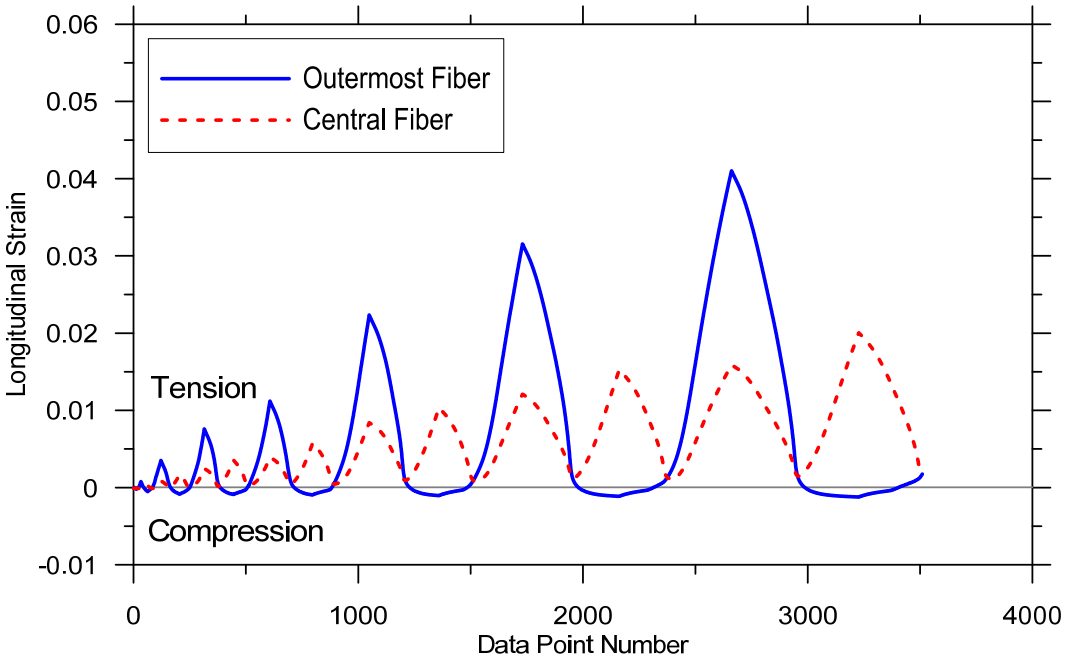

Figure 3.6 Analytical strain histories at outermost and central wall fibers.

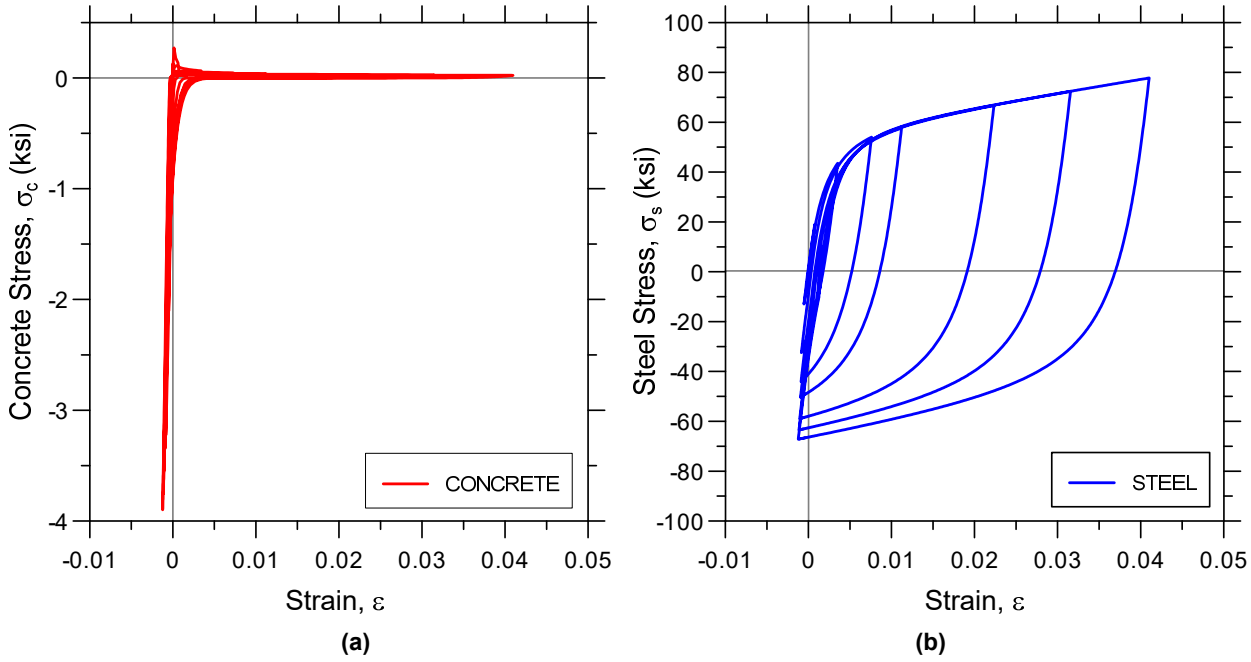

Figure 3.7 **Analytically predicted stress–strain relationships at wall outermost fiber: (a) concrete and (b) steel.**

3.2.2 Simulation of Shear-Flexural Behavior of a Medium-Rise RC Wall Specimen under Cyclic Loading using the *SFI-MVLEM* Model.

As an example of applying the *SFI-MVLEM* to predict the pronounced shear-flexure interaction behavior in medium-rise RC walls, behavior of the RC wall specimen RW-A15-P10-S78 [Tran and Wallace 2012] tested under constant axial load and cyclic lateral displacement history applied at the top of the wall was predicted using the *SFI-MVLEM* model. The specimen was 6 in. thick, 48 in. long, and 72 in. high, which corresponds to an aspect (or shear-span-to-depth) ratio of 1.5 (moderate-aspect-ratio wall). Wall boundary reinforcement consisted of four #5 and four #6 bars with typical A706 Grade 60 material properties; web reinforcement consisted of Grade 60 #3 bars placed at 5 in. spacing in both the vertical and horizontal direction [Figure 3.8(b)]. Concrete peak compressive strength at the time of testing was equal to 8.09 ksi based on a standard cylinder test.

The specimen was subjected to constant axial load of approximately 10% of wall axial capacity. Parameters of the concrete (*ConcreteCM*) and steel (*SteelMPF*) material models were calibrated to match as-tested material properties. Specimen geometry along the height was discretized using five *SFI-MVLEM* elements as shown in Figure 3.8(a), where the bottom two elements, 12 in. high, represented the plastic-hinge region of the wall observed in the experiment. Discretization of the model cross section was performed using five RC panel (macro-fiber) elements, where the outer two fibers represented confined wall boundaries and the three inner fibers represented the unconfined web of the wall [Figure 3.8(b)]. Detailed information about the test specimen can be found in Tran and Wallace [2012]; details on model calibration and validation are provided by Kolozvari [2013] and Kolozvari et al.[2015b]. Complete input files used to generate the analytical model of specimen RW-A15-P10-S78, as well as to apply gravity and lateral load cases, are provided in Appendices B.3, B.4, and B.5, respectively.

Analytically predicted and experimentally obtained lateral load versus top total displacement responses and wall cracking patterns are compared in Figure 3.9; lateral load versus flexural and shear deformations are shown in Figure 3.10. Total top displacement was obtained from the top-node recorder, shear force was recorded using *globalForce* element recorder, total shear displacement was obtained using *shearDef* element recorder, and crack orientations were obtained using *RCPanel* and *cracking_angles* element recorders.

As shown in Figure 3.9(a), the analytical model captured reasonably well the overall load-deformation behavior of Specimen RW-A15-P10-S78, including loading and unloading stiffness, pinching characteristics, and lateral load capacity of the wall in positive loading direction; the wall capacity was slightly underestimated in negative loading direction at intermediate drift levels (between 0.5 and 1.5% drift); it is assumed this was due to same reasons described in the previous section for Specimen RW2. Significant strength degradation observed during the experiment caused by buckling of vertical reinforcing bars in the wall boundary and shear sliding adjacent to wall base was not captured in analytical results because of the model's inability to simulate these strength–loss mechanisms. Figure 3.9(b) reveals that analytically predicted distribution and orientation of cracks agree well with the experimentally recorded cracking pattern, indicating that the assumptions related to cracking criteria and crack orientations in the formulation of the FSAM are reasonable.

As shown in Figure 3.10, the analytical model successfully captured the nonlinear flexural and shear deformations and their coupling throughout the entire cyclic loading history. As demonstrated in both the experimental and analytical results, flexural and shear yielding occurred almost simultaneously for the wall specimen at a lateral load level of approximately 180 kips. In addition, the model successfully reproduced the shapes of the load versus flexural and shear-deformation responses, with the flexural response characterized by minimal pinching and shear behavior characterized by a highly pinched load-deformation response. Although the analytical model captured the flexural stiffness of the wall at all drift levels, shear stiffness was overestimated at drift levels lower than 0.5%. The magnitudes of nonlinear flexural and shear deformation components predicted by the model generally matched the experimentally measured values throughout the cyclic loading history. However, as depicted in Figure 3.10(a), the analytical model underestimated the shear deformations measured during the experiment during the second loading cycle to 3.0% drift in the positive direction because of its inability to capture the shear sliding adjacent to wall base observed during the test, which caused progressively increasing lateral strength degradation. Further information regarding model calibration and validation for this wall specimen, as well as other medium-rise wall specimens, is provided by Kolozvari [2013] and Kolozvari et al. [2015b].

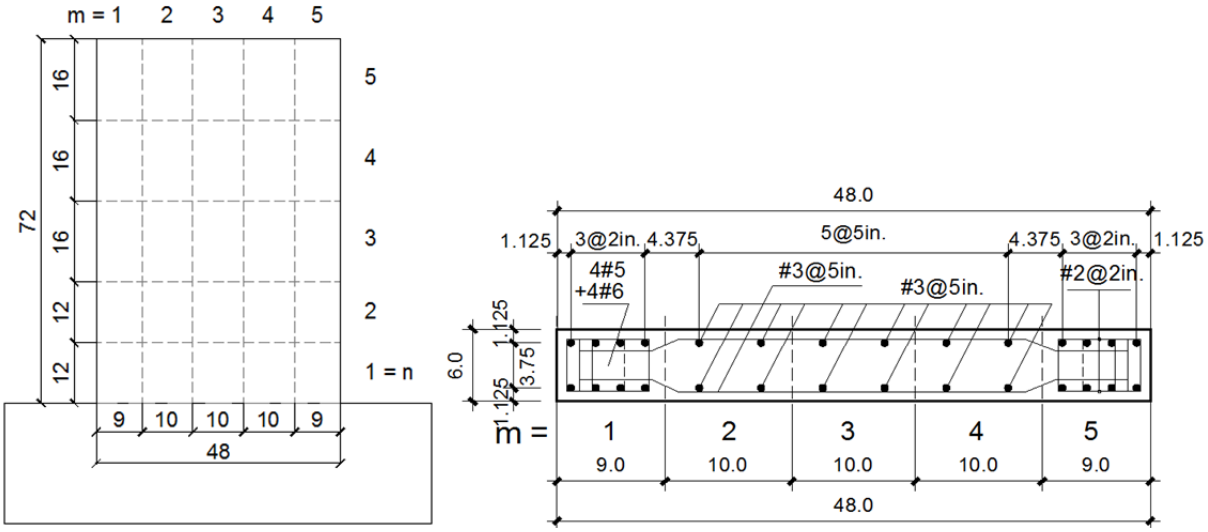

(a) (b)

Figure 3.8 Model discretization: (a) plan view and (b) cross section.

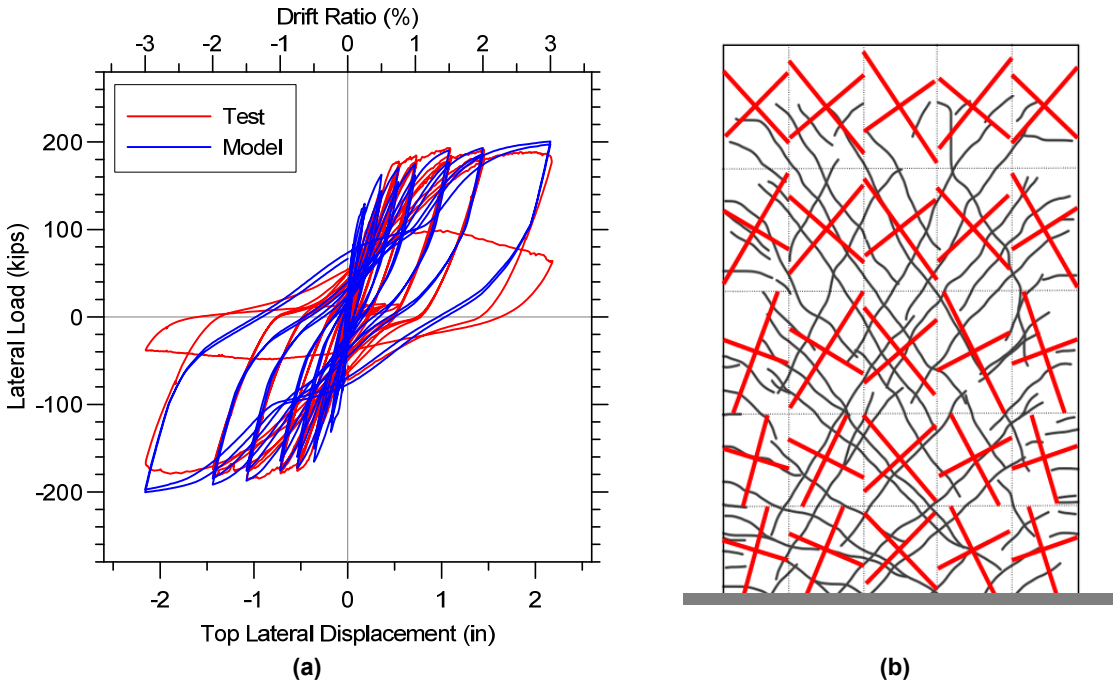

(a) (b)

Figure 3.9 Wall responses: (a) lateral load versus top displacement behavior, and (b) cracking patterns.

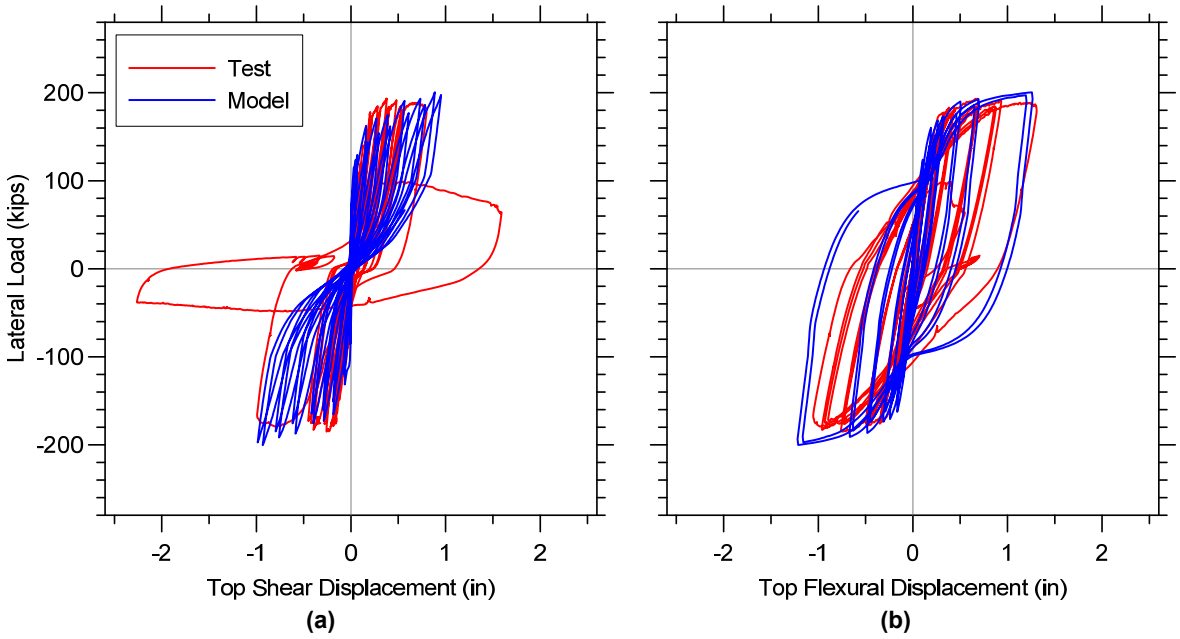

Figure 3.10 Load versus deformation behavior for (a) shear and (b) flexure.

Analytically-predicted wall responses at the model element level and the constitutive RC panel (macro-fiber) level are presented next, with the primary purpose of illustrating possible output available from the analytical model formulation implemented in OpenSees. In addition to various responses presented, references to corresponding recorders adopted for the new element and material models are provided. Figure 3.11 plots analytically predicted lateral load versus total, flexural, and shear-displacement responses, as well as moment versus curvature response for the bottom wall model element. Lateral force was recorded using *globalForce* element recorder, shear deformation was obtained using *ShearDef* element recorder, and element curvature was recorded using *Curvature* element recorder (see Appendix A.2 for available output from the *SFI-MVLEM* element and Appendix B.3 for the input file).

Figure 3.12 plots strain versus total (resultant from concrete and steel, smeared on concrete) stress relationships in the *x*–*y* plane for a single RC panel (macro-fiber) located at the wall boundary in the bottom wall element, including both axial and shear components of the strain–stress field. Strain and stress fields for a single panel were obtained using *RCPanel* element recorders, and *panel_strain* and *panel_stress* commands. Note that one inherent assumption of the *SFI-MVLEM* is that the resultant horizontal stress associated with steel and concrete (i.e., resultant smeared stress σ_x) along the length of the wall is equal to zero, as described in Section 2.1.2.1; therefore, axial stresses in horizontal direction shown on Figure 3.12(a) represent the computational error tolerance.

Figure 3.13 presents the strain–stress relationships along two inclined concrete struts for the outermost RC panel (fiber) of the bottom wall element, the orientations of which correspond to direction of principle strains at the instance of cracking. The responses were obtained using element *RCPanel* recorders with *strain_stress_concrete1* and *strain_stress_concrete2* commands. In addition, analytically predicted strain–stress relationships for horizontal and vertical steel reinforcement for the same macro-fiber are shown in Figure 3.14. Reinforcing steel

responses were recorded using element *RCPanel* recorders, and *strain_stress_steelX* and *strain_stress_steelY* commands. Available RC panel (macro-fiber) output from the FSAM constitutive model and corresponding commands are described in Appendix A.3; the input file used to generate the recorders is provided in Appendix B.3.

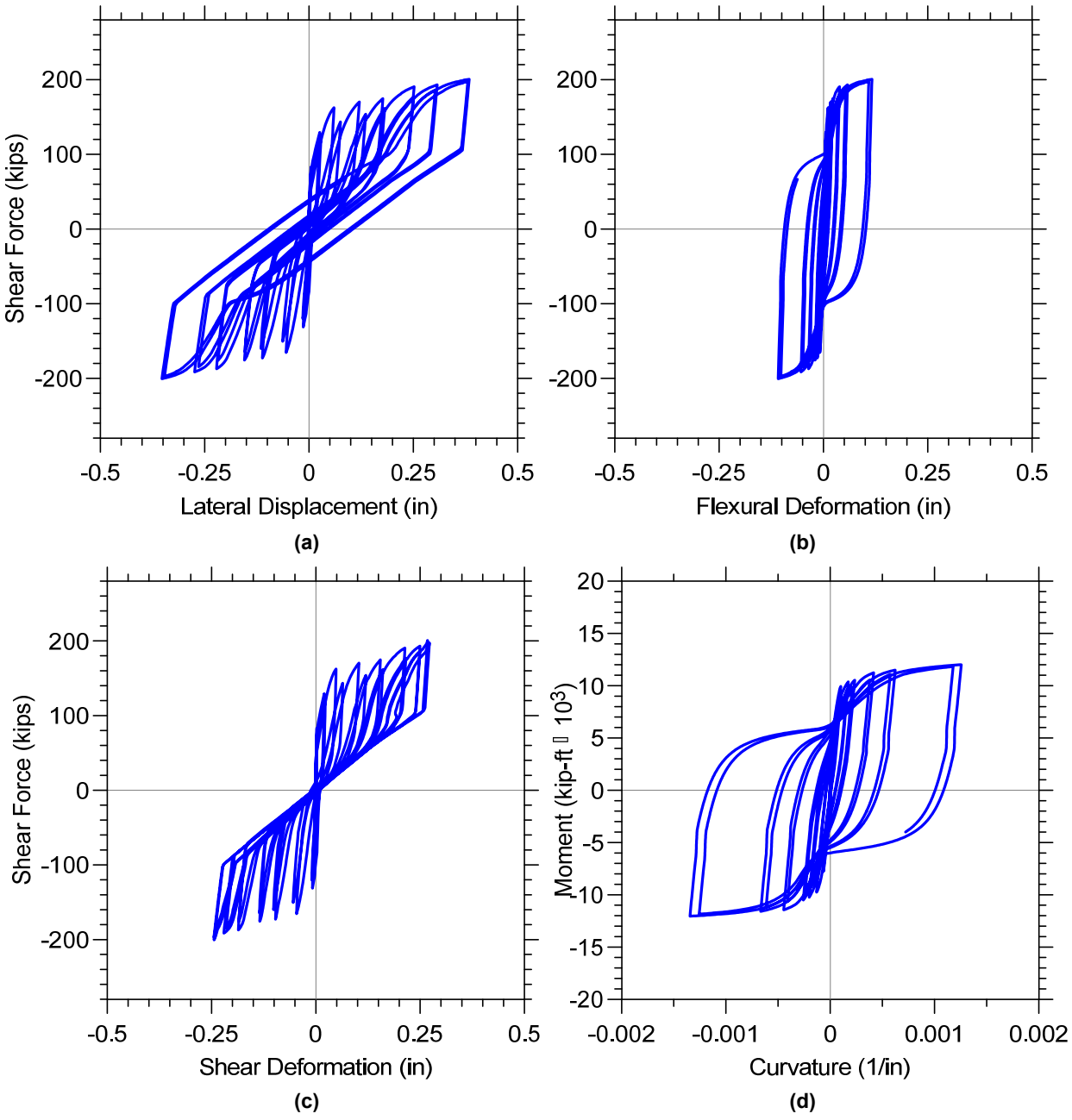

Figure 3.11 **Model element responses: (a) force versus total deformation; (b) force versus flexural deformation; (c) force versus shear deformation; and (d) moment versus curvature.**

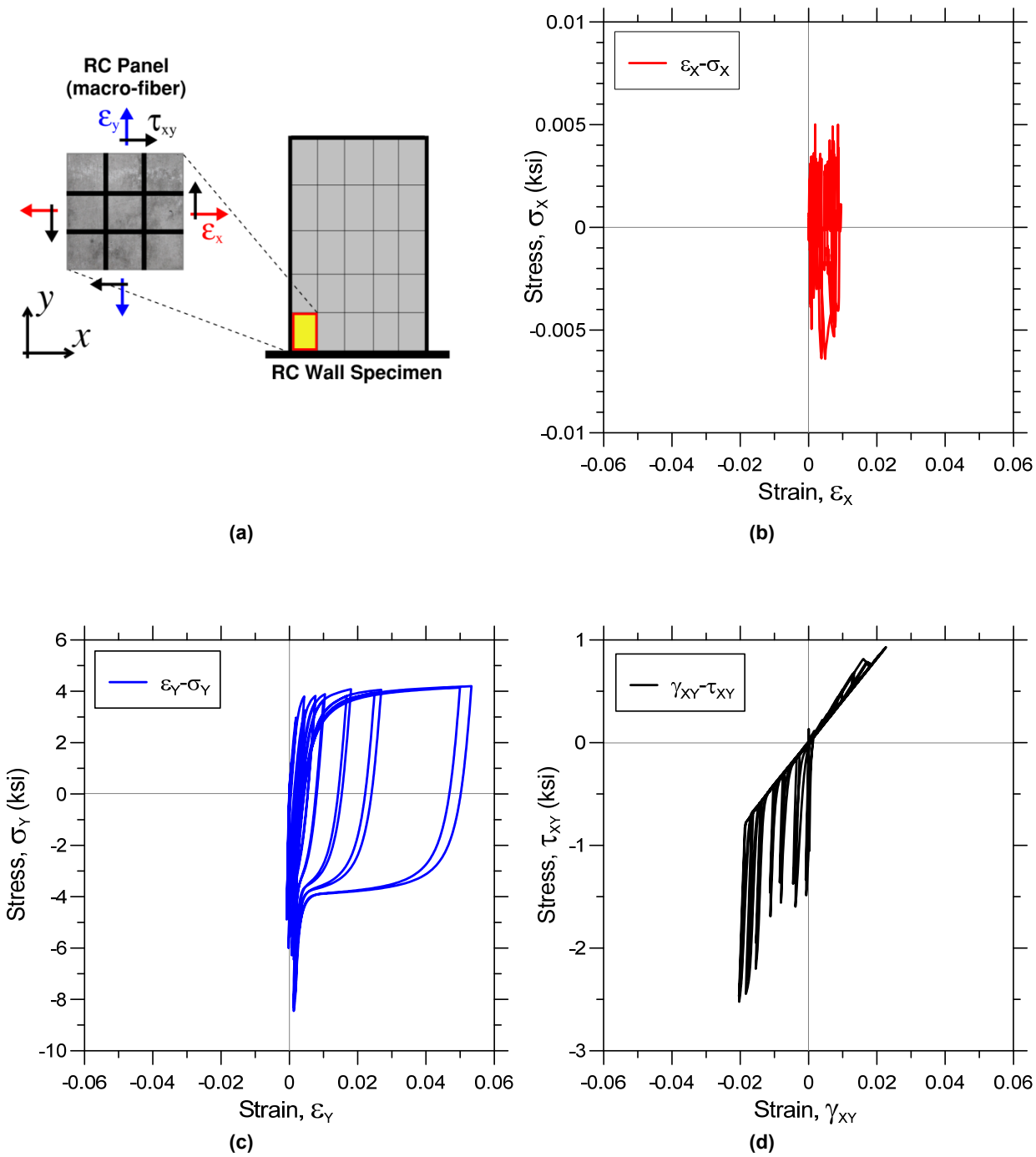

Figure 3.12 **Reinforced concrete panel resultant stress versus strain responses: (a) considered RC panel; (b) axial-horizontal; (c) axial-vertical; and (d) shear.**

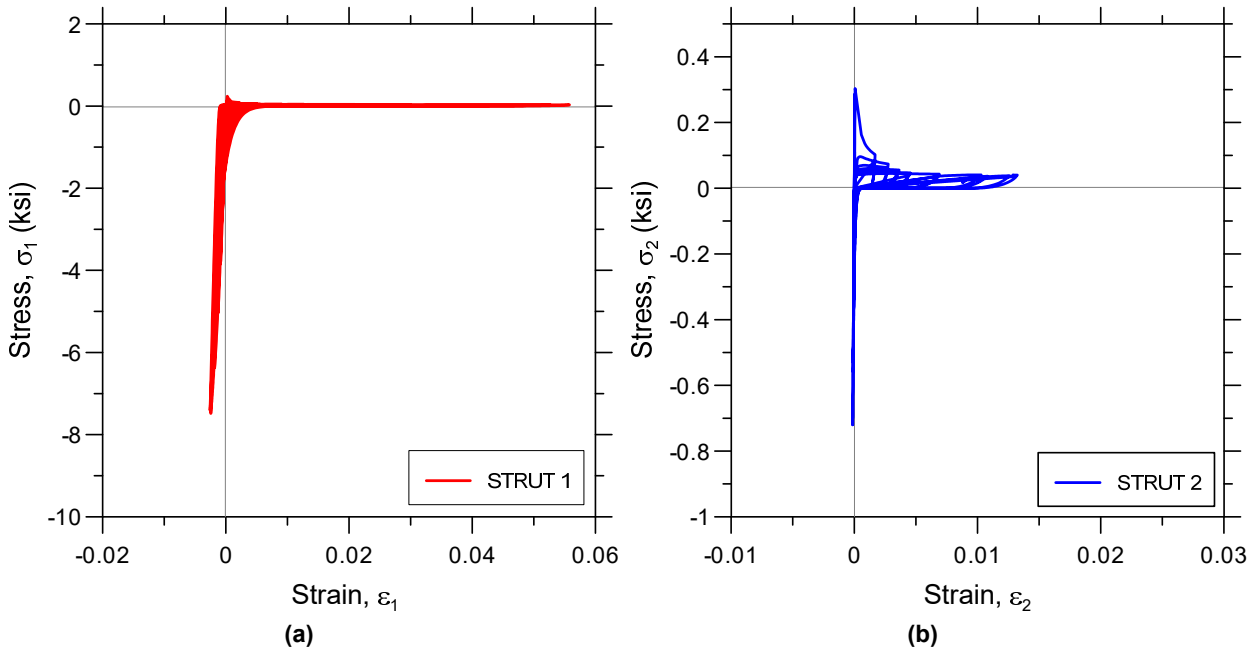

Figure 3.13 **Predicted stress–strain behavior for concrete: (a) Strut 1 and (b) Strut 2.**

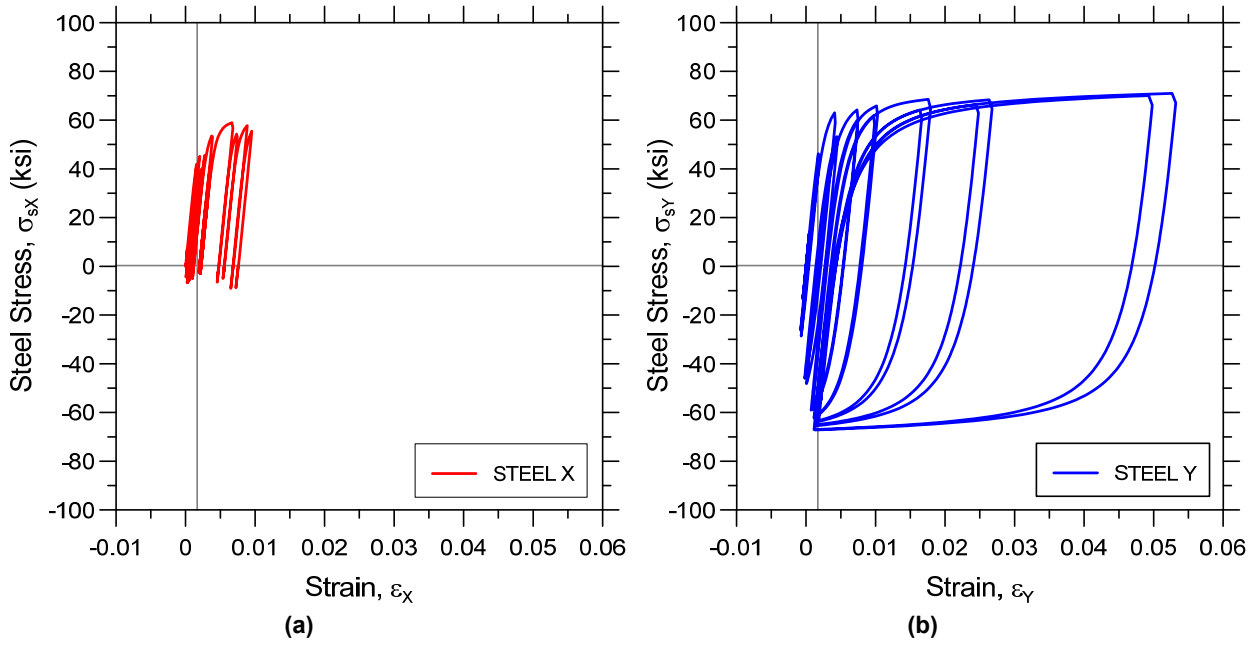

Figure 3.14 **Predicted stress–strain behavior for steel: (a) horizontal (*X*) and (b) vertical (*Y*).**

3.3 DYNAMIC ANALYSIS OF A REINFORCED CONCRETE BUILDING WALL-FRAME SYSTEM

Application of the *SFI-MVLEM* wall model to dynamic analysis of a structural system is illustrated in an example of a five-story building coupled wall-frame system analyzed under a single ground-motion time history. Description of the building characteristics and the analytical model are provided in the following sections.

3.3.1 Building Geometry

Plan and elevation/section views of the archetype building are shown in Figure 3.15. The building footprint is 140 ft × 60 ft, with 20-ft-long spans. Analysis was conducted for shaking in the transverse direction only, where the lateral-force-resisting elements include two identical one-bay frames located along the building perimeter [axes 1 and 8, Figure 3.15(b)] and two identical walls located near the center of the building [axes 4 and 5, Figure 3.15(c)]. An iterative design procedure, outlined in the following section, resulted in cross-sectional dimensions of 12 in. × 240 in. (walls), 18 in. × 32 in. (beams; width × depth), and 28 in. × 28 in. (columns).

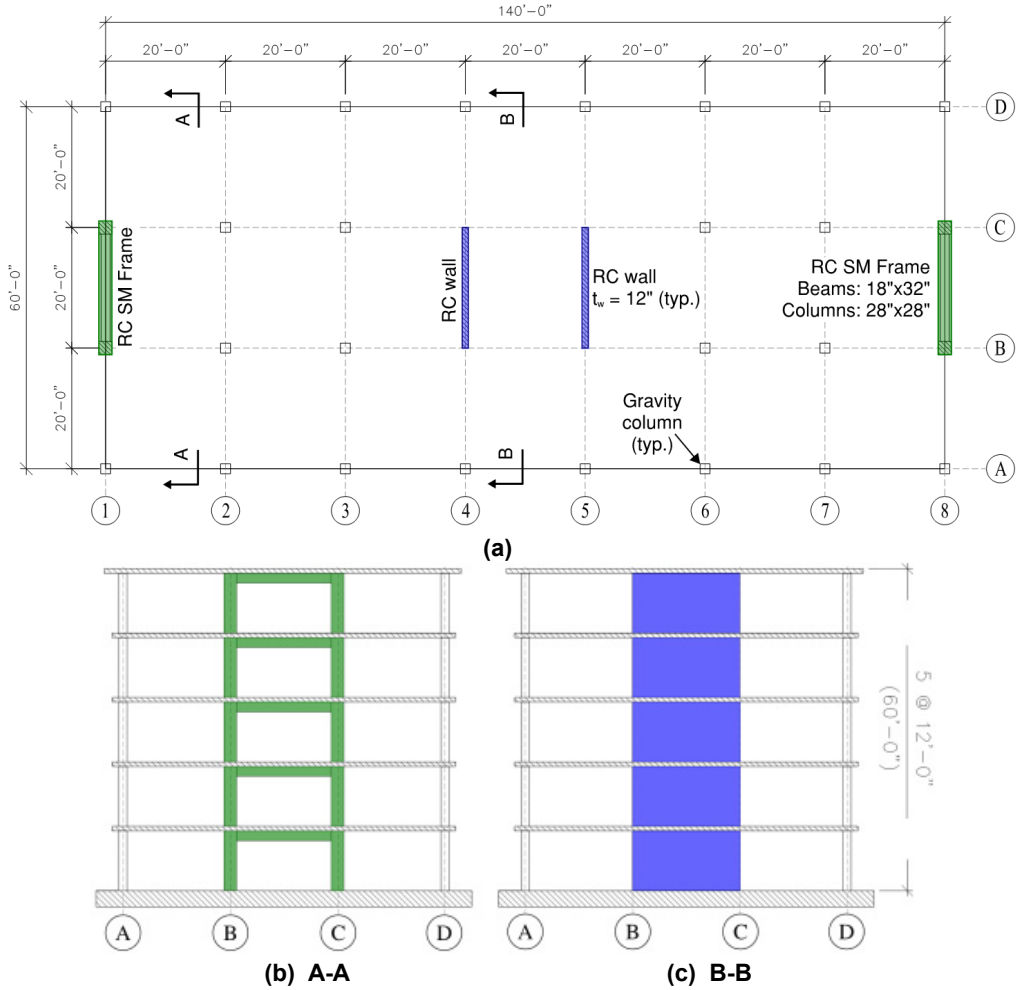

Figure 3.15 Building views: (a) plan view; (b) frame elevation; and (c) wall elevation.

3.3.2 Design Approach

The structural design was performed for a residential building characterized with an importance factor of I = 1.0, risk category I, and design category D, according to ASCE 7-10 S11.5 and S11.6. The frame was designed to resist 25% of the earthquake lateral load, which classifies the building structural system as Dual System according to ASCE 7-10 [2013]. A concrete compressive strength of f_c' = 5.0 ksi and reinforcing steel (both longitudinal and transversal reinforcement) with yield strength f_y = 60.0 ksi were used. Uniformly distributed dead load of 150 psf and live load of 40 psf (ASCE 7-10, Table 4-1, Residential Building) were used for the design, whereas load combinations were adopted according to ASCE 7-10 S2.3. Since only one bay seismic-resisting perimeter frame on each side of the structure was used, which also resists less than 35% of the base shear, the redundancy factor (ASCE 7-10 S12.3.4) was taken as ρ = 1.3.

Seismic lateral loads on the building were calculated using the Equivalent Lateral Force (ELF) procedure (ASCE 7-10, S12.8) based on the code-prescribed spectrum characterized with mapped short-period and 1-sec-period accelerations of S_S =1.5g and S_1 = 0.6g, respectively, assuming Site Class B (F_a = 1.0, F_v = 1.0), and design spectral acceleration parameters of S_{DS} = 1.0g and S_{D1} = 0.6g, which yielded T_0 = 0.12 sec and T_S = 0.6 sec; see Figure 3.18(b). Based on the fundamental period of the building computed according to ASCE 7-10 12.8.2 (T = 0.6 sec), a base shear of $V = C_sW$ = 0.19W = 1200 kips was obtained, where the effective seismic weight of the entire building was W = 6300 kips. Axial demands due to gravity loads on walls and columns were computed based on prescribed dead and live loads (reduced according to ASCE 7-10 S4.7) according to tributary areas for the considered load combinations, whereas axial load due to seismic actions (horizontal and vertical) were computed according to ASCE 7-10 S12.14.3.

Instead of using linear analysis, a simple (and approximate) collapse mechanism approach was used to determine design strength requirements for walls, beams, and columns, using the vertical distribution of seismic lateral forces (ASCE 7-10 S12.8.3). Assumed collapse mechanism of the building structural system included wall and column yielding at the base, and beam yielding at each level (beam negative nominal moment capacity was assumed to be one-half of the positive nominal beam capacity, ACI 318-11 21.5.2.2), as well as strong-column–weak-beam condition at each joint (exterior connection). Determined flexural demands were M_{uW} = 27,760 kip-ft, M_{uB} = 798 kip-ft, and M_{uC} = 479 kip-ft for each wall, and for the beams and columns, respectively.

A detailed assessment of the building was conducted to evaluate whether the design of the lateral load-resisting system, i.e., the walls and frames, satisfied ASCE 7-10 [2013] and ACI 318-11 [2011] provisions. A 20-ft-long and 12-in.-thick structural wall, with sixteen #11 bars located at each boundary [Figure 3.16(a)], satisfied P–M strength requirements and the "stress-based" approach (S21.9.6.3) was used to determine if special boundary elements satisfying S21.9.6.4 were required [Figure 3.16(a)]. Wall shear strength corresponding to minimum horizontal web reinforcing ratio of ρ_t = 0.0025 (#5 bars @ 18 in., α_c = 2.0) of ϕV_n = 629 kips (ACI 318-11, S21.9.4) was sufficient to resist wall-shear demands corresponding to 100% of seismic force (V_u = 1200/2 = 600 kips).

A one-bay five-story frame as shown in Figure 3.16(b) was design to resist 25% of the lateral seismic demand obtained using ELF procedure. Based on axial and flexural demands, a 28 × 28 in. column with twelve #11 bars was adopted along the height of the building [Figure

3.16(b)]; the column P–M strengths satisfy ACI 318-11 (S10.3) requirements. The beam design was characterized by a 18 ×3 two-in. cross section, with seven #9 bars at the top and five #8 bars at the bottom of the beam [Figure 3.16(c)], which was sufficient to resist beam flexural demand and satisfy the requirements of ACI 318-11 S10.5 and S21.5.2. The strong column–weak beam provision of ACI 318-11 S21.6.2 was checked at all floor levels. Beams and columns were assumed to satisfy shear strength requirements of ACI 318-11 S21.5.4 and S21.6.5, respectively, and detailing requirements of S21.5.3 and S21.6.4, respectively. The design of beam–column joints was performed according to ACI 318-11 S21.7 for an exterior connection (ϕ_v = 0.85 and γ_v = 12, S21.7.4), assuming that the beams that frame into beam–column joints would yield prior to the columns. Finally, building lateral displacements computed using linear analysis according to ASCE 7-10 (S12.8.6) yielded story drifts of 0.0035, 0.0091, 0.0126, 0.0144, and 0.0151, which were less than allowable story drift of $0.02h_{sx}/\rho = 1.3 = 0.0154h_{sx}$ (ASCE 7-10, Table 12.12-1).

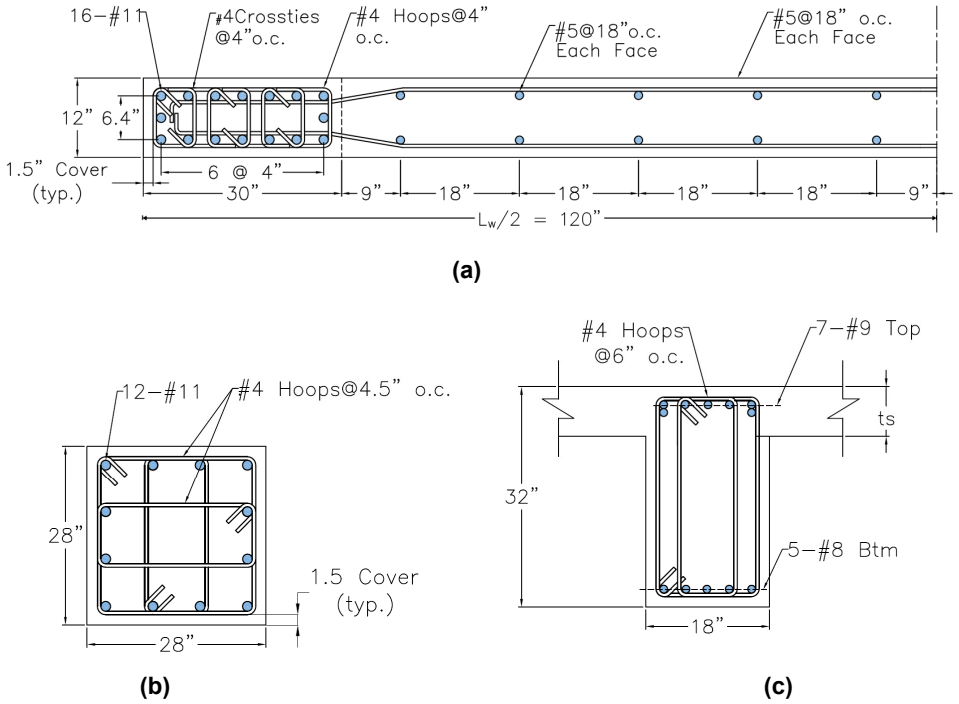

Figure 3.16 Member cross sections: (a) wall, (b) column, and (c) beam.

3.3.3 Analytical Modeling

3.3.3.1 Model Description

The analytical model of the building lateral-load-resisting system was generated in OpenSees [McKenna et al 2000] according to the adopted geometry, cross sections, and material properties of the structural members; see Figure 3.17(a). Based on the symmetry of the building, a 2D model was used, consisting of one frame and one wall; therefore, torsion effects were neglected in the analysis. The gravity system was not included in the model [ASCE 7-10 2013], and the rigid diaphragm assumption was used at each story level. Tributary mass was assigned at the element nodes at each story level at the axis locations of the vertical members (i.e., wall and columns), whereas gravity load (dead and live) was assigned according to corresponding tributary areas as either nodal load at wall-element nodes at each story or uniformly distributed

load along the beams of the frame. OpenSees input files used to generate the model and perform modal and dynamic time-history analyses are provided in Appendix C.

Reinforced concrete frame elements (i.e., beams and columns) were modeled using elastic beam–column elements by assuming the location of plastic hinges to be at the faces of beam–column joints [Figure 3.17(b)]; their behavior was simulated using zero-length elements at hinge locations and the elasto-plastic moment-rotation hysteretic model using the modified Ibarra Krawinkler Deterioration Model [Lignos and Krawinkler 2011], with modeling parameters adopted according to beam and column flexural capacities and the ASCE 41 backbone relationships [Figure 3.17(b)]. The reduction of flexural stiffness after cracking was considered using stiffness modifiers for elastic portions of beam and column elements according to Table 6.5 in ASCE 41. The behavior of the RC walls was simulated using the *SFI-MVLEM* element described in Section 2.1 [Kolozvari et al. 2015a, b]. As show in Figure 3.17(a), the RC wall was modeled using ten equal-length elements along the building height (i.e., two elements per story height). Wall discretization in the horizontal direction was performed using six macro-fibers to represent the wall cross section; two outer macro-fibers were used to represent the confined wall boundaries and the remaining four represent the unconfined wall web.

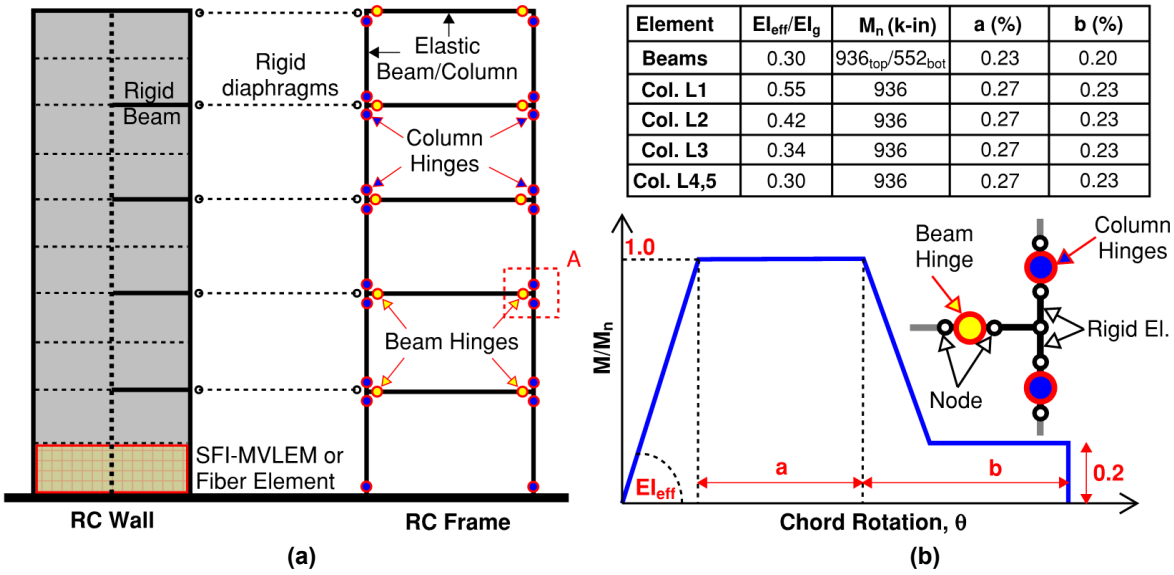

Figure 3.17 Analytical model of building system: (a) modeling approach and (b) plastic hinge model.

3.3.3.2 Material Calibration

Steel stress–strain relationship – The reinforcing steel stress–strain relationship described by the Menegotto and Pinto [1973] model (*Steel02*) was calibrated to represent the typical properties of Grade-60 reinforcing bars. Monotonic parameters used for the calibration of the steel stress–strain relationship are yield strength f_y = 60 ksi and strain hardening ratio b = 0.015. The parameters describing the cyclic stiffness degradation characteristics of the reinforcing bars were calibrated as R_0 = 20, a_1 = 18.5, and a_2 = 0.15, as proposed originally by Menegotto and Pinto [1973].

Concrete stress–strain relationship – In this study the behavior of RC, both confined and unconfined, was simulated using the uniaxial material model proposed by Chang and Mander [1994] and implemented in OpenSees (*ConcreteCM* described in Section 2.3). The monotonic envelope of the stress–strain model for unconfined concrete in compression proposed by Chang and Mander was calibrated to agree with monotonic envelope proposed by Saatcioglu and Razvi [1992], by matching the compressive strength f'_c, the strain at compressive strength ε'_c, initial tangent modulus E_c, and the parameter r defining the shape of the monotonic stress–strain curve. The stress–strain envelopes for confined concrete in compression were obtained by computing the peak stress of confined concrete (f'_{cc}) and the strain at peak stress (ε'_{cc}) based on the area, configuration, spacing, and yield stress of the transverse reinforcement, using the confinement model by Mander et al. [1988]; the initial tangent modulus for confined concrete (E_{cc}) and corresponding shape parameter (r_c) were obtained based on the peak stress of confined concrete (f'_{cc}) using empirical relations proposed by Chang and Mander [1994] (see also Orakcal and Wallace [2006]). The tensile strength of concrete was determined from the relationship $f_t = 0.31\sqrt{f'_c}$ (MPa), and a value of 0.00008 was selected for the strain at the peak monotonic tensile stress ε_t, as suggested by Belarbi and Hsu [1994]. The shape of the monotonic tension envelope of the Chang and Mander [1994] model was calibrated via the parameter r to reasonably represent the average post-crack stress–strain relation proposed by Belarbi and Hsu [1994], which represents tension stiffening effects on concrete. The parameters used for calibrating the stress–strain model for concrete in compression and tension are presented in Table 3.2.

Table 3.2 Concrete material parameters.

Compression			Tension	
Parameter	**Boundary (confined)**	**Web (unconf.)**	**Parameter**	**Confined and unconfined**
f'_c, ksi	7.705	5.00	f_t, ksi	2.13
ε'_c	0.005	0.002	ε_t	0.00008
E_c, ksi	38810	34963	E_c, ksi	34963
x_{cr}^-	1.015	1.03	x_{cr}^+	∞
r	15	13	r	1.2

3.3.3.3 Ground-Motion Record

Nonlinear analysis was performed using a single horizontal ground motion applied in the transverse direction of the building. The ground-motion record was selected from the PEER NGA database, with a peak ground acceleration (PGA) of 0.30*g*; see Figure 3.18(a). The Response spectrum of the selected ground-motion record used in the analysis is shown in Figure 3.18(b), where it is compared with adopted code-design spectrum.

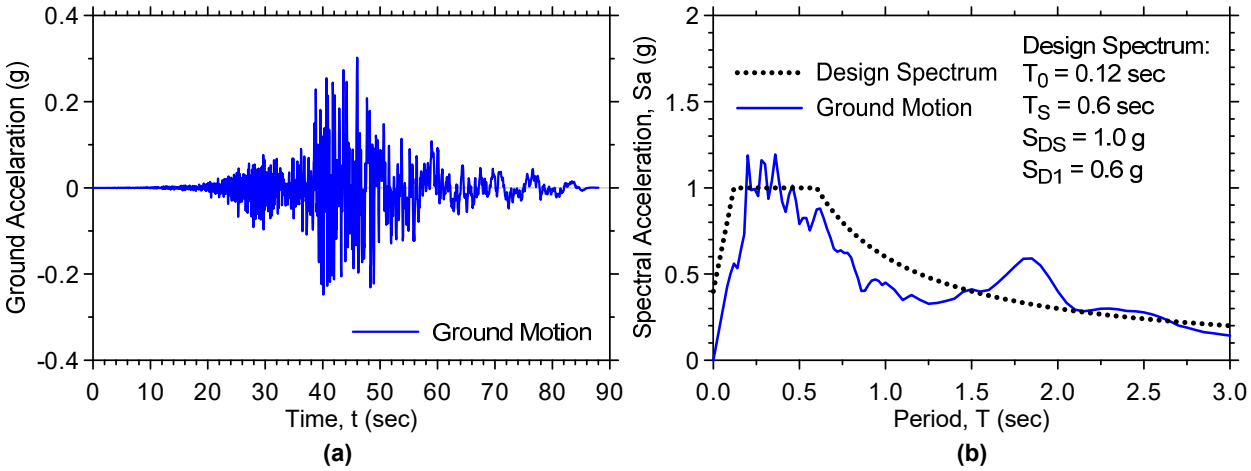

Figure 3.18 Ground-motion data: (a) acceleration time history and (b) response spectra.

3.3.4 Dynamic Analysis Results

Various wall responses obtained from dynamic analysis of the building wall–frame system described above are presented to illustrate available output from the *SFI-MVLEM* element implemented in OpenSees; references to recorders used to generate the results are provided. Analytically obtained wall responses presented in this section include modal properties of the building structure, time histories of wall top displacement and base shear force, wall global responses including vertical profiles (along the height of the wall) of maximum lateral deformations, drifts, shear forces, and bending moments, as well as wall local responses including vertical profiles of maximum and minimum vertical strains and rotations. Additional local wall responses obtained at the model element level are presented, including time histories of force-deformation relationships for the bottom wall element and strain–stress relationships for the outermost RC panel. Responses of the structural elements comprising the RC frame are not considered.

3.3.4.1 Dynamic Properties

First two fundamental periods and mode shapes obtained for the building are presented in Figure 3.19.

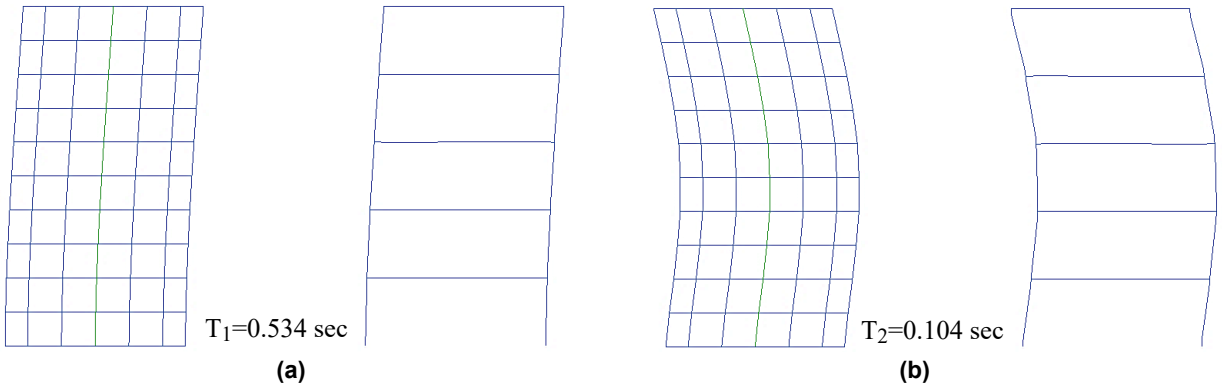

Figure 3.19 Mode shapes: (a) first mode and (b) second mode.

3.3.4.2 Time-History Responses

Time histories of ground-motion acceleration, wall top nodal lateral displacement, and wall-base shear force (force reaction at the wall bottom) are presented in Figure 3.20; the responses were obtained using *globalForce* and *Reactions Node* recorders.

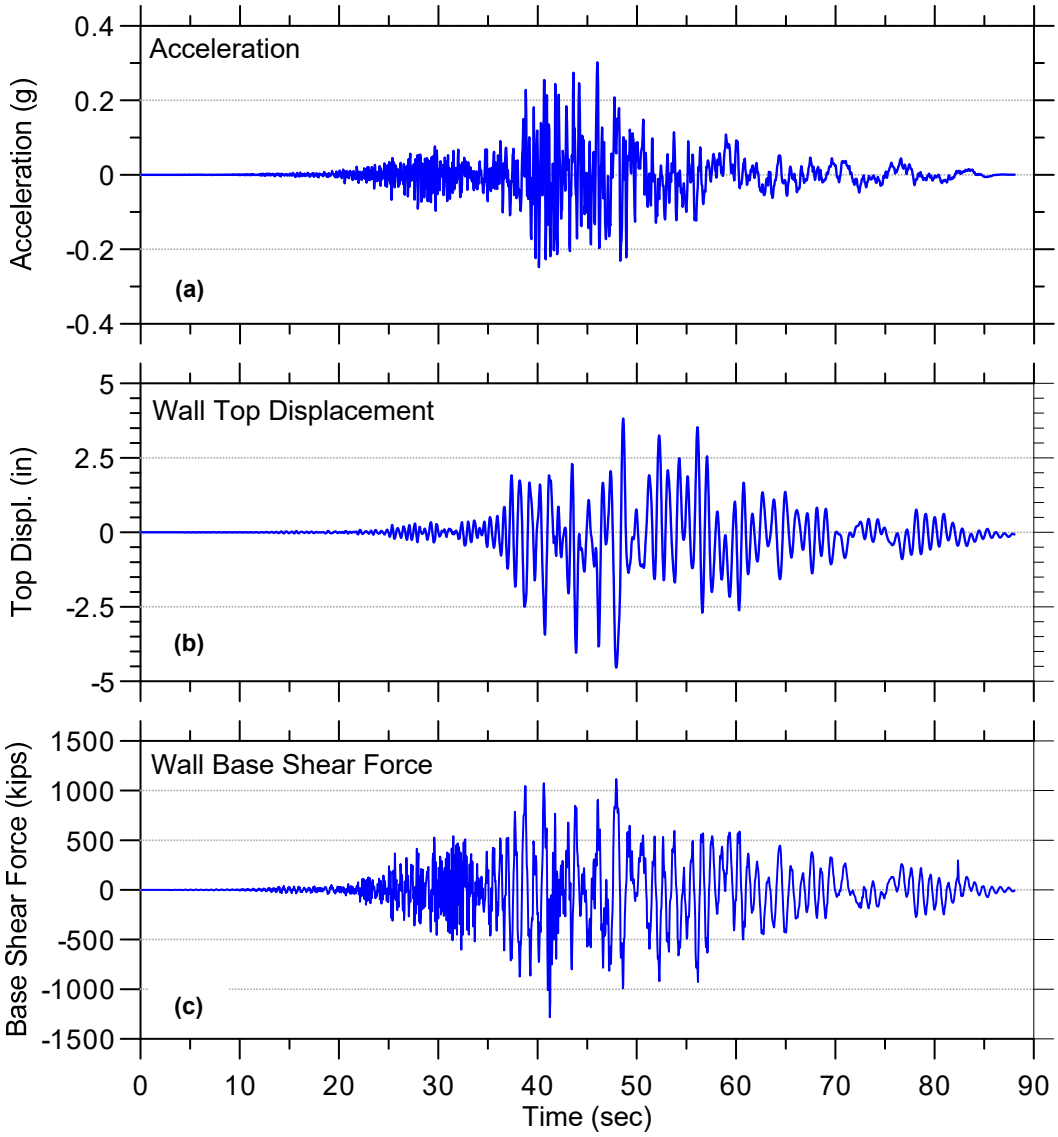

Figure 3.20 Building global responses: (a) acceleration; (b) wall top displacement; and (c) wall-base shear force.

3.3.4.3 Maximum Global Responses over Wall Height

Maximum envelopes of wall lateral displacements and interstory drifts, and shear forces and bending moments are presented in Figure 3.21 and Figure 3.22, respectively. Wall lateral displacements and drifts were obtained using corresponding *Node* recorders (*disp* and *drift*); shear force and bending moments over the wall height were recorded using element recorders *globalForce*.

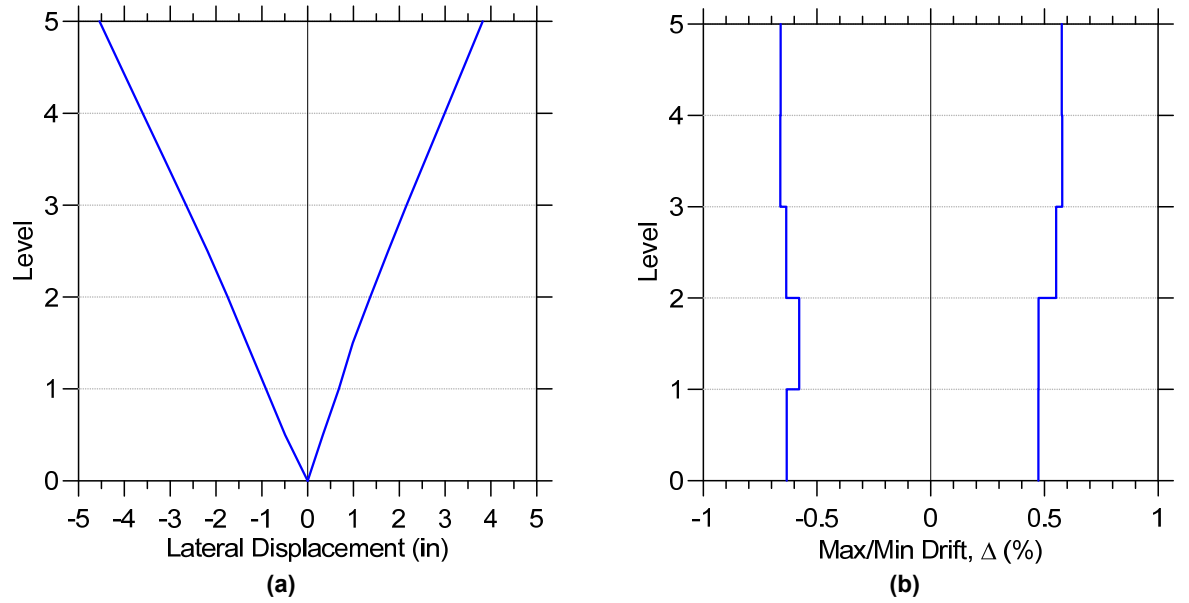

Figure 3.21 **Maximum deformation responses: (a) lateral displacements and (b) interstory drifts.**

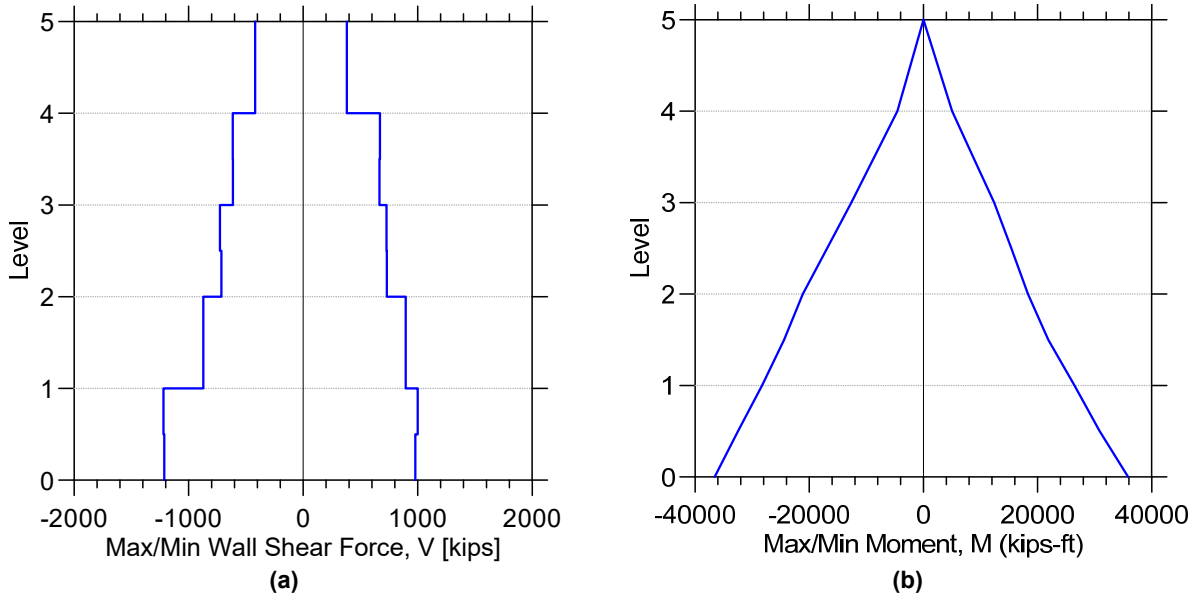

Figure 3.22 **Maximum force responses over wall height: (a) shear force and (b) moment.**

3.3.4.4 Bottom Wall Element Responses

Figure 3.23 plots the responses of the bottom wall element, including lateral load versus total, flexural, and shear displacements, and moment versus curvature relationship obtained from the dynamic analysis. Wall–element shear displacement and curvature time histories were obtained using *SFI_MVLEM* element recorders *ShearDef* and *Curvature*, respectively; shear forces and bending moments were recorded using element recorder *globalForce* (see Appendix A.2 for available output from the *SFI-MVLEM* element; input file is provided in Appendix C.1 for recorder generation).

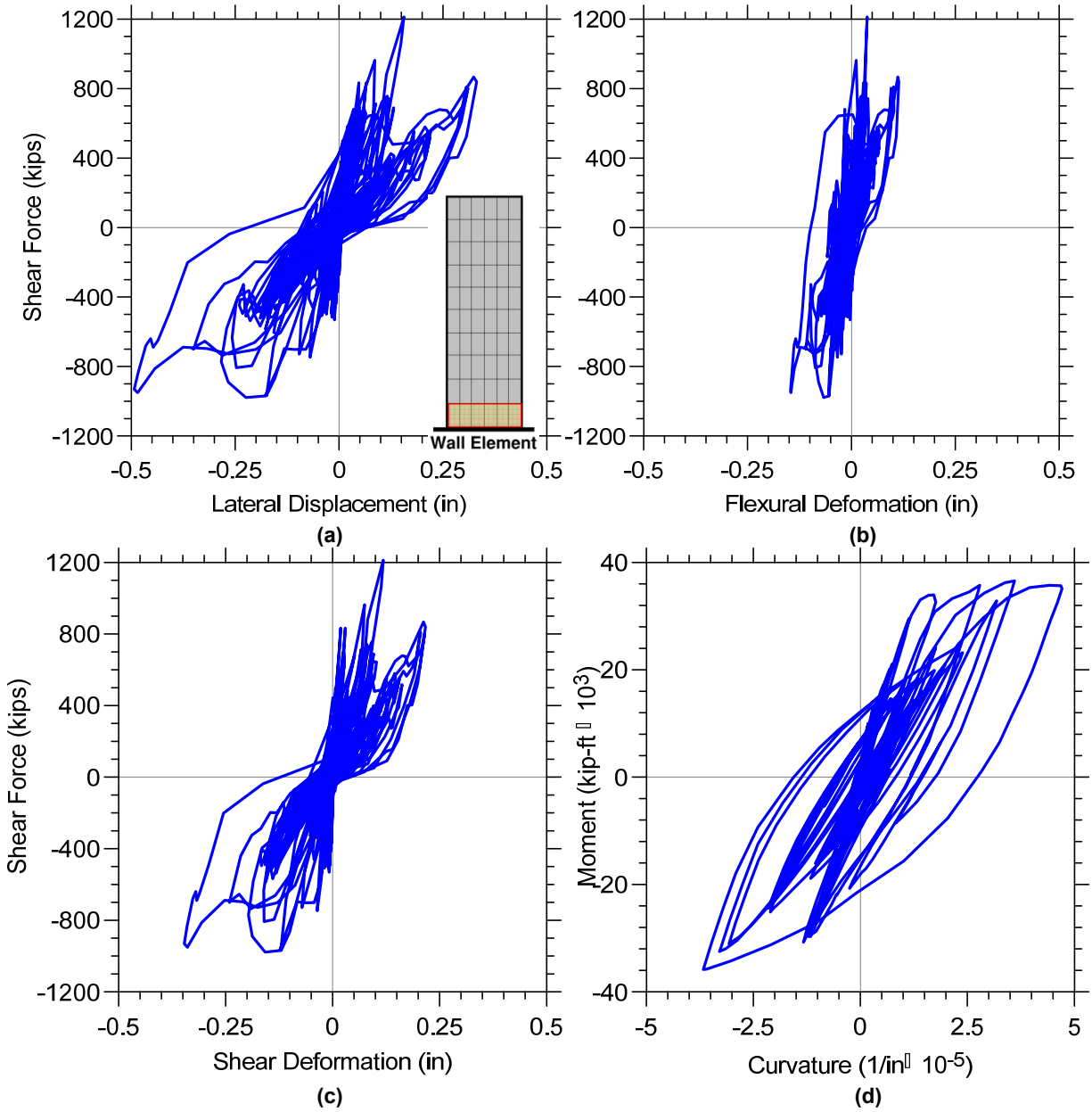

Figure 3.23 **Model element responses: (a) lateral load versus total lateral displacement; (b) lateral load versus flexural deformation; (c) lateral load versus shear deformation; and (d) moment versus curvature.**

3.3.4.5 Single RC Panel Responses

Analytically predicted strain versus resultant (smeared) stress responses for a single RC panel (macro-fiber) located at the left wall boundary of the bottom wall element are presented in Figure 3.24. Global panel stress–strain relationships presented in Figure 3.24 were obtained using element recorder *RCPanel* with commands *panel_strain* and *panel_stress*; the uniaxial behavior of concrete along the two concrete struts presented in Figure 3.25 were recorded using *strain_stress_concrete1* and *strain_stress_concrete2* commands; uniaxial stress–strain behavior of horizontal and vertical reinforcing steel presented in Figure 3.26 were obtained using

strain_stress_steelX and *strain_stress_steelY* commands. Other possible panel output is described in Appendices A.2 and A.3, and can be plotted in a similar manner.

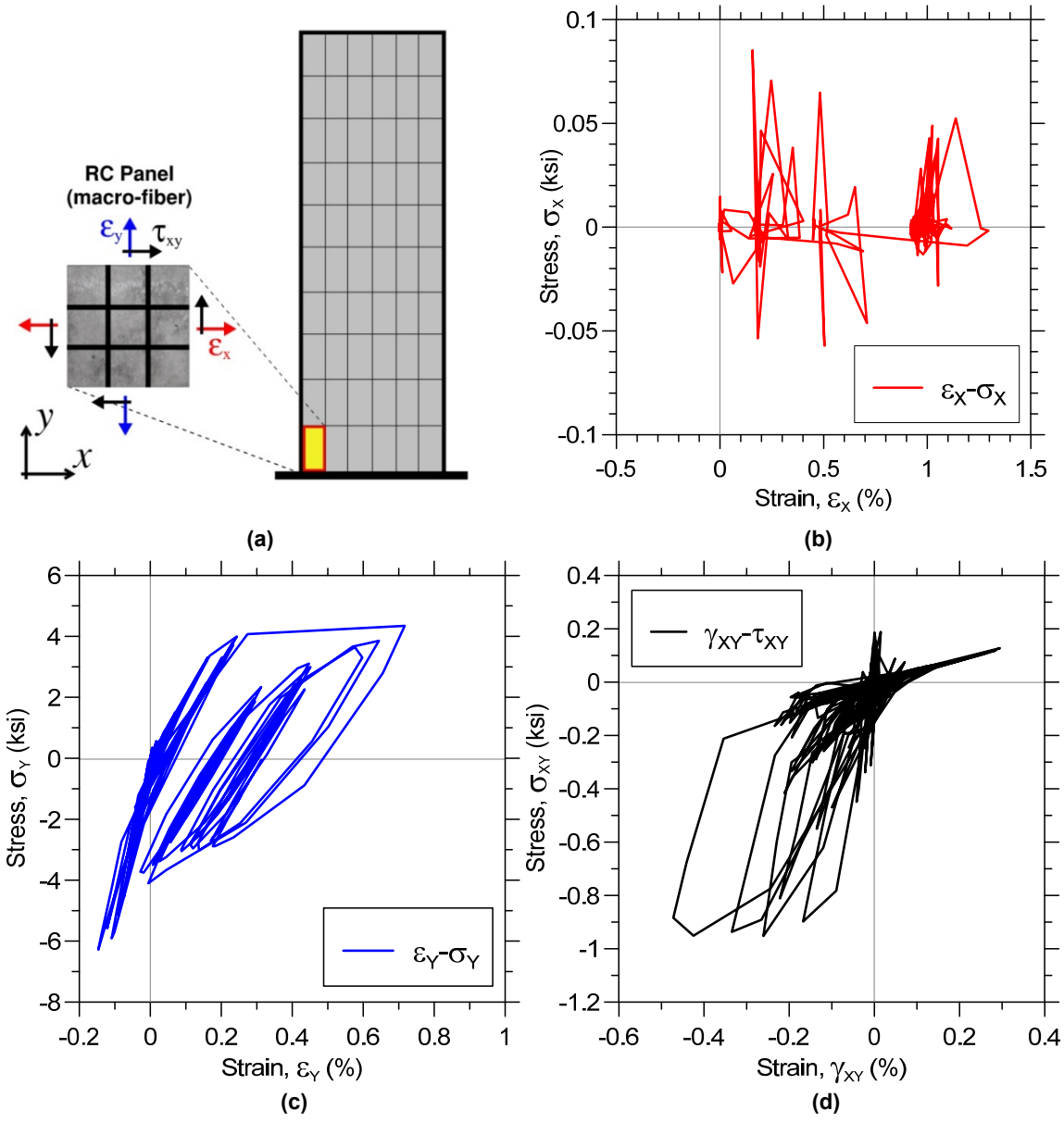

Figure 3.24 **Panel resultant stress versus strain responses: (a) considered RC panel; (b) axial-horizontal; (c) axial-vertical; and (d) shear.**

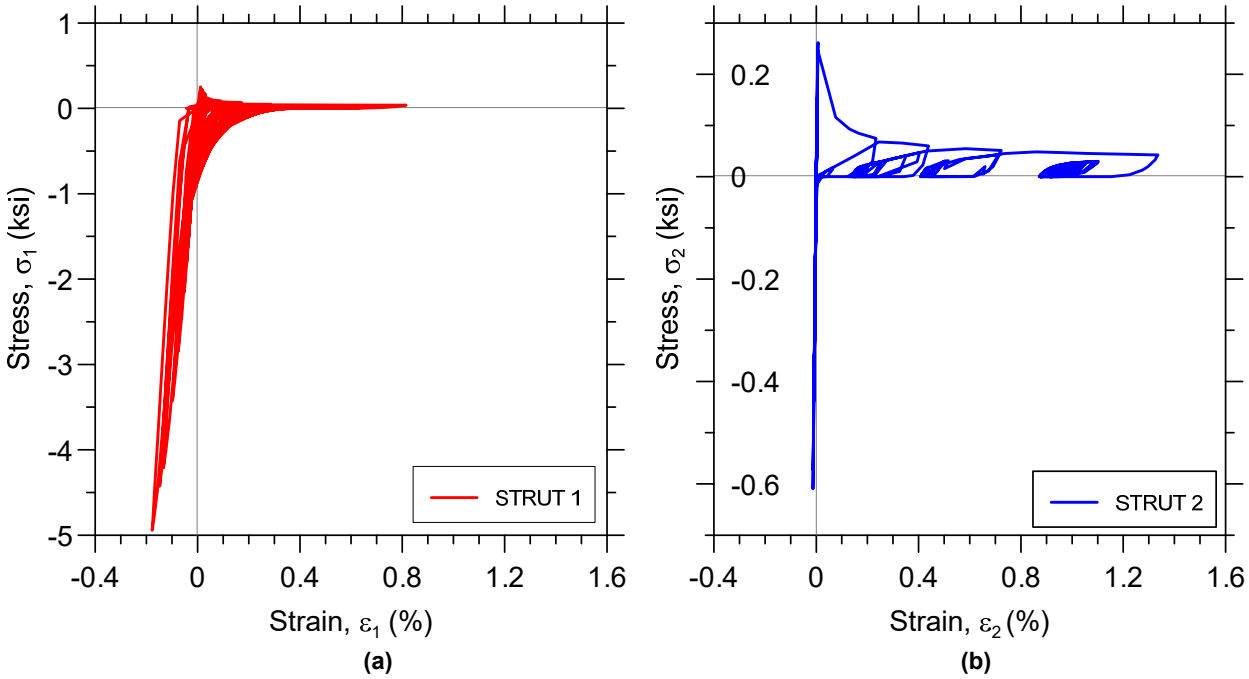

Figure 3.25 **Predicted stress–strain behavior for concrete: (a) Strut 1 and (b) Strut 2.**

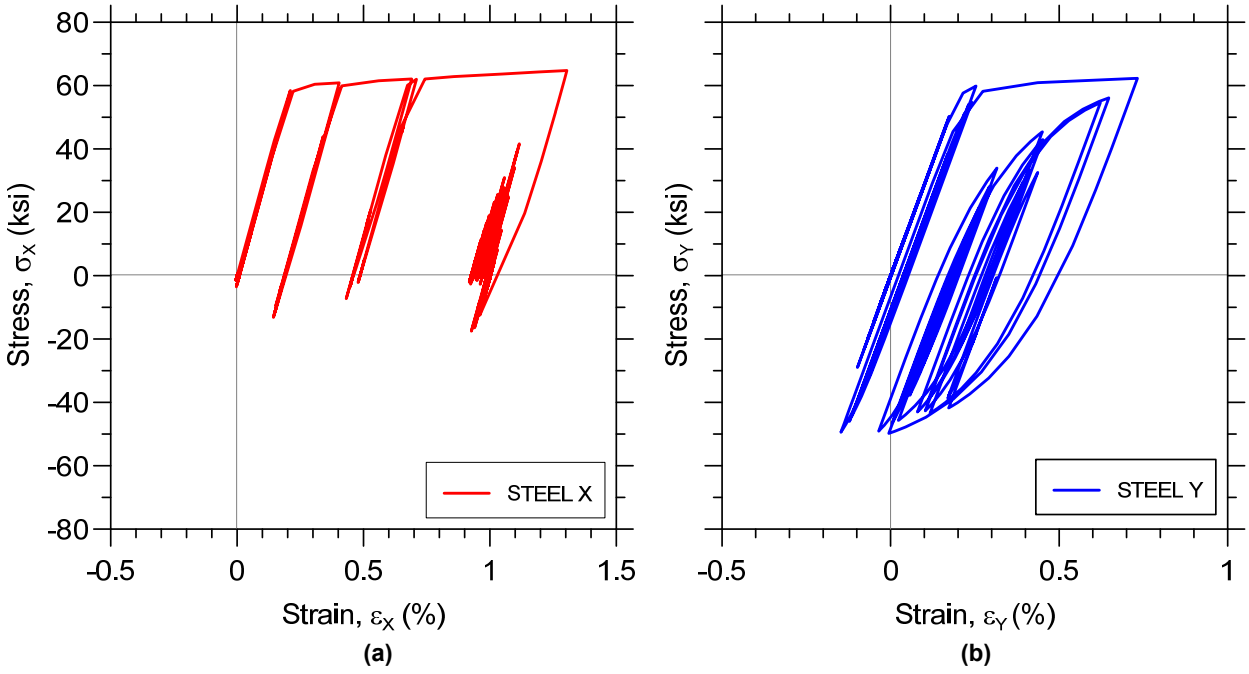

Figure 3.26 **Predicted stress–strain behavior for steel: (a) horizontal (*X*) and (b) vertical (*Y*).**

Finally, vertical profiles of maximum vertical strains [Figure 3.27(a)] were obtained using the element recorder with *RCPanel* and *panel_strain* recorder commands, whereas maximum wall rotations over wall height [Figure 3.27(b)] were derived from the element *Curvature* recorder. Similarly, the distribution of other wall response characteristics (e.g., shear deformations, etc.) can be plotted over the wall height.

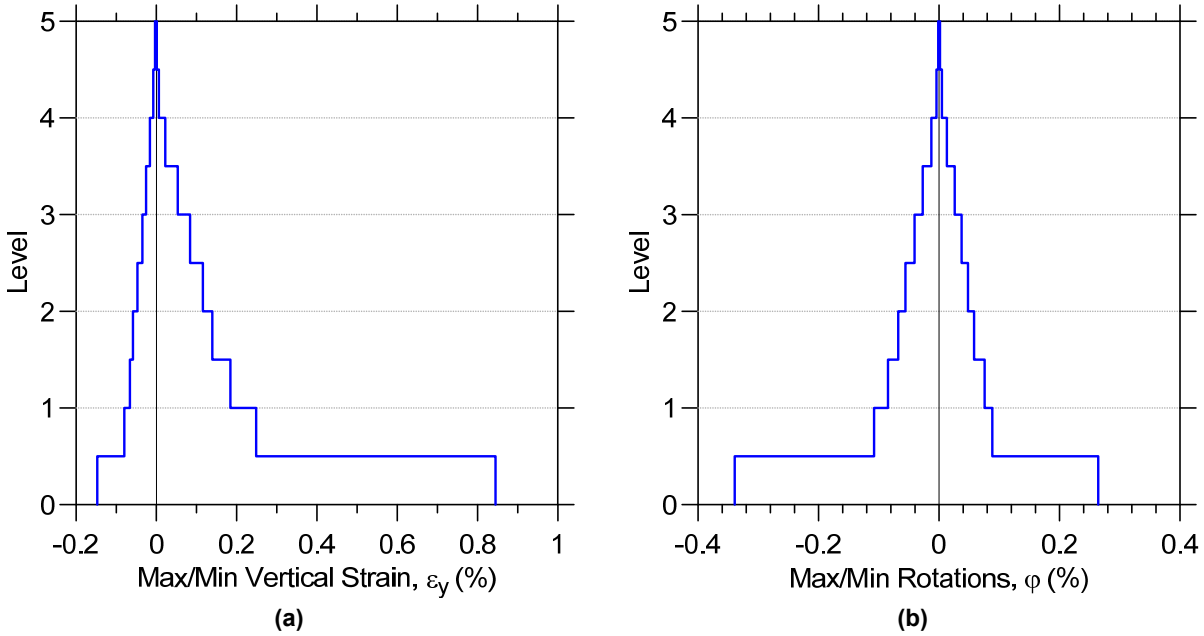

Figure 3.27 Local responses–vertical profiles of maximum: (a) vertical strains and (b) rotations.

4 Summary and Conclusions

An analytical model that integrates axial/flexural and shear responses, and simulates their interaction under cyclic loading conditions has been developed and implemented into the open-source computational platform developed by the Pacific Earthquake Engineering Research (PEER) Center, OpenSees. The proposed analytical model, called the *SFI-MVLEM*, incorporates RC panel behavior described by a fixed-crack-angle modeling approach (FSAM), into the fiber-based Multiple-Vertical-Line-Element-Model (*MVLEM*). The interaction of axial and shear modes of behavior is simulated at the RC panel (macro-fiber) level, which further captures interaction between shear and flexural responses at the model element level. The implementation of the novel shear-flexure interaction model included incorporation of five new features into OpenSees software including:

- model element based on original formulation of the Multiple-Vertical-Line-Element-Model (*MVLEM*) with uncoupled axial/flexural and shear behavior
- model element based on the formulation of Shear-Flexure-Interaction Multiple-Vertical-Line-Element-Model (*SFI-MVLEM*), that captures interaction between nonlinear axial/flexural and shear responses
- 2D in-plane constitutive panel model based on a fixed-strut-angle modeling approach (*FSAM*)
- uniaxial material model for concrete (*ConcreteCM*)
- uniaxial material model for steel (*SteelMPF*)

Examples of applications of new analytical models to simulation of nonlinear behavior of RC walls, columns, and building systems are provided including complete input files, detailed analysis results, as well as user manuals for new OpenSees classes, all of which also available on the OpenSees Wiki web page.

The analytical models implemented into OpenSees were validated against experimental results obtained from tests on RC columns with circular and rectangular cross sections, as well as slender RC wall specimen with flexure-dominated behavior, and moderately slender RC wall specimen with significantly pronounced shear-flexure interaction. Comparisons between experimentally measured and analytically predicted load-deformation responses using the model indicated that the *SFI-MVLEM* implemented in OpenSees is capable of capturing reasonably well the hysteretic load-deformation behavior of the RC column and wall specimens considered, by adequately capturing interaction between axial-flexural and shear behavior. Comparisons of the lateral load versus top displacement responses demonstrate that the proposed modeling approach

captures the lateral load capacity, stiffness degradation, and pinching characteristics of RC walls and columns for a range of specimen characteristics (e.g., span-to-depth ratio, axial load levels, and reinforcing ratios); overestimation of unloading stiffness was observed for only one of the four column specimens considered. Based on the response comparisons, a major shortcoming of the model is related to its inability to capture strength degradation reported in the experimental results; the model failed to simulate certain failure mechanisms (e.g., buckling/fracture of reinforcing bars; shear failure).

It is suggested that future studies focus on using a large number of test results available in the literature to calibration extensively a broader range of wall and column specimens with different geometries, reinforcement characteristics, and axial load levels, as well as model validation against dynamic tests on building and bridge components and systems. In addition, future research should focus on development and implementation of more robust constitutive models to represent shear transfer mechanisms along the cracks. In addition, development and implementation of rebar buckling and fracture behavior should be incorporated into the constitutive relationship for reinforcing steel and constitutive modeling of the sliding shear mechanism above the base of a wall, which would enable the analytical model to capture failure modes associated with these mechanisms. Future work will also include dissemination of research through various training and education activities, such as workshops, seminars, and webinars in collaboration with Pacific Earthquake Engineering Research Center (PEER), Earthquake Engineering Research Institute (EERI), and SAVI (Virtual International Institute for Seismic Performance Assessment of Structural Wall Systems).

REFERENCES

ACI (2011). *Building Code Requirements for Structural Concrete–ACI 318-11*, American Concrete Institute, Farmington Hills, Michigan.

ASCE 7-10 (2013). *Minimum Design Loads for Buildings and other Structures*, American Society of Civil Engineers, Reston, Virginia.

ASCE 41-13 (2014), *Seismic Evaluation and Retrofit of Existing Buildings*, American Society of Civil Engineers, Reston, Virginia.

Belarbi H., Hsu T.C.C. (1994). Constitutive laws of concrete in tension and reinforcing bars stiffened by concrete, American Concrete Institute, *ACI Struct. J.,* 91(4): 465–474.

Beyer K., Dazio A., Priestley M.J.N. (2011). Shear deformations of slender reinforced concrete walls under seismic loading, American Concrete Institute, *ACI Struct. J.,* 108(2): 167–177.

Chang G.A., Mander J.B. (1994). Seismic energy based fatigue damage analysis of bridge columns: Part I – Evaluation of seismic capacity, *NCEER Technical Report No. NCEER-94-0006*, State University of New York, Buffalo, NY.

Colotti V. (1993). Shear behavior of RC structural walls, ASCE, *J. Struct. Eng*., 119(3): 728–746.

Elmorsi M., Kianush M.R., Tso W.K. (1998). Nonlinear analysis of cyclically loaded reinforced concrete Structures, *ACI Struct. J.*, 95(6): 725–739.

Elwood K.J. (2002). *Shake Table Tests and Analytical Studies on the Gravity Load Collapse of Reinforced Concrete Frames*, PhD Dissertation, Department of Civil and Environmental Engineering, University of California, Berkeley, 419 pgs.

Filippou F.C., Popov E.P., Bertero V.V. (1983). Effects of bond deterioration on hysteretic behavior of reinforced concrete joints, *Report EERC 83-19*, Earthquake Engineering Research Center, University of California, Berkeley, CA.

Fischinger M., Rejec K., Isakovic T. (2012). Modeling inelastic shear response of RC walls, *Proceedings, 15th World Conference on Earthquake Engineering*, Lisbon, Portugal.

Gullu M.F., Horoz B., Orakcal K. (2015). Modeling of coupled shear and flexural responses in reinforced concrete structural walls (in Turkish), *Proceedings, 8th National Conference on Earthquake Engineering*, Istanbul, Turkey.

Gullu M.F., Orakcal, K. (2014). Nonlinear finite element modeling of reinforced concrete structural walls, *Proceedings, 2nd European Conference on Earthquake Engineering and Seismology*, Istanbul, Turkey.

Gullu M.F., Orendil A.E., and Orakcal K. (2014). "Finite Element Modeling of Low-Rise Structural Walls with Shear-Controlled Responses." Proceedings, 11th International Congress on Advances in Civil Engineering, Istanbul, Turkey.

Horoz B., Gullu M.F., Orakcal K. (2015). Modeling of coupled nonlinear shear and flexural responses in medium-rise RC walls, *Proceedings, 3rd Conference on Smart Monitoring, Assessment, and Rehabilitation of Civil Structures*, Antalya, Turkey.

Hsu T.C., Zhang L. (1996). Tension stiffening in reinforced concrete membrane elements, American Concrete Institute, *ACI Struct. J.*, 93(1): 108–115.

Jiang H., Kurama Y. (2010). Analytical modeling of medium-rise reinforced concrete shear walls, American Concrete Institute, *ACI Struct. J.,* 107(4.): 400–410.

Kabeyasawa T., Shiohara H., Otani S., Aoyama H. (1983). Analysis of the full-scale seven-story reinforced concrete test structure, *Proceedings, Second US-Japan Workshop on Performance-Based Earthquake Engineering Methodology for Reinforced Concrete Building Structures*, pp. 17–29, Hokkaido, Japan.

Kolozvari K. (2013). *Analytical Modeling of Cyclic Shear-Flexure Interaction in Reinforced Concrete Structural Walls*, PhD Dissertation, Department of Civil and Environmental Engineering, University of California, Los Angeles, CA.

Kolozvari K., Orakcal K., Wallace J.W. (2015a). Modeling of cyclic shear-flexure interaction in reinforced concrete structural walls. i: theory. ASCE, *J. Struct. Eng*., 141(5): 04014135.

Kolozvari K., Tran T., Orakcal K., Wallace J.W. (2015b). Modeling of cyclic shear-flexure interaction in reinforced concrete structural walls. ii: experimental validation, ASCE, *J. Struct. Eng*., 141(5): 04014136.

Kunnath S.K., Heo Y., Mohle J.P. (2009). Nonlinear uniaxial material model for reinforcing steel bars, ASCE, *J. Struct. Eng*., 135(4): 335–343.

Lignos D.G., Krawinkler H. (2011). Deterioration modeling of steel components in support of collapse prediction of steel moment frames under earthquake loading, ASCE, *J. Struct. Eng*., 137 (11): 1291–1302.

Lynn A.C., Moehle J.P. Mahin S.A., Holmes T.W. (1996). Seismic evaluation of existing reinforced concrete building columns, *Earthq. Spectra*, 12(4): 715–739.

Mander J.B., Priestley M.J.N., Park R. (1988). Theoretical stress-strain model for confined concrete, ASCE, *J. Struct. Eng*., 114(8): 1804–1826.

Mansour M.Y., Hsu T.C. (2005). Behavior of reinforced concrete elements under cyclic shear, ASCE, *J. Struct. Eng*., 131(1): 44–53.

Massone L.M., Orakcal K., Wallace J. W. (2006). Modeling flexural/shear interaction in rc walls, ACI-SP-236, deformation capacity and shear strength of reinforced concrete members under cyclic loadings, American Concrete Institute, Farmington Hills, MI, Paper 7, pp. 127–150.

Massone L.M., Orakcal K., Wallace J.W. (2009). Modeling of squat structural walls controlled by shear, American Concrete Institute, *ACI Struct. J.,* 106(5): 646–655.

Massone L.M., Wallace J.W. (2004). Load–deformation responses of slender reinforced concrete walls, American Concrete Institute, *ACI Struct. J.*, 101(1): 103–113.

McDaniel C. (1997). *Scale Effects on the Shear Strength of circular Reinforced Concrete Columns,* PhD Dissertation, Department of Structural Engineering, University of California, San Diego, CA.

McKenna F., Fenves G. L., Scott M. H., and Jeremic B. (2000). *Open System for Earthquake Engineering Simulation* (*OpenSees*). Pacific Earthquake Engineering Research Center, University of California, Berkeley, CA.

Menegotto M., Pinto E. (1973). Method of analysis for cyclically loaded reinforced concrete plane frames including changes in geometry and non-elastic behavior of elements under combined normal force and bending, *Proceedings, IABSE Symposium*, Lisbon, Portugal.

Mullapudi R.T., Ayuob A.S. (2009). Fiber beam element formulation using the softened membrane model, American Concrete Institute, *ACI Special Publication,* 265: 283–308.

Mullapudi R.T., Charkhchi P., Ayuob A.S. (2009). Evaluation of behavior of reinforced concrete shear walls through finite element analysis, *ACI Special Publication*, 265: 73–100.

Oesterle R., Aristizabal-Ochoa J., Fiorato A., Russel H., Corley W. (1979). *Earthquake Resistant Structural Walls—Tests of Isolated Walls: Phase II*, Portland Cement Association, Skokie, IL, 327 pgs.

Orakcal K. (2004). *Nonlinear Modeling and Analysis of Slender Reinforced Concrete Walls*, Ph.D. Dissertation, Department of Civil and Environmental Engineering, University of California, Los Angeles, CA.

Orakcal K., Conte J.P., Wallace J.W. (2004). Flexural modeling of reinforced concrete structural walls - model attributes, American Concrete Institute, *ACI Struct. J.,* 101(5): 688–698.

Orakcal K., Wallace J.W. (2006). Flexural modeling of reinforced concrete walls - Experimental verification, American Concrete Institute, *ACI Struct. J.,* 103(2): 196–206.

Orakcal K., Massone L.M., Ulugtekin D. (2012). Constitutive modeling of reinforced concrete panel behavior under cyclic loading, *Proceedings, 15th World Conference on Earthquake Engineering*, Lisbon, Portugal.

Pang D., Hsu T.C. (1996). Fixed angle softened truss model for reinforced concrete, American Concrete Institute, *ACI Struct. J.*, 93(2): 197–207.

Panagiotou M., Restrepo J.I., Schoettler M., Kim G. (2012). Nonlinear cyclic truss model for reinforced concrete walls, American Concrete Institute, *ACI Struct. J.,* 109(2): 205–214.

Priestley M.J.N., Benzoni G. (1996). Seismic performance of circular columns with low longitudinal reinforcement ratios, American Concrete Institute, *ACI Struct. J.,* 93(4): 474–485.

Priestley M.J.N., Seible F., Calvi G.M. (1996). *Seismic Design and Retrofit of Bridges*, John Wiley, New York, NY.

Saatcioglu M., Ozcebe G. (1989). Response of reinforced concrete columns to simulated seismic loading, American Concrete Institute, *ACI Struct. J.*, Vol. 86, No. 1, p.p. 3–12.

Saatcioglu M., Razvi S.R. (1992). Strength and ductility of confined concrete, ASCE, *J. Struct. Eng*., 118(6): 1590–1607.

Sayre B. (2003). *Performance Evaluation of Steel Reinforced Shear Walls*, MS Thesis, Department of Civil and Environmental Engineering University of California, Los Angeles, CA.

Shanmugam S.P. (2009). *Seismic Behavior of Circular Reinforced Concrete Bridge Columns under Combined Loading including Torsion*, PhD Dissertation, Department of Civil, Architectural, and Environmental Engineering, Missouri University of Science and Technology, Rolla, MO.

Thomsen J.H., Wallace J.W. (1995). Displacement-based design of reinforced concrete structural walls: an experimental investigation of walls with rectangular and t-shaped cross-sections, *Report No. CU/CEE-95/06*, Department of Civil Engineering, Clarkson University, Potsdam, NY.

Tran T.A. and Wallace J.W. (2012). "Experimental study of nonlinear flexural and shear deformations of reinforced concrete structural walls", Proceedings, 15th World Conference on Earthquake Engineering, Lisbon, Portugal.

Tsai W.T. (1988). Uniaxial compressional stress-strain relation of concrete, ASCE, *J. Struct. Eng*., 114(9): 2133–2136.

Ulugtekin D. (2010). *Analytical Modeling of Reinforced Concrete Panel Elements under Reversed Cyclic Loadings*, M.S. Thesis, Bogazici University, Istanbul, Turkey.

Vecchio and Collins (1986).

Vulcano A., Bertero V.V., Colotti V. (1988). Analytical modeling of rc structural Walls, *Proceedings, 9th World Conference on Earthquake Engineering*, Vol. 6, pp. 41–46, Tokyo-Kyoto, Japan.

Xu S.-Y., Zhang J. (2010). Hysteretic shear-flexure interaction model of reinforced concrete columns for seismic response assessment of bridges, *Earthq. Eng. Struct. Dyn*., 4(3): 315–337.

Appendix A User Manuals

A.1 ELEMENT MVLEM

Description:

The *MVLEM* element command is used to generate a two-dimensional Multiple-Vertical-Line-Element-Model (*MVLEM*, Vulcano et al. [1988], Orakcal et al. [2004]) for simulation of flexure-dominated RC wall behavior. A single model element incorporates six global DOFs, three of each located at the center of rigid top and bottom beams, as illustrated in Figure A.1(a). The axial/flexural response of the *MVLEM* is simulated by a series of uniaxial elements (or macro-fibers) connected to the rigid beams at the top and bottom (e.g., floor) levels, whereas the shear response is described by a shear spring located at height *ch* from the bottom of the model element. Shear and flexural responses of the model element are uncoupled. The relative rotation between top and bottom faces of the wall element occurs around the point located on the central axis of the element at height *ch* [Figure A.1(b)]. Rotations and resulting transverse displacements are calculated based on the wall curvature, derived from section and material properties, corresponding to the bending moment at height *ch* of each element; see Figure A.1(b). A value of $c = 0.4$ was recommended by Vulcano et al. [1988] based on comparison of the model response with experimental results. Flexural and shear behavior of the *MVLEM* element are uncoupled.

Source: /usr/local/cvs/OpenSees/SRC/element/MVLEM/

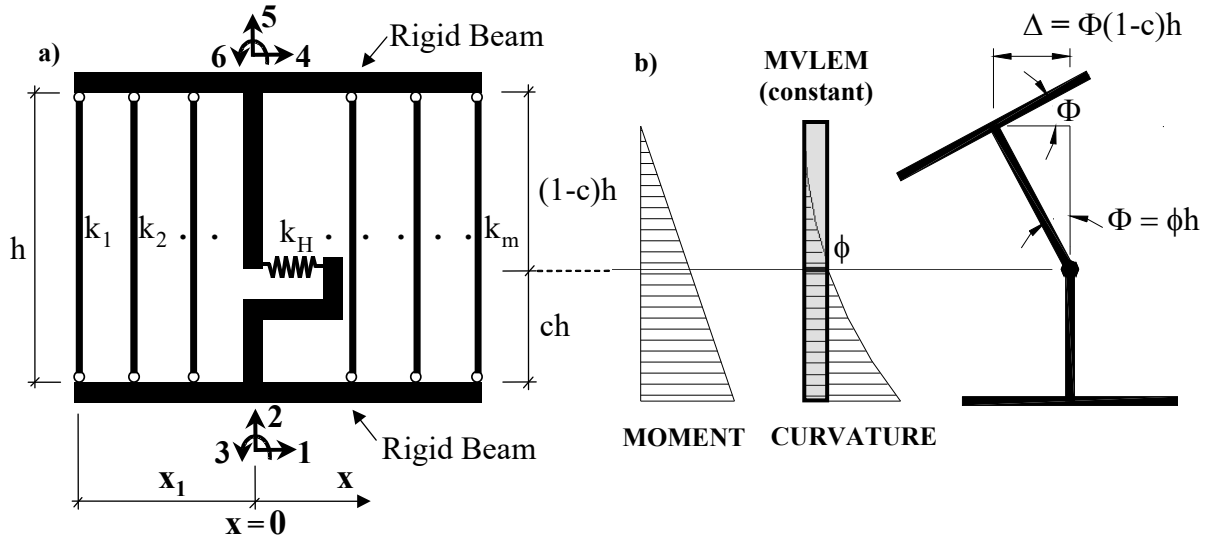

Figure A.1 Modeling approach: a) MVLEM element, b) MVLEM rotations and displacements.

The uniaxial behavior of the vertical fibers and the horizontal (shear) spring is represented using uniaxial material models available in OpenSees. Concrete (e.g., *ConcreteCM*) and steel material models (e.g., *SteelMPF*) need to be assigned to the vertical fibers to represent the axial-flexural behavior of a RC wall, while the force-deformation behavior of the horizontal spring is simulated using a single uniaxial material model (e.g., *Elastic* or *Hysteretic* material).

Input Parameters:

Element MVLEM $eleTag $Dens $iNode $jNode $m $c -thick <Thicknesses> -width <Widths> -rho <Reinforcing_ratios> -matConcrete <Concrete_tags> -matSteel <Steel_tags> -matShear <Shear_tag>

$eleTag	Unique element object tag
$Dens	Wall density
$iNode $jNode	End node tags
$m	Number of element macro-fibers
$c	Location of center of rotation with from the *iNode*; c = 0.4 (recommended)
<Thicknesses>	Array of *m* macro-fiber thicknesses
<Widths>	Array of *m* macro-fiber widths
<Reinforcing_ratios>	Array of *m* reinforcing ratios corresponding to macro-fibers; for each fiber: rho,i = As,i/Agross,i (1 < i < m)
<Concrete _tags>	Array of *m uniaxialMaterial* tags for concrete
<Steel_tags>	Array of *m uniaxialMaterial* tags for steel
<Shear_tag>	Tag of *uniaxialMaterial* for shear material behaior

Output Parameters:

The following output is available from the ***MVLEM*** element:

globalForce	Element global forces
Curvature	Element curvature
Shear_Force_Deformation	Element shear force-deformation relationship
Fiber_Strain	Vertical strain in *m* fibers along the cross-section
Fiber_Stress_Concrete	Vertical concrete stress in *m* fibers along the cross-section
Fiber_Stress_Steel	Vertical steel stress in *m* fibers along the cross-section

Examples:

Element MVLEM $eleTag $Dens $iNode $jNode $m $c -thick <Thicknesses> -width <Widths> -rho <Reinforcing_ratios> -matConcrete <Concrete_tags> -matSteel <Steel_tags> -matShear <Shear_tag>

Element MVLEM 1 0.0 1 2 8 0.4 -thick 4 4 4 4 4 4 4 4 -width 7.5 1.5 7.5 7.5 7.5 7.5 1.5 7.5 -rho 0.0293 0.0 0.0033 0.0033 0.0033 0.0033 0.0 0.0293 -matConcrete 3 4 4 4 4 4 4 3 -matSteel 1 2 2 2 2 2 2 1 -matShear 5

Recorder Element -file MVLEM_Fgl.out -time -ele 1 globalForce

Recorder Element -file MVLEM_FiberStrain.out -time -ele 1 Fiber_Strain

A.2 ELEMENT SFI_MVLEM

Description:

The *SFI_MVLEM* command is used to construct a Shear-Flexure Interaction Multiple-Vertical-Line-Element Model (SFI-MVLEM, Kolozvari et al. [2014a, b], which captures interaction between axial/flexural and shear behavior of RC structural walls and columns under cyclic loading. The *SFI_MVLEM* element [Figure A.2(a)] incorporates 2-D RC panel behavior described by the Fixed-Strut-Angle-Model (*nDMaterial FSAM*, Figure A.2(b); Ulugtekin [2010]), into a 2D macroscopic fiber-based model (*MVLEM*). The interaction between axial and shear behavior is captured at each RC panel (macro-fiber) level, which further incorporates interaction between shear and flexural behavior at the *SFI_MVLEM* element level.

Source: /usr/local/cvs/OpenSees/SRC/element/SFI_MVLEM/

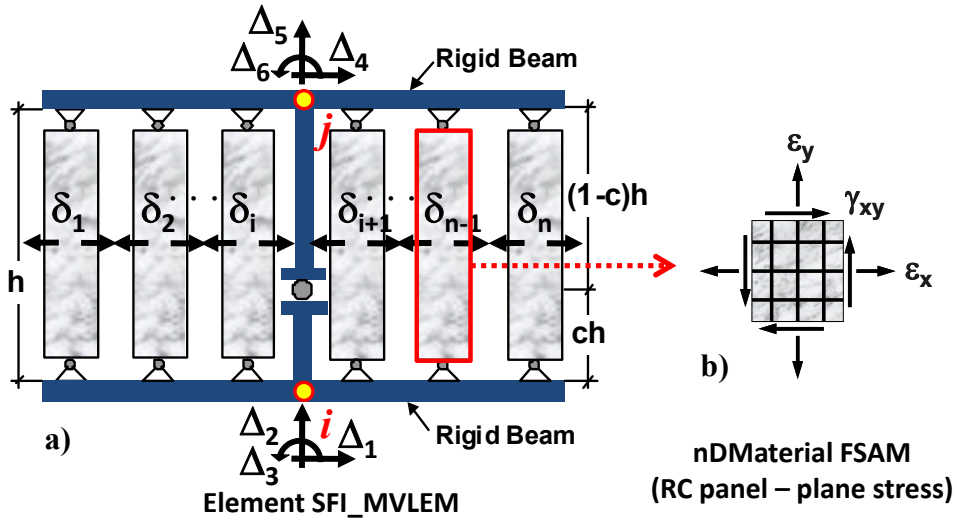

Figure A.2 Modeling approach: (a) SFI_MVLEM element; and (b) RC panel element.

Input Parameters:

Element SFI_MVLEM $eleTag $Dens $iNode $jNode $m $c -thick <thicknesses> -width <widths> -mat <material_tags>

$eleTag	Unique element object tag
$iNode $jNode	End node tags
$m	Number of element macro-fibers
$c	Location of center of rotation (c × element height) with respect to *iNode* - c = 0.4 (recommended)
<thicknesses>	Array of *m* macro-fiber thicknesses
<widths>	Array of *m* macro-fiber widths
<material_tags>	Array of *m* macro-fiber *nDMaterial* [1] tags

[1] ***SFI_MVLEM*** element shall be used with ***nDMaterial FSAM***, which is a 2-D plane-stress constitutive relationship representing reinforced concrete panel behavior.

Output Parameters:

The following output is available from the ***SFI_MVLEM*** element:

globalForce	Element global forces
ShearDef	Element shear deformation
Curvature	Element curvature
RCPanel $fibTag $Response	Returns RC panel (macro-fiber) *$Response* for a $*fibTag*-th panel (1<*fibTag*<*m*). For available *$Response*-s refer to Appendix A.3.

Examples:

```
Element SFI_MVLEM $eleTag $iNode $jNode $m $c -thick <thicknesses> -width <widths>
-mat <material_tags>
Element SFI_MVLEM 1  1  2  5  0.4  -thick 6 6 6 6 6  -width 9 10 10 10 9  -mat 7 6 6 6 7

Recorder Element -file MVLEM_Fgl.out  -time  -ele  1  2  3  globalForce

Recorder Element -file MVLEM_panel_strain.out -time -ele  1  RCPanel  1  panel_strain
```

A.3 NDMATERIAL FSAM

Description:

This command is used to construct an *nDMaterial FSAM* (Fixed-Strut-Angle-Model, Figure A.3), which is a plane-stress constitutive model for simulating the behavior of RC panel elements under generalized, in-plane, reversed-cyclic loading conditions [Ulugtekin 2010; Orakcal et al. 2012]. In the *FSAM*, the strain fields acting on concrete and reinforcing steel components of an RC panel are assumed to be equal to each other, implying perfect bond assumption between concrete and reinforcing steel bars. While the reinforcing steel bars develop uniaxial stresses under strains in their longitudinal direction, the behavior of concrete is defined using stress–strain relationships in biaxial directions, the orientation of which is governed by the state of cracking in concrete. Although the concrete stress–strain relationship used in the *FSAM* is fundamentally uniaxial in nature, it also incorporates biaxial softening effects including compression softening and biaxial damage. For transfer of shear stresses across the cracks, a friction-based elasto-plastic shear aggregate interlock model is adopted, together with a linear elastic model for representing dowel action on the reinforcing steel bars [Kolozvari 2013].

Source: /usr/local/cvs/OpenSees/SRC/material/nD/reinforcedConcretePlaneStress/FSAM/

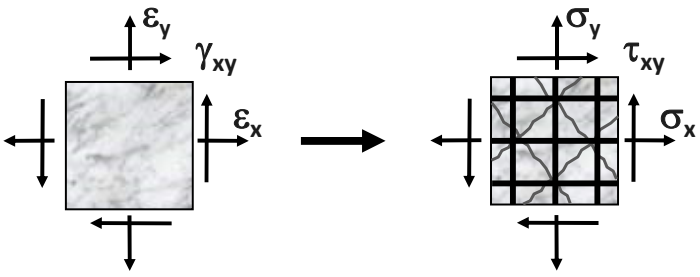

Figure A.3 FSAM for converting in-plane strains to smeared stresses on a RC panel element.

Input Parameters:

nDMaterial FSAM $mattag $rho $sX $sY $conc $rouX $rouY $nu $alfadow

$mattag	Unique *nDMaterial* tag
$rho	Material density
$sX	Tag of *uniaxialMaterial* simulating horizontal (-X) reinforcement
$sY	Tag of *uniaxialMaterial* simulating vertical (-Y) reinforcement
$conc	Tag of *uniaxialMaterial* [2] simulating concrete
$rouX	Reinforcing ratio in horizontal (-X) direction
$rouY	Reinforcing ratio in vertical (-Y) direction
$nu	Concrete friction coefficient ($0.0 < \$nu < 1.5$)
$alfadow	Stiffness coefficient of reinf. dowel action ($0.0 < \$alfadow < 0.05$)

Recommended values for parameter of a shear resisting mechanism (*nu* and *alfadow*, Figure A.4) are provided above. Details about the sensitivity of analytical predictions using SFI_MVLEM to changes in these parameters are presented by Kolozvari (2013).

Output Parameters:

The following output is available from the ***FSAM*** RC panel model:

panel_strain	Strains ε_x, ε_y, γ_{xy} (Figure A.3)
panel_stress	Resulting panel stresses σ_x, σ_y, τ_{xy} (concrete and steel, Figure A.3)
panel_stress_concrete	Resulting panel concrete stresses σ_{xc}, σ_{yc}, τ_{xyc} (Figure A.4b)
panel_stress_steel	Resulting panel steel stresses σ_{xs}, σ_{ys}, τ_{xys} (Figure A.4d)
strain_stress_steelX	Uniaxial strain and stress of horizontal reinforcement ε_x, σ_{xxs}
strain_stress_steelY	Uniaxial strain and stress of vertical reinforcement ε_y, σ_{yys}
strain_stress_concrete1	Uniaxial strain and stress of concrete strut 1 ε_{c1}, σ_{c1}
strain_stress_concrete2	Uniaxial strain and stress of concrete strut 2 ε_{c2}, σ_{c2}
strain_stress_interlock1	Shear strain and stress along concrete strut 1 γ_{cr1}, τ_{cr1} (Figure A.4c)
strain_stress_interlock2	Shear strain and stress along concrete strut 2 γ_{cr2}, τ_{cr2} (Figure A.4c)
cracking_angles	Orientation of concrete cracks

Note that recorders for a RC panel (marco-fiber) are invoked as ***SFI-MVLEM*** element recorders using command ***RCPanel*** and one of the desired commands listed above. Currently, it is possible to output values only for one macro-fiber within one or multiple elements.

Examples:

```
nDMaterial FSAM $mattag  $rho  $sX  $sY  $conc  $rouX    $rouY   $nu  $alfadow

nDMaterial FSAM      1    0.0    1    2      4  0.0073  0.0606  0.1      0.01

Recorder Element -file MVLEM_panel_strain.out -time -ele 1 RCPanel 1 panel_strain
```

[2] ***nDMaterial FSAM*** shall be used with ***uniaxialMaterial ConcreteCM***.

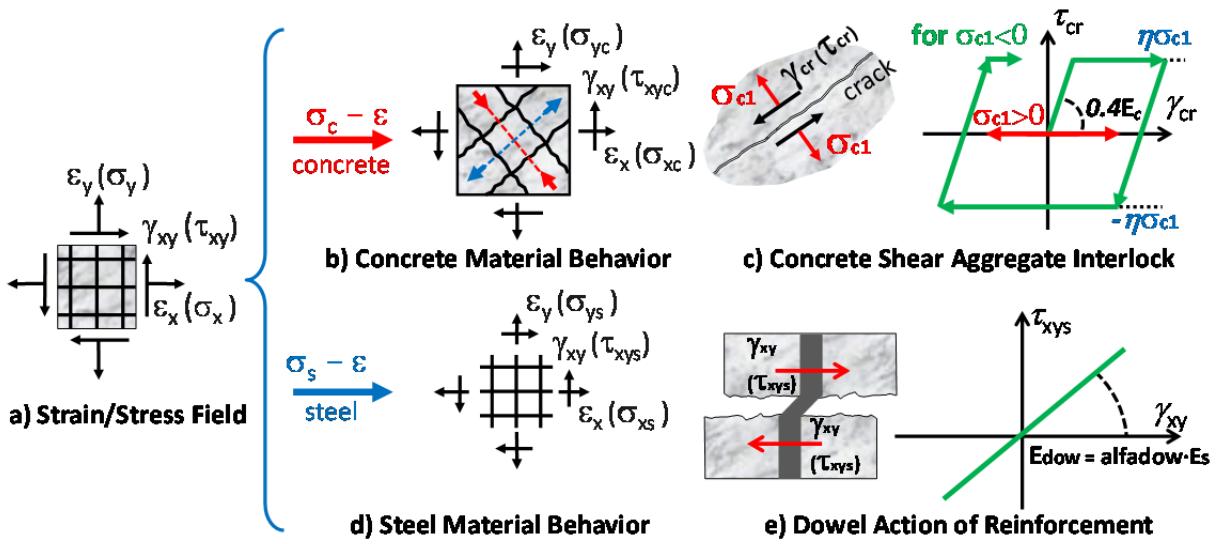

Figure A.4 **Behavior and input/output parameters of the FSAM constitutive model.**

A.4 UNIAXIALMATERIAL CONCRETE_CM

Description:

This command is used to construct a *uniaxialMaterial ConcreteCM*, which is a uniaxial hysteretic constitutive model for concrete developed by Chang and Mander [1994]. This model is a refined, rule-based, generalized, and non-dimensional constitutive model that allows calibration of the monotonic and hysteretic material modeling parameters, and can simulate the hysteretic behavior of confined and unconfined, ordinary and high-strength concrete, in both cyclic compression and tension (Figure A.5). The model addresses important behavioral features, such as continuous hysteretic behavior under cyclic compression and tension, progressive stiffness degradation associated with smooth unloading and reloading curves at increasing strain values, and gradual crack closure effects. Details of the model are available in the report by Chang and Mander [1994]. Note that *ConcreteCM* incorporates the unloading/reloading rules defined originally by Chang and Mander [1994], as opposed to *Concrete07*, which adopts simplified hysteretic rules.

The Chang and Mander [1994] model successfully generates continuous hysteretic stress–strain relationships with slope continuity for confined and unconfined concrete in both compression and tension. The compression envelope curve of the model is defined by the initial tangent slope, (**Ec**), the peak coordinate (**epcc, fpcc**), a parameter (**rc**) from Tsai's [1988] equation defining the shape of the envelope curve, and a parameter (**xcrn**) to define normalized (with respect to **epcc**) strain where the envelope curve starts following a straight line, until zero compressive stress is reached at the spalling strain, ε_{sp}. These parameters can be controlled based on specific experimental results for a refined calibration of the compression envelope (Figure A.6). Chang and Mander [1994] proposed empirical relationships for parameters **Ec**, **epcc**, and **rc** for unconfined concrete with compressive strength **fpcc**, based on review of previous research. Parameters **fpcc**, **epcc**, **Ec**, **rc**, and **xcrn** can also be calibrated to represent the stress–strain behavior of confined concrete in compression, to follow the constitutive relationships for confined concrete proposed by Mander et al (1988) or similar.

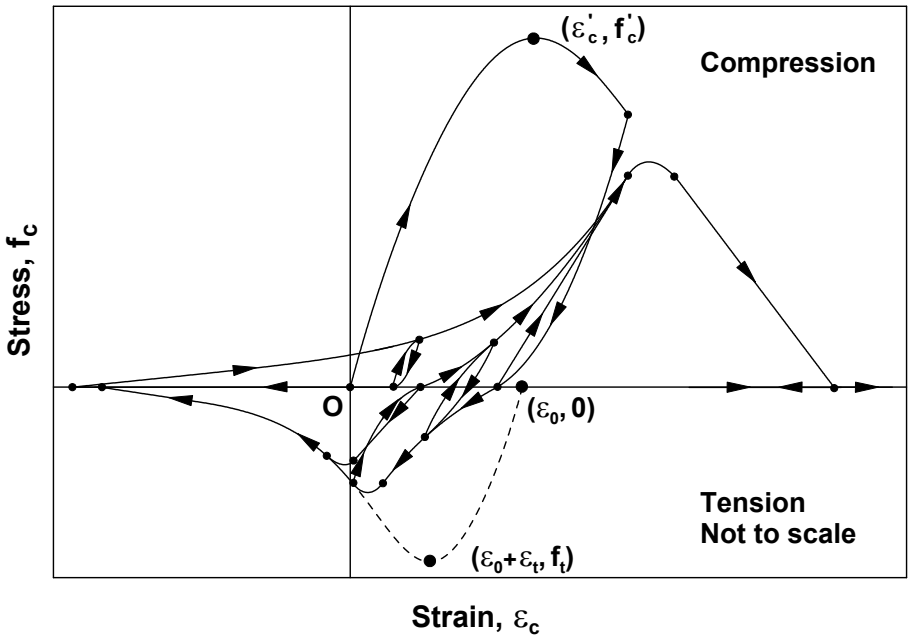

Figure A.5 Hysteretic constitutive model for concrete by Chang and Mander [1994].

The shape of the tension envelope curve in the model is the same as that of the compression envelope; however, the tension envelope curve is shifted to a new origin that is based on the unloading strain from the compression envelope (Figure A.6). As well, the strain ductility experienced previously on the compression envelope is also reflected on the tension envelope. The parameters associated with the tension envelope curve include the tensile strength of concrete (**ft**), the monotonic strain at tensile strength (**et**), a parameter (**rt**) from Tsai's [1988] equation defining the shape of the tension envelope curve, and a parameter (**xcrp**) to define normalized (with respect to **et**) strain where the tension envelope curve starts following a straight line, until zero tensile stress is reached at a strain of ε_{crk}. These parameters can also be controlled and calibrated based on specific experimental results or empirical relations proposed by other researchers (e.g., Belarbi and Hsu [1994]) to model the behavior of concrete in tension and the tension stiffening phenomenon. Concrete experiencing tension stiffening can be considered not to crack completely; that is, a large value for parameter **xcrp** (e.g., 10000) can be defined.

An optional input parameter gap is introduced in the *ConcreteCM* model implemented in OpenSees for providing the users with the opportunity to control the intensity of gap closure in the stress–strain behavior of concrete, which in-turn influences the level of pinching in the lateral load-displacement behavior of a RC wall. The original Chang and Mander [1994] model adopts a non-zero tangent stiffness at zero stress level upon unloading from the tension envelope, which is represented by gap = 1 in *ConcreteCM*. Using gap = 0 (default) produces less gradual gap closure, since it assumes zero tangent stiffness at zero stress level upon unloading from the tension envelope, and is suitable for most analyses. Example 1 compares flexural response predictions of a slender wall obtained using more gradual (gap = 1) and less gradual (gap = 0) gap closure behavior, to illustrate the impact of this parameter on the analytical results. Examples of hysteretic stress–strain histories generated by the model code are illustrated in Figure A.7.

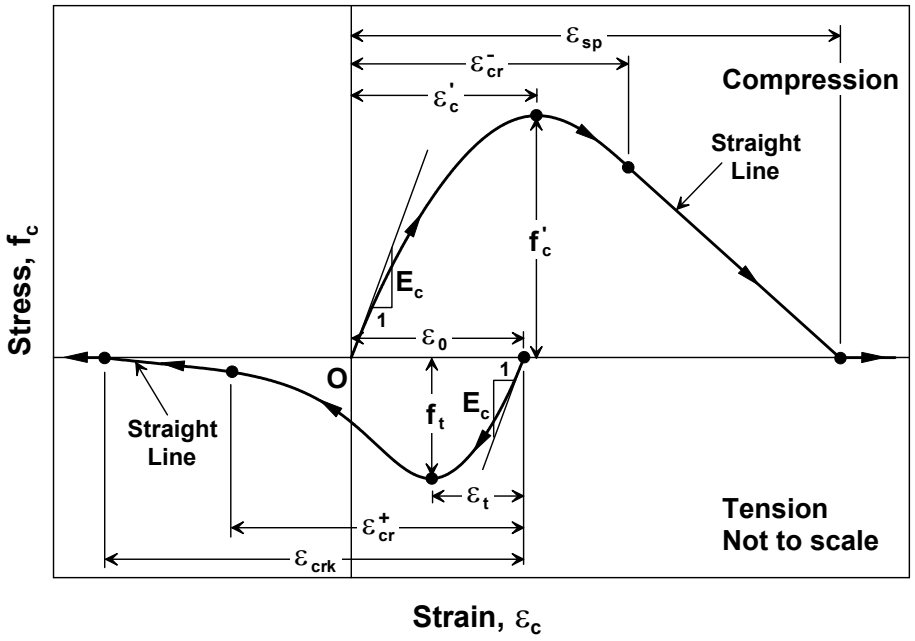

Figure A.6 Compression and tension envelope curves.

Input Parameters:

uniaxialMaterial ConcreteCM $mattag $fpcc $epcc $Ec $rc $xcrn $ft $et $rt $xcrp <-GapClose $gap>

$mattag	Unique *nDMaterial* tag
$fpcc	Compressive strength
$epcc	Strain at compressive strength
$Ec	Initial tangent modulus
$rc	Shape parameter in Tsai's equation defined for compression
$xcrn	Non-dimensional critical strain on compression envelope (where the envelope curve starts following a straight line)
$ft	Tensile strength
$et	Monotonic strain at tensile strength
$rt	Shape parameter in Tsai's equation defined for tension
$xcrp	Non-dimensional critical strain on tension envelope (where the envelope curve starts following a straight line – large value [e.g., 10000] recommended when tension stiffening is considered)
<-GapClose $gap>	**gap** = 0, less gradual gap closure (default); **gap** = 1, more gradual gap closure

Examples:

```
uniaxialMaterial ConcreteCM $mattag  $fpcc   $epcc    $Ec  $rc  $xcrn   $ft    $et    $rt  $xcrp
uniaxialMaterial ConcreteCM    1     -6.2  -0.0021  4500   7   1.035  0.30  0.00008  1.2  10000
```

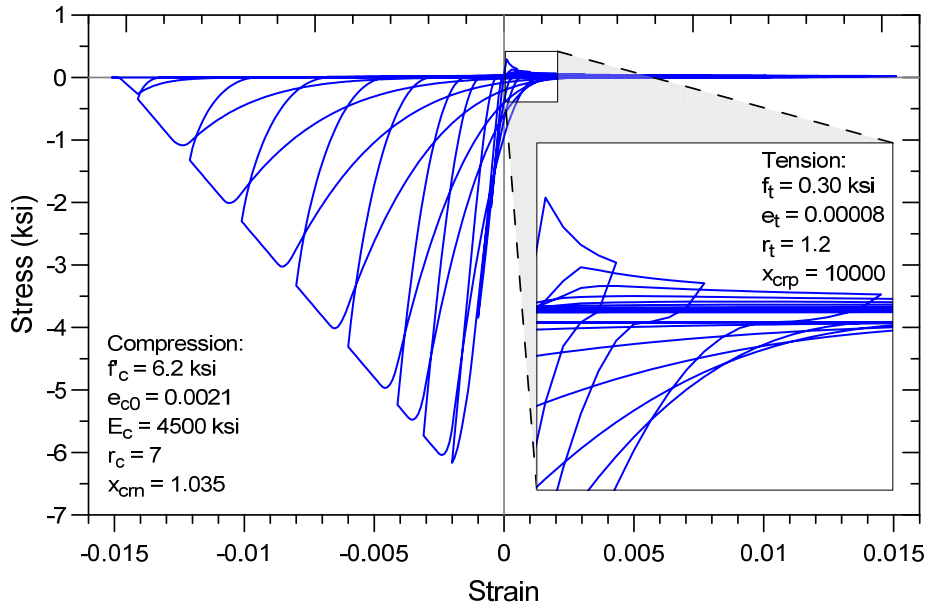

Figure A.7 Sample oncrete stress–strain behavior.

A.5 UNIAXIALMATERIAL STEELMPF

Description:

This command is used to construct a *uniaxialMaterial SteelMPF*, which represents the well-known uniaxial constitutive nonlinear hysteretic material model for steel proposed by Menegotto and Pinto [1973], and extended by Filippou et al. [1983] to include isotropic strain hardening effects. The relationship is in the form of curved transitions (Figure A.8), each from a straight-line asymptote with slope E_0 (modulus of elasticity) to another straight-line asymptote with slope $E_1 = bE_0$ (yield modulus) where b is the strain hardening ratio. The curvature of the transition curve between the two asymptotes is governed by a cyclic curvature parameter R, which permits the Bauschinger effect to be represented, and is dependent on the absolute strain difference between the current asymptote intersection point and the previous maximum or minimum strain reversal point depending on whether the current strain is increasing or decreasing, respectively. The strain and stress pairs (ε_r, σ_r) and (ε_0, σ_0) shown on Figure A.8 are updated after each strain reversal. The model allows calibration of isotropic hardening parameters in both compression and tension through optional input variables a_1 and a_2 for isotropic strain hardening in compression, and a_3 and a_4 for isotropic strain hardening tension, and uses default values of $a_1 = a_3 = 0.0$ and $a_2 = a_4 = 1.0$ that yield no isotropic strain hardening for either compression or tension. To incorporate isotropic strain hardening in compression, the recommended parameters are $a_1 = 0.01$ and $a_2 = 7.0$. To incorporate isotropic strain hardening in tension, the recommended parameters are $a_3 = 0.01$ and $a_4 = 7.0$.

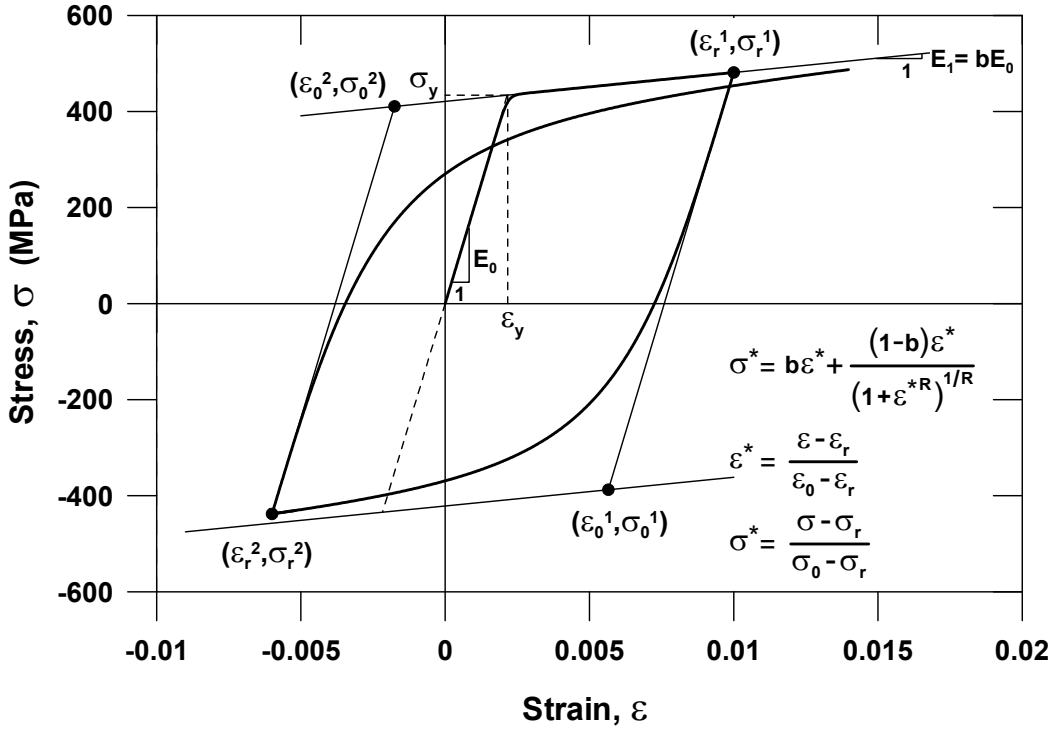

Figure A.8 Constitutive model for steel [Menegotto and Pinto 1973].

Although the Menegotto-Pinto model extended by Filippou et al.is already available in OpenSees (e.g., *Steel02*), the formulation of *SteelMPF* brings several distinctive features compared to the existing models. For example, the implemented model allows definition of different yield stresses and strain hardening ratios for compression and tension, which allows consideration of tension stiffening effects on the tensile stress–strain behavior of reinforcing bars embedded in concrete. As well, the implemented model considers degradation of the cyclic curvature parameter *R* for strain reversals in both pre- and post- yielding regions of the hysteretic stress–strain behavior, which may provide more accurate predictions of the yield capacity of RC structural members under cyclic loading, whereas *Steel02* considers the cyclic curvature degradation after formation of post-yield strains only. Figure A.9 compares strain-stress relationships obtained using *SteelMPF* and *Steel02* for a strain history that includes strain reversals at strain values equal to one-half of the yield strain (e.i., $\varepsilon_r = \pm 0.001 = \varepsilon_y/2$).

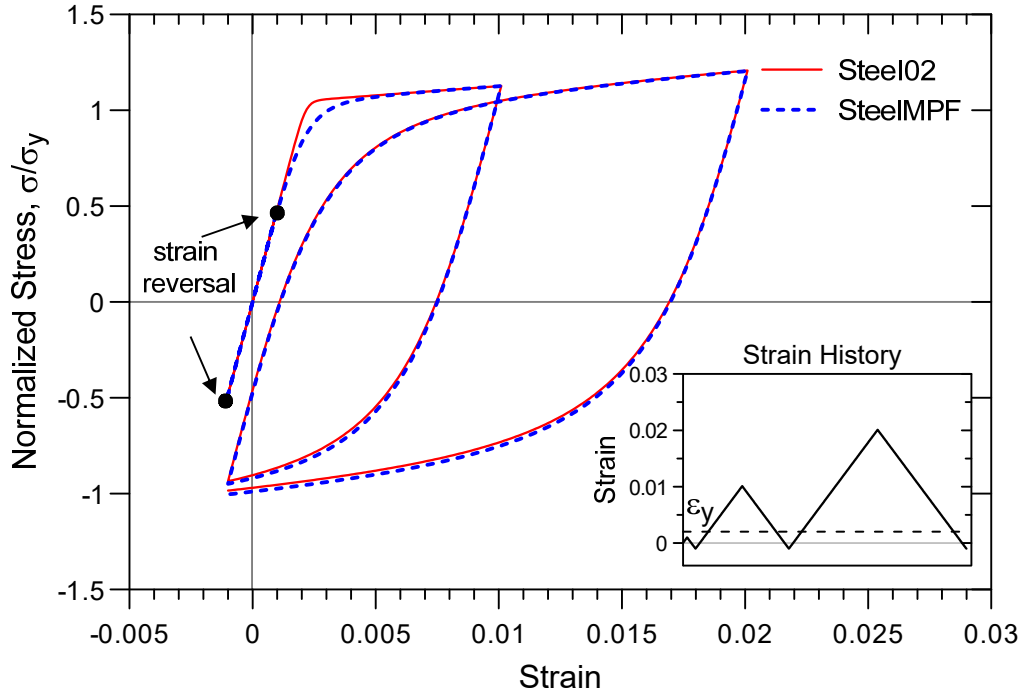

Figure A.9 ***Steel02*** **and** ***SteelMPF*** **– degradation of cyclic curvature in pre-yielding region.**

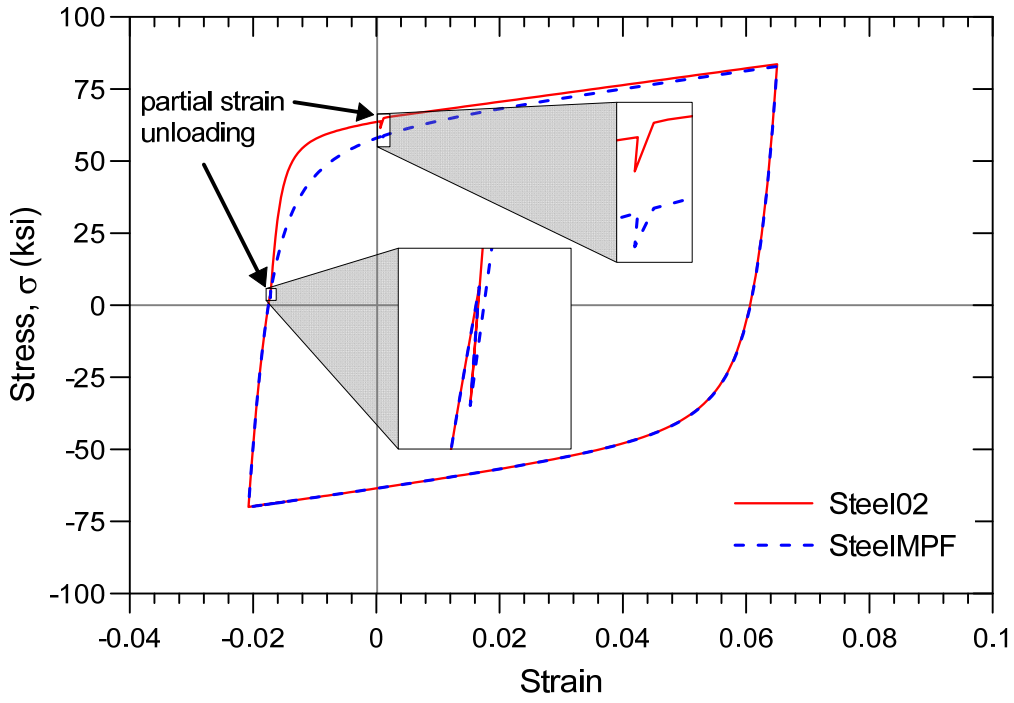

Figure A.10 **Comparison of** ***Steel02*** **and** ***SteelMPF*****: stress overshooting upon reloading from low-amplitude unloading.**

Furthermore, it has been observed from the strain-stress relationships obtained from quasi-static or dynamic analyses using existing steel models in OpenSees (e.g., *Steel02*) that after partial unloading occurs in a model element caused by dynamic loading or stress re-distribution under quasi-static loading due to concrete cracking or crushing, the Menegotto-Pinto formulation produces stress overshooting in the cyclic stress–strain behavior of reinforcing steel. This overshooting effect is not behavioral and causes non-physical hardening in the stress–strain behavior, upon reloading from the partial unloading loop. This phenomenon is illustrated in Figure A.10 for the *Steel02* model. This anomaly results in overestimation of steel stresses predicted by the *Steel02* model upon return from partial unloading, yielding strain-stress curve that may not represent the physical constitutive behavior of reinforcing steel under cyclic loading. The overshooting effect observed in *Steel02* has been remedied in *SteelMPF*, via manipulating the model formulation so that reloading behavior after partial unloading cannot overshoot the previous loading loop in the cyclic stress–strain behavior. The comparison between strain-stress relationships obtained using *SteelMPF* and *Steel02* for a strain history that includes low-amplitude unloading followed by reloading is presented in Figure A.10.

Input Parameters:

uniaxialMaterial SteelMPF $mattag $fyp $fyn $E0 $bp $bn $R0 $cR1 $cR2 <$a1 $a2 $a3 $a4>

$mattag	Unique *nDMaterial* tag
$fyp	Yield strength in tension (positive loading direction)
$fyn	Yield strength in compression (negative loading direction)
$E0	Initial tangent modulus
$bp	Strain hardening ratio in tension (positive loading direction)
$bn	Strain hardening ratio in compression (negative loading direction)
$R0	Initial value of the curvature parameter R (R0 = 20 recommended)
$cR1	Curvature degradation parameter (a1 = 0.925 recommended)
$cR2	Curvature degradation parameter (a2 = 0.15 or 0.0015 recommend.)
$a1	Isotropic hardening in compression parameter (optional, default = 0.0). Shifts compression yield envelope by a proportion of compressive yield strength after a maximum plastic tensile strain of $a2($fyp/$E0).
$a2	Isotropic hardening in compression parameter (optional, default = 1.0). See explanation of #a1.
$a3	Isotropic hardening in tension parameter (optional, default = 0.0). Shifts tension yield envelope by a proportion of tensile yield strength after a maximum plastic compressive strain of $a3($fyn/$E0).
$a4	Isotropic hardening in tension parameter (optional, default = 1.0). See explanation of #a3.

Example:

```
uniaxialMaterial SteelMPF $mattag  $fyp  $fyn   $E0   $bp  $bn   $R0  $cR1 $cR2 <$a1 $a2 $a3 $a4>
uniaxialMaterial SteelMPF       1    60    60 29000 0.02 0.02   20.0  18.5 0.15
```

Appendix B Input Files: Cyclic Analysis of Reinforced Concrete Wall and Column Specimens

B.1 CIRCULAR COLUMN SPECIMEN H/D(3)-T/M(0)/1.32% – SFI_MVLEM MODEL GENERATION

```
# ------------------------------------------------------------------
# Simulation of circular column cyclic behavior using SFI_MVLEM
# Specimen: H/D(3)-T/M(0)/1.32%, Shanmugam (2009)
# File Name: SFI_MVLEM_Shanmugam.tcl
# ------------------------------------------------------------------

# ---------------------------------------------------------
# Start of model generation (Units: kip, in, sec, ksi)
# ---------------------------------------------------------

# Set Up Directories
set modelName "Shanmugam";         # Model Name
set dataDir SFI_MVLEM_$modelName; # Name of output folder
file mkdir $dataDir;

# Create ModelBuilder for 2D element (with two-dimensions and 3 DOF/node)
model basic -ndm 2 -ndf 3

# ------------------------------------------------------------------------
# Set geometry, nodes, boundary conditions
# ------------------------------------------------------------------------

# Column Geometry
# Column height
set H 72;

# Column Fiber Widths
set w1 4.83;
set w2 4.55;
set w3 5.25;
set w4 $w2;
set w5 $w1;

# Column Fiber Thicknesses
set t1 13.89;
```

```
set t2 21.50;
set t3 23.50;
set t4 $t2;
set t5 $t1;

# Create nodes & add to Domain
# node nodeId xCrd yCrd
node 1 0 0;
node 2 0 18;
node 3 0 36;
node 4 0 54;
node 5 0 $H;

# Boundary conditions
fix 1 1 1 1;

# Set Control Node and DOF
set IDctrlNode 5;
set IDctrlDOF 1;

# ------------------------------------------------------------------------
# Define uniaxial materials for 2D nDMaterial FSAM
# ------------------------------------------------------------------------

# STEEL .....................................................
# uniaxialMaterial Steel02 $tag $fy $Es $b $R0 $cR1 $cR2 $a1 $a2 $a3 $a4;

# steel X
set fyX 65.2;    # fy
set bx 0.01;     # strain hardening

# steel Y
set fyY 65.4;    # fy
set by 0.01;     # strain hardening

# steel misc
set Es 29000.0; # ksi
set R0 10.0;     # initial value of curvature parameter
set cR1 0.925;   # curvature degradation parameter
set cR2 0.15;    # curvature degradation parameter
set a1 0.01;     # isotropic strain hardening parameter
set a2 7.0;      # isotropic strain hardening parameter
set a3 0.01;     # isotropic strain hardening parameter
set a4 7.0;      # isotropic strain hardening parameter

# Build steel materials
uniaxialMaterial    Steel02  1 $fyX  $Es $bx  $R0 $cR1 $cR2 $a1 $a2 $a3
$a4; # steel X
uniaxialMaterial    Steel02  2 $fyY  $Es $by  $R0 $cR1 $cR2 $a1 $a2 $a3
$a4; # steel Y

# CONCRETE ..................................................
# uniaxialMaterial ConcreteCM $mattag $fpcc $epcc $Ec $rc $xcrn $ft $et
$rt $xcrp
```

```
# unconfined
set fpc 3.74;          # peak compressive stress
set ec0 -0.002;        # strain at peak compressive stress
set ft 0.335798;       # peak tensile stress
set et 0.00008;        # strain at peak tensile stress
set Ec 3486;           # Young's modulus
set xcrnu 1.022;       # cracking strain - compression
set xcrp 10000;        # cracking strain - tension
set ru 15;             # shape parameter - compression
set rt 1.2;            # shape parameter - tension

# confined
set fpcc    5.93;      # peak compressive stress
set ec0c    -0.0078;   # strain at peak compressive stress
set Ecc     4390;      # Young's modulus
set xcrnc   1.045;     # cracking strain - compression
set rc      15;        # shape parameter - compression

# Build concrete materials
uniaxialMaterial ConcreteCM 3 -$fpc   $ec0   $Ec  $ru  $xcrnu  $ft  $et
$rt  $xcrp; # unconfined concrete
uniaxialMaterial ConcreteCM 4 -$fpcc  $ec0c  $Ecc $rc  $xcrnc  $ft  $et
$rt  $xcrp; # confined concrete

# ------------------------------------------------------------------
#  Define 2D RC Panel Material FSAM
# ------------------------------------------------------------------

# Set Material Input Parameters
# Reinforcing ratios
set rouX1 0.0043; # X
set rouX2 0.0056;
set rouX3 0.0057;
set rouX4 $rouX2;
set rouX5 $rouX1;

set rouY1  0.0353; # Y
set rouY2  0.0162;
set rouY3  0.0128;
set rouY4  $rouY2;
set rouY5  $rouY1;

# Shear resisting mechanisms
set nu 0.2;            # friction coefficient
set alfadow 0.002;     # dowel action stiffness

# nDMaterial FSAM $mattag $rho $sX $sY $conc $rouX $rouY $nu $alfadow
nDMaterial FSAM   5    0   1     2     4  $rouX1 $rouY1  $nu  $alfadow;
nDMaterial FSAM   6    0   1     2     4  $rouX2 $rouY2  $nu  $alfadow;
nDMaterial FSAM   7    0   1     2     4  $rouX3 $rouY3  $nu  $alfadow;
nDMaterial FSAM   8    0   1     2     4  $rouX4 $rouY4  $nu  $alfadow;
nDMaterial FSAM    9    0   1     2     4  $rouX5 $rouY5  $nu  $alfadow;
```

```
# ------------------------------------------------------------------
#  Define SFI_MVLEM elements
# ------------------------------------------------------------------

# element SFI_MVLEM eleTag iNode jNode m c -thick fiberThick -width
fiberWidth -mat matTags
element SFI_MVLEM  1  1  2  5  0.4 -thick $t1 $t2 $t3 $t4 $t5 -width $w1
$w2 $w3 $w4 $w5 -mat 5 6 7 8 9
element SFI_MVLEM  2  2  3  5  0.4 -thick $t1 $t2 $t3 $t4 $t5 -width $w1
$w2 $w3 $w4 $w5 -mat 5 6 7 8 9
element SFI_MVLEM  3  3  4  5  0.4 -thick $t1 $t2 $t3 $t4 $t5 -width $w1
$w2 $w3 $w4 $w5 -mat 5 6 7 8 9
element SFI_MVLEM  4  4  5  5  0.4 -thick $t1 $t2 $t3 $t4 $t5 -width $w1
$w2 $w3 $w4 $w5 -mat 5 6 7 8 9

# ------------------------------
# End of model generation
# ------------------------------

# Initialize
initialize

# ------------------------------
# Recorder generation
# ------------------------------

# Nodal recorders
recorder Node -file $dataDir/MVLEM_Dtop.out -time -node $IDctrlNode -dof 1
2 disp

recorder Node -file $dataDir/MVLEM_DOFs.out -time -node 1 2 3 4 -dof 1 2 3
disp

# Element recorders
recorder Element -file $dataDir/MVLEM_Fgl.out -time -ele 1 2 3 globalForce

recorder Element -file $dataDir/MVLEM_Dsh.out -time -ele 1 2 3 ShearDef

recorder Element -file $dataDir/MVLEM_Curvature.out -time -ele 1 2 3
Curvature

recorder Element -file $dataDir/MVLEM_panel_strain.out -time -ele 1
RCPanel 1 panel_strain

recorder Element -file $dataDir/MVLEM_panel_stress.out -time -ele 1
RCPanel 1 panel_stress

recorder Element -file $dataDir/MVLEM_panel_stress_concrete.out -time -ele
1 RCPanel 1 panel_stress_concrete

recorder Element -file $dataDir/MVLEM_panel_stress_steel.out -time -ele 1
RCPanel 1 panel_stress_steel
```

```
recorder Element -file $dataDir/MVLEM_strain_stress_steel1.out -time -ele
1 RCPanel 1 strain_stress_steelX

recorder Element -file $dataDir/MVLEM_strain_stress_steel2.out -time -ele
1 RCPanel 1 strain_stress_steelY

recorder Element -file $dataDir/MVLEM_strain_stress_concrete1.out -time -
ele 1 RCPanel 1 strain_stress_concrete1

recorder Element -file $dataDir/MVLEM_strain_stress_concrete2.out -time -
ele 1 RCPanel 1 strain_stress_concrete2

recorder Element -file $dataDir/MVLEM_strain_stress_interlock1.out -time -
ele 1 RCPanel 1 strain_stress_interlock1

recorder Element -file $dataDir/MVLEM_strain_stress_interlock2.out -time -
ele 1 RCPanel 1 strain_stress_interlock2

recorder Element -file $dataDir/MVLEM_cracking_angles.out -time -ele 1
RCPanel 1 cracking_angles

# ---------------------------
# Define Axial Load
# ---------------------------

set N [expr 118.4]

# ------------------------------
# Set parameters for cyclic analysis
# ------------------------------

set iDmax "0.0028 0.0050 0.0081 0.0098 0.0150 0.0204 0.0258 0.0310 0.0417
0.0518 0.0622 0.0822 0.1026";# vector of displacement-cycle peaks, in
terms of storey drift ratio
set Dincr 0.1;         # displacement increment for pushover.
set CycleType Full;    # type of cyclic analysis: Full / Push / Half
set Ncycles 2;         # specify the number of cycles at each peak
set Tol 1.0e-4;
set LunitTXT "inch";
```

B.2 WALL SPECIMEN RW2: MVLEM MODEL GENERATION

```
# ------------------------------------------------------------------
# Simulation of wall flexural response using MVLEM
# Specimen: RW2 (Thomsen and Wallace, 1995)
# File Name: MVLEM_RW2.tcl
# ------------------------------------------------------------------

# ---------------------------------------------------------
# Start of model generation (Units: kip, in, sec, ksi)
# ---------------------------------------------------------

# Set Up Directories
set modelName "RW2";                # Model Name
set dataDir MVLEM_$modelName;       # Name of output folder
file mkdir $dataDir;

# Create ModelBuilder for 2D element (with two-dimensions and 3 DOF/node)
model BasicBuilder -ndm 2 -ndf 3

# -------------------------------------------
# Set geometry, nodes, boundary conditions
# -------------------------------------------

# Wall Geometry
set H 144.0;      # Wall height
set t 4.0;        # Wall thickness

# Create nodes
# node nodeId xCrd yCrd
node 1 0 0;
node 2 0 1.25;
node 3 0 1.75;
node 4 0 2.0;
node 5 0 5.25;
node 6 0 9.0;
node 7 0 18.0;
node 8 0 30.0;
node 9 0 36.0;
node 10 0 37.25;
node 11 0 37.75;
node 12 0 54.0;
node 13 0 72.0;
node 14 0 90.0;
node 15 0 108.0;
node 16 0 126.0;
node 17 0 $H;

# Boundary conditions
fix 1 1 1 1;      # Fixed condition at node 1

# Set Control Node and DOF
```

```
set IDctrlNode 17;
set IDctrlDOF 1;

# ------------------------------------------------------------------------
# Define uniaxial materials
# ------------------------------------------------------------------------
# STEEL .....................................................
# uniaxialMaterial SteelMPF $mattag $fyp $fyn $E0 $bp $bn $R0 $a1 $a2

# steel Y boundary
set fyYbp 57.3;  # fy - tension
set bybp 0.0185; # strain hardening - tension
set fyYbn 63.0;  # fy - compression
set bybn 0.02;         # strain hardening - compression

# steel Y web
set fyYwp 48.8;  # fy - tension
set bywp 0.035;  # strain hardening - tension
set fyYwn 65.0;  # fy - compression
set bywn 0.02;   # strain hardening - compression

# steel misc
set Es 29000.0;  # Young's modulus
set R0 20.0;     # initial value of curvature parameter
set a1 18.5;     # curvature degradation parameter
set a2 0.0015;   # curvature degradation parameter

# Build steel materials
# steel Y boundary
uniaxialMaterial    SteelMPF  1 $fyYbp $fyYbn $Es $bybp $bybn $R0 $a1 $a2;
# steel Y web
uniaxialMaterial    SteelMPF  2 $fyYwp $fyYwn $Es $bywp $bywn $R0 $a1 $a2;

# Set MVLEM Reinforcing Ratios
set rouYb 0.029333;    # Y boundary
set rouYw 0.003333;    # Y web

# CONCRETE ..................................................
# uniaxialMaterial ConcreteCM $mattag  $fpcc  $epcc  $Ec  $rc  $xcrn   $ft
$et  $rt   $xcrp <-GapClose $gap>

# unconfined
set fpc 6.2;           # peak compressive stress
set ec0 -0.0021;       # strain at peak compressive stress
set ft 0.295;          # peak tensile stress
set et 0.00008;        # strain at peak tensile stress
set Ec 4500;           # Young's modulus
set xcrnu 1.039;       # cracking strain - compression
set xcrp 10000;        # cracking strain - tension
set ru 7;              # shape parameter - compression
set rt 1.2;            # shape parameter - tension

# confined
set fpcc 6.9036;       # peak compressive stress
set ec0c -0.0033;      # strain at peak compressive stress
```

```
set Ecc 5091.3;        # Young's modulus
set xcrnc 1.0125;      # cracking strain - compression
set rc 7.3049;         # shape parameter - compression
# Build concrete materials
# confined concrete
uniaxialMaterial ConcreteCM 3 -$fpcc  $ec0c  $Ecc $rc  $xcrnc  $ft  $et
$rt  $xcrp -GapClose 1;
# unconfined concrete
uniaxialMaterial ConcreteCM 4 -$fpc   $ec0   $Ec  $ru  $xcrnu  $ft  $et
$rt  $xcrp -GapClose 1;

# SHEAR .....................................................
# uniaxialMaterial Elastic $matTag $E <$eta> <$Eneg>
# NOTE: large shear stiffness assigned since only flexural response
set Ashweb 192;                    # Gross area of the wall cross section
set G 1875000;                     # Shear Modulus
set GAs [expr $G * $Ashweb];       # Shear Stiffness

# Build shear material
uniaxialMaterial Elastic 5 $GAs;

# ------------------------------
#  Define MVLEM elements
# ------------------------------

# element MVLEM eleTag iNode jNode m c -thick fiberThick -width fiberWidth
-rho Rho -matConcrete matTagsConcrete -matSteel matTagsSteel -matShear
matTagShear"

element MVLEM  1  0.0 1   2  8 0.4 -thick $t $t $t $t $t $t $t $t -width
7.5 1.5 7.5 7.5 7.5 7.5 1.5 7.5 -rho $rouYb 0.0 $rouYw $rouYw $rouYw
$rouYw 0.0 $rouYb -matConcrete 3 4 4 4 4 4 4 3 -matSteel 1 2 2 2 2 2 2 1 -
matShear 5

element MVLEM  2  0.0 2   3  8 0.4 -thick $t $t $t $t $t $t $t $t -width
7.5 1.5 7.5 7.5 7.5 7.5 1.5 7.5 -rho $rouYb 0.0 $rouYw $rouYw $rouYw
$rouYw 0.0 $rouYb -matConcrete 3 4 4 4 4 4 4 3 -matSteel 1 2 2 2 2 2 2 1 -
matShear 5

element MVLEM  3  0.0 3   4  8 0.4 -thick $t $t $t $t $t $t $t $t -width
7.5 1.5 7.5 7.5 7.5 7.5 1.5 7.5 -rho $rouYb 0.0 $rouYw $rouYw $rouYw
$rouYw 0.0 $rouYb -matConcrete 3 4 4 4 4 4 4 3 -matSteel 1 2 2 2 2 2 2 1 -
matShear 5

element MVLEM  4  0.0 4   5  8 0.4 -thick $t $t $t $t $t $t $t $t -width
7.5 1.5 7.5 7.5 7.5 7.5 1.5 7.5 -rho $rouYb 0.0 $rouYw $rouYw $rouYw
$rouYw 0.0 $rouYb -matConcrete 3 4 4 4 4 4 4 3 -matSteel 1 2 2 2 2 2 2 1 -
matShear 5

element MVLEM  5  0.0 5   6  8 0.4 -thick $t $t $t $t $t $t $t $t -width
7.5 1.5 7.5 7.5 7.5 7.5 1.5 7.5 -rho $rouYb 0.0 $rouYw $rouYw $rouYw
$rouYw 0.0 $rouYb -matConcrete 3 4 4 4 4 4 4 3 -matSteel 1 2 2 2 2 2 2 1 -
matShear 5
```

```
element MVLEM  6  0.0 6   7  8 0.4 -thick $t $t $t $t $t $t $t $t -width
7.5 1.5 7.5 7.5 7.5 7.5 1.5 7.5 -rho $rouYb 0.0 $rouYw $rouYw $rouYw
$rouYw 0.0 $rouYb -matConcrete 3 4 4 4 4 4 4 3 -matSteel 1 2 2 2 2 2 2 1 -
matShear 5

element MVLEM  7  0.0 7   8  8 0.4 -thick $t $t $t $t $t $t $t $t -width
7.5 1.5 7.5 7.5 7.5 7.5 1.5 7.5 -rho $rouYb 0.0 $rouYw $rouYw $rouYw
$rouYw 0.0 $rouYb -matConcrete 3 4 4 4 4 4 4 3 -matSteel 1 2 2 2 2 2 2 1 -
matShear 5

element MVLEM  8  0.0 8   9  8 0.4 -thick $t $t $t $t $t $t $t $t -width
7.5 1.5 7.5 7.5 7.5 7.5 1.5 7.5 -rho $rouYb 0.0 $rouYw $rouYw $rouYw
$rouYw 0.0 $rouYb -matConcrete 3 4 4 4 4 4 4 3 -matSteel 1 2 2 2 2 2 2 1 -
matShear 5

element MVLEM  9  0.0 9   10 8 0.4 -thick $t $t $t $t $t $t $t $t -width
7.5 1.5 7.5 7.5 7.5 7.5 1.5 7.5 -rho $rouYb 0.0 $rouYw $rouYw $rouYw
$rouYw 0.0 $rouYb -matConcrete 3 4 4 4 4 4 4 3 -matSteel 1 2 2 2 2 2 2 1 -
matShear 5

element MVLEM  10 0.0 10  11 8 0.4 -thick $t $t $t $t $t $t $t $t -width
7.5 1.5 7.5 7.5 7.5 7.5 1.5 7.5 -rho $rouYb 0.0 $rouYw $rouYw $rouYw
$rouYw 0.0 $rouYb -matConcrete 3 4 4 4 4 4 4 3 -matSteel 1 2 2 2 2 2 2 1 -
matShear 5

element MVLEM  11 0.0 11  12 8 0.4 -thick $t $t $t $t $t $t $t $t -width
7.5 1.5 7.5 7.5 7.5 7.5 1.5 7.5 -rho $rouYb 0.0 $rouYw $rouYw $rouYw
$rouYw 0.0 $rouYb -matConcrete 3 4 4 4 4 4 4 3 -matSteel 1 2 2 2 2 2 2 1 -
matShear 5

element MVLEM  12 0.0 12  13 8 0.4 -thick $t $t $t $t $t $t $t $t -width
7.5 1.5 7.5 7.5 7.5 7.5 1.5 7.5 -rho $rouYb 0.0 $rouYw $rouYw $rouYw
$rouYw 0.0 $rouYb -matConcrete 3 4 4 4 4 4 4 3 -matSteel 1 2 2 2 2 2 2 1 -
matShear 5

element MVLEM  13 0.0 13  14 8 0.4 -thick $t $t $t $t $t $t $t $t -width
7.5 1.5 7.5 7.5 7.5 7.5 1.5 7.5 -rho $rouYb 0.0 $rouYw $rouYw $rouYw
$rouYw 0.0 $rouYb -matConcrete 3 4 4 4 4 4 4 3 -matSteel 1 2 2 2 2 2 2 1 -
matShear 5

element MVLEM  14 0.0 14  15 8 0.4 -thick $t $t $t $t $t $t $t $t -width
7.5 1.5 7.5 7.5 7.5 7.5 1.5 7.5 -rho $rouYb 0.0 $rouYw $rouYw $rouYw
$rouYw 0.0 $rouYb -matConcrete 3 4 4 4 4 4 4 3 -matSteel 1 2 2 2 2 2 2 1 -
matShear 5

element MVLEM  15 0.0 15  16 8 0.4 -thick $t $t $t $t $t $t $t $t -width
7.5 1.5 7.5 7.5 7.5 7.5 1.5 7.5 -rho $rouYb 0.0 $rouYw $rouYw $rouYw
$rouYw 0.0 $rouYb -matConcrete 3 4 4 4 4 4 4 3 -matSteel 1 2 2 2 2 2 2 1 -
matShear 5

element MVLEM  16 0.0 16  17 8 0.4 -thick $t $t $t $t $t $t $t $t -width
7.5 1.5 7.5 7.5 7.5 7.5 1.5 7.5 -rho $rouYb 0.0 $rouYw $rouYw $rouYw
$rouYw 0.0 $rouYb -matConcrete 3 4 4 4 4 4 4 3 -matSteel 1 2 2 2 2 2 2 1 -
matShear 5
```

```
# ------------------------------
# End of model generation
# ------------------------------

# Initialize
initialize

# ------------------------------
# Recorder generation
# ------------------------------

# Nodal recorders
recorder Node -file $dataDir/MVLEM_Dtop.out -time -node $IDctrlNode -dof 1
disp
recorder Node -file $dataDir/MVLEM_DOFs.out -time -node 1 2 3 4 -dof 1 2 3
disp

# Element recorders
recorder Element -file $dataDir/MVLEM_Fgl.out -time -ele 1 2 3 globalForce
recorder Element -file $dataDir/MVLEM_Curvature.out -time -ele 1 2 3
Curvature

# Fiber responses
recorder Element -file $dataDir/MVLEM_fiber_strain.out -time -ele 1
fiber_strain
recorder Element -file $dataDir/MVLEM_fiber_stress_concrete.out -time -ele
1 fiber_stress_concrete
recorder Element -file $dataDir/MVLEM_fiber_stress_steel.out -time -ele 1
fiber_stress_steel

# Shear spring response
recorder Element -file $dataDir/MVLEM_shear_force_def.out -time -ele 1
shear_force_deformation

# ---------------------
# Define Axial Load
# ---------------------

set N [expr 85.0]; # kips

# ------------------------------------------------------
# Set parameters for displacement controlled analysis
# ------------------------------------------------------

# vector of displacement-cycle peaks in terms of wall drift ratio
(flexural displacements)
set iDmax "0.000330792 0.001104233 0.002925758 0.004558709 0.006625238
0.010816268 0.014985823 0.019655056";
set Dincr 0.01;              # displacement increment for displacement
controlled analysis.
set CycleType Full;          # type of static analysis: Full / Push / Half
set Ncycles 1;               # specify the number of cycles at each peak
set Tol 1.0e-5;
set LunitTXT "inch";
```

B.3 WALL SPECIMEN RW-A15-P10-S78: SFI_MVLEM MODEL GENERATION

```
# ------------------------------------------------------------------
# Simulation of wall cyclic behavior using SFI_MVLEM
# Specimen: RW-A15-P10-S78 (Tran and Wallace, 2012)
# File Name: SFI_MVLEM_SP4.tcl
# ------------------------------------------------------------------

# ---------------------------------------------------------
# Start of model generation (Units: kip, in, sec, ksi)
# ---------------------------------------------------------

# Set Up Directories
set modelName "SP4";                    # Model Name
set dataDir SFI_MVLEM_$modelName;       # Name of output folder
file mkdir $dataDir;

# Create ModelBuilder for 2D element (with two-dimensions and 3 DOF/node)
model BasicBuilder -ndm 2 -ndf 3

# ------------------------------------------
# Set geometry, nodes, boundary conditions
# ------------------------------------------

# Wall Geometry
set H 72;         # Wall height
set t 6;          # Wall thickness

# Create nodes
# node nodeId xCrd yCrd
node 1 0 0;
node 2 0 12;
node 3 0 24;
node 4 0 40;
node 5 0 56;
node 6 0 $H;

# Boundary conditions
fix 1 1 1 1;      # Fixed condition at node 1

# Set Control Node and DOF
set IDctrlNode 6;
set IDctrlDOF 1;

# ------------------------------------------------------------------------
# Define uniaxial materials for 2D RC Panel Constitutive Model (FSAM)
# ------------------------------------------------------------------------

# STEEL .....................................................
# uniaxialMaterial SteelMPF $mattag $fyp $fyn $E0 $bp  $bn $R0 $a1 $a2

# steel X
set fyX 58.4103;        # fy
set bx 0.02;            # strain hardening
```

```
# steel Y web
set fyYw 58.4103;      # fy
set byw 0.02;          # strain hardening

# steel Y boundary
set fyYb 69.0;         # fy
set byb 0.005;         # strain hardening

# steel misc
set Esy 29000.0;       # Young's modulus
set Esx $Esy;          # Young's modulus
set R0 20.0;           # initial value of curvature parameter
set A1 18.5;           # curvature degradation parameter
set A2 0.0015;         # curvature degradation parameter

# Build steel materials
# steel X
uniaxialMaterial    SteelMPF  1 $fyX $fyX $Esx $bx $bx $R0 $A1 $A2;
# steel Y web
uniaxialMaterial    SteelMPF  2 $fyYw $fyYw $Esy $byw $byw $R0 $A1 $A2;
# steel Y boundary
uniaxialMaterial    SteelMPF  3 $fyYb $fyYb $Esy $byb $byb $R0 $A1 $A2;

# CONCRETE .....................................................
# uniaxialMaterial ConcreteCM $mattag  $fpcc  $epcc  $Ec  $rc  $xcrn   $ft
$et  $rt   $xcrp <-GapClose $gap>

# unconfined
set fpc 8.09;          # peak compressive stress
set ec0 -0.002371;     # strain at peak compressive stress
set ft 0.335798;       # peak tensile stress
set et 0.00008;        # strain at peak tensile stress
set Ec 5403.2172;      # Young's modulus
set xcrnu 1.022;       # cracking strain - compression
set xcrp 10000;        # cracking strain - tension
set ru 15;             # shape parameter - compression
set rt 1.2;            # shape parameter - tension

# confined
set fpcc 10.479723; # peak compressive stress
set ec0c -0.005873; # strain at peak compressive stress
set Ecc 5953.9187;     # Young's modulus
set xcrnc 1.023; # cracking strain - compression
set rc 12.072964;# shape parameter - compression

# Build concrete materials
uniaxialMaterial ConcreteCM 4 -$fpc   $ec0   $Ec  $ru  $xcrnu  $ft  $et
$rt  $xcrp -GapClose 0; # unconfined concrete
uniaxialMaterial ConcreteCM 5 -$fpcc  $ec0c  $Ecc $rc  $xcrnc  $ft  $et
$rt  $xcrp -GapClose 0; # confined concrete
```

```
# ------------------------------------
# Define 2D RC Panel Material (FSAM)
# ------------------------------------

# Reinforcing ratios
set rouXw 0.0074;      # X web
set rouXb 0.0082;      # X boundary
set rouYw 0.0074;      # Y web
set rouYb 0.0587;      # Y boundary

# Shear resisting mechanism parameters
set nu 0.8;            # friction coefficient
set alfadow 0.01;      # dowel action stiffness parameter

# nDMaterial FSAM $mattag   $rho  $sX  $sY  $conc  $rouX  $rouY  $nu
$alfadow
nDMaterial FSAM         6    0.0   1     2     4  $rouXw $rouYw  $nu
$alfadow; # Web (unconfined concrete)
nDMaterial FSAM         7    0.0   1     3     5  $rouXb $rouYb  $nu
$alfadow; # Boundary (confined concrete only)

# ------------------------------
# Define SFI_MVLEM elements
# ------------------------------

# element SFI_MVLEM eleTag iNode jNode m c -thick fiberThick -width
fiberWidth -mat matTags
element SFI_MVLEM  1  1  2 5 0.4 -thick $t $t $t $t $t -width 9 10 10 10 9
-mat 7 6 6 6 7
element SFI_MVLEM  2  2  3 5 0.4 -thick $t $t $t $t $t -width 9 10 10 10 9
-mat 7 6 6 6 7
element SFI_MVLEM  3  3  4 5 0.4 -thick $t $t $t $t $t -width 9 10 10 10 9
-mat 7 6 6 6 7
element SFI_MVLEM  4  4  5 5 0.4 -thick $t $t $t $t $t -width 9 10 10 10 9
-mat 7 6 6 6 7
element SFI_MVLEM  5  5  6 5 0.4 -thick $t $t $t $t $t -width 9 10 10 10 9
-mat 7 6 6 6 7

# ------------------------------
# End of model generation
# ------------------------------

# Initialize
initialize

# ------------------------------
# Recorder generation
# ------------------------------

# Nodal recorders
recorder Node -file $dataDir/MVLEM_Dtop.out -time -node $IDctrlNode -dof 1
disp
recorder Node -file $dataDir/MVLEM_DOFs.out -time -node 1 2 3 4 5 6 -dof 1
2 3 disp
```

```
# Element recorders
recorder Element -file $dataDir/MVLEM_Fgl.out -time -ele 1 2 3 4 5
globalForce
recorder Element -file $dataDir/MVLEM_Dsh.out -time -ele 1 2 3 4 5
ShearDef
recorder Element -file $dataDir/MVLEM_Curvature.out -time -ele 1 2 3 4 5
Curvature

# Single RC panel (macro-fiber) responses
recorder Element -file $dataDir/MVLEM_panel_strain.out -time -ele 1
RCPanel 1 panel_strain
recorder Element -file $dataDir/MVLEM_panel_stress.out -time -ele 1
RCPanel 1 panel_stress
recorder Element -file $dataDir/MVLEM_panel_stress_concrete.out -time -ele
1 RCPanel 1 panel_stress_concrete
recorder Element -file $dataDir/MVLEM_panel_stress_steel.out -time -ele 1
RCPanel 1 panel_stress_steel
recorder Element -file $dataDir/MVLEM_strain_stress_steel1.out -time -ele
1 RCPanel 1 strain_stress_steelX
recorder Element -file $dataDir/MVLEM_strain_stress_steel2.out -time -ele
1 RCPanel 1 strain_stress_steelY
recorder Element -file $dataDir/MVLEM_strain_stress_concrete1.out -time -
ele 1 RCPanel 1 strain_stress_concrete1
recorder Element -file $dataDir/MVLEM_strain_stress_concrete2.out -time -
ele 1 RCPanel 1 strain_stress_concrete2
recorder Element -file $dataDir/MVLEM_strain_stress_interlock1.out -time -
ele 1 RCPanel 1 strain_stress_interlock1
recorder Element -file $dataDir/MVLEM_strain_stress_interlock2.out -time -
ele 1 RCPanel 1 strain_stress_interlock2

# Cracking angles for all panels
recorder Element -file $dataDir/MVLEM_cracking_angles1.out -time -ele 1 2
3 4 5 RCPanel 1 cracking_angles
recorder Element -file $dataDir/MVLEM_cracking_angles2.out -time -ele 1 2
3 4 5 RCPanel 2 cracking_angles
recorder Element -file $dataDir/MVLEM_cracking_angles3.out -time -ele 1 2
3 4 5 RCPanel 3 cracking_angles
recorder Element -file $dataDir/MVLEM_cracking_angles4.out -time -ele 1 2
3 4 5 RCPanel 4 cracking_angles
recorder Element -file $dataDir/MVLEM_cracking_angles5.out -time -ele 1 2
3 4 5 RCPanel 5 cracking_angles

# ---------------------
# Define Axial Load
# ---------------------

set N [expr 149.0]; # kips

# ------------------------------------------------------
# Set parameters for displacement controlled analysis
# ------------------------------------------------------

# vector of displacement-cycle peaks in terms of wall drift ratio
set iDmax "0.001 0.0025 0.005 0.0075 0.01 0.015 0.02 0.03";
```

```
set Dincr 0.01;        # displacement increment
set CycleType Full;    # type of cyclic analysis: Full / Push / Half
set Ncycles 2;         # specify the number of cycles at each peak
set Tol 1.0e-5;
set LunitTXT "inch";
```

B.4 GRAVITY ANALAYSIS

```
# ------------------------------
# Gravity load analysis
# File Name: gravity.tcl
# ------------------------------

# Generate the model and load input variables
source MVLEM_RW2.tcl;        # model generation (RW2)
# source SFI_MVLEM_SP4.tcl;  # model generation (RW-A15-P10-S78)
# source SFI_MVLEM_Shanmugam.tcl; # model generation (H/D(3)-T/M(0)/1.32%)

# Create a Plain load pattern with a linear TimeSeries
pattern Plain 1 "Linear" {

    # Create the nodal load - command: load nodeID xForce yForce
    load $IDctrlNode  0.0 [expr  -$N]  0.0
}

# ------------------------------
# Analysis generation
# ------------------------------

# Create the integration scheme, the LoadControl scheme using steps of 0.1
integrator LoadControl 0.1

# Create the system of equation, a sparse solver with partial pivoting
system BandGeneral

# Create the convergence test, the norm of the residual with a tolerance
of
# 1e-5 and a max number of iterations of 100
test NormDispIncr $Tol  100 1

# Create the DOF numberer, the reverse Cuthill-McKee algorithm
numberer RCM

# Create the constraint handler, the transformation method
constraints Transformation

# Create the solution algorithm, a Newton-Raphson algorithm
algorithm Newton  # -initialThenCurrent

# Create the analysis object
analysis   Static

# Run analysis
analyze 10
```

B.5 LATERAL ANALYSIS (DISPLACEMENT-CONTROLLED)

```
# ----------------------------------------------------
# Displacement Controlled Analysis
# File Name: dispControl.tcl
# ----------------------------------------------------

source gravity.tcl; # gravity analysis file

puts "Model generated and gravity load applied successfully";

# Set the gravity loads to be constant & reset the time in the domain
loadConst -time 0.0

set Fact $H; # scale drift ratio by story height for displacement cycles

# Set lateral load pattern with a Linear TimeSeries
set Plateral 1.0;      # Reference lateral load
pattern Plain 200 "Linear" {

      load $IDctrlNode $Plateral 0.0 0.0
}

set load_step 1;

# set up analysis parameters
source LibAnalysisStaticParameters.tcl;

#  perform Static Cyclic Displacements Analysis
source LibGeneratePeaks.tcl

set fmt1 "%s Cyclic analysis: CtrlNode %.3i, dof %.1i, Disp=%.4f %s";
      # format for screen/file output of DONE/PROBLEM analysis

foreach Dmax $iDmax {

      set iDstep [GeneratePeaks $Dmax $Dincr $CycleType $Fact];# this proc
is defined above

      for {set i 1} {$i <= $Ncycles} {incr i 1} {

            set zeroD 0
            set D0 0.0
            foreach Dstep $iDstep {
                  set D1 $Dstep
                  set Dincr [expr $D1 - $D0]
                  integrator DisplacementControl $IDctrlNode $IDctrlDOF
$Dincr
                  analysis Static
                  # first analyze command
                  set ok [analyze 1]
                  # if convergence failure
                  if {$ok != 0} {
                        # if analysis fails, we try some other stuff
```

```
                        if {$ok != 0} {
                              puts "Trying Newton with Initial Tangent .."
                              test NormDispIncr   $Tol 2000 0
                              algorithm Newton -initial
                              set ok [analyze 1]
                              test $testTypeStatic $TolStatic
$maxNumIterStatic    0
                              algorithm $algorithmTypeStatic 200 1
                        }
                        if {$ok != 0} {
                              puts "Trying Broyden .."
                              algorithm Broyden 300
                              set ok [analyze 1 ]
                              algorithm $algorithmTypeStatic
                        }
                        if {$ok != 0} {
                              puts "Trying NewtonWithLineSearch .."
                              algorithm NewtonLineSearch 0.8
                              set ok [analyze 1]
                              algorithm $algorithmTypeStatic
                        }
                        if {$ok != 0} {
                              set putout [format $fmt1 "PROBLEM"
$IDctrlNode $IDctrlDOF [nodeDisp $IDctrlNode $IDctrlDOF] $LunitTXT]
                              puts $putout
                              return -1
                        }; # end if
                  }; # end if
                  # -----------------------------------------------------
                  set D0 $D1;            # move to next step

                  # print load step on the screen
                  puts "Load Step: [expr $load_step]"
                  set load_step [expr $load_step+1]

            }; # end Dstep

      };    # end i

};    # end of iDmaxCycl
# ------------------------------------------------------------------------

if {$ok != 0 } {
      puts [format $fmt1 "PROBLEM" $IDctrlNode $IDctrlDOF [nodeDisp
$IDctrlNode $IDctrlDOF] $LunitTXT]
} else {
      puts [format $fmt1 "DONE"  $IDctrlNode $IDctrlDOF [nodeDisp
$IDctrlNode $IDctrlDOF] $LunitTXT]
}

# Print the state at control node
print node $IDctrlNode
```

B.6 DEFINITION OF STATIC ANALYSIS PARAMETERS

```
# ----------------------------------------------------
# File Name: LibAnalysisStaticParameters.tcl
# ----------------------------------------------------

# static analysis parameters
# All variables set as global variables (rather than set command)
#    so that these variables can be uploaded by a procedure
#                                  Silvia Mazzoni & Frank McKenna, 2006

# CONSTRAINTS handler -- Determines how the constraint equations are
enforced in the analysis
(http://opensees.berkeley.edu/OpenSees/manuals/usermanual/617.htm)
#          Plain Constraints -- Removes constrained DOFs from the system
of equations (only for homogeneous equations)
#          Lagrange Multipliers -- Uses the method of Lagrange multipliers
to enforce constraints
#          Penalty Method -- Uses penalty numbers to enforce constraints -
-good for static analysis with non-homogeneous eqns (rigidDiaphragm)
#          Transformation Method -- Performs a condensation of constrained
DOFs
variable constraintsTypeStatic Plain;               # default;
if {  [info exists RigidDiaphragm] == 1} {
      if {$RigidDiaphragm=="ON"} {
            variable constraintsTypeStatic Lagrange;# for large model, try
Transformation
      };    # if rigid diaphragm is on
};          # if rigid diaphragm exists
constraints $constraintsTypeStatic

# DOF NUMBERER (number the DOFs in the domain):
(http://opensees.berkeley.edu/OpenSees/manuals/usermanual/366.htm)
#   determines the mapping between equation numbers and degrees-of-freedom
#          Plain -- Uses the numbering provided by the user
#          RCM -- Renumbers the DOF to minimize the matrix band-width
using the Reverse Cuthill-McKee algorithm
set numbererTypeStatic RCM
numberer $numbererTypeStatic

# SYSTEM(http://opensees.berkeley.edu/OpenSees/manuals/usermanual/371.htm)
# Linear Equation Solvers (how to store and solve the system of equations
in the analysis)
#   -- provide the solution of the linear system of equations Ku = P. Each
solver is tailored to a specific matrix topology.
#          ProfileSPD -- Direct profile solver for symmetric positive
definite matrices
#          BandGeneral -- Direct solver for banded unsymmetric matrices
#          BandSPD -- Direct solver for banded symmetric positive definite
matrices
#          SparseGeneral -- Direct solver for unsymmetric sparse matrices
#          SparseSPD -- Direct solver for symmetric sparse matrices
#          UmfPack -- Direct UmfPack solver for unsymmetric matrices
set systemTypeStatic BandGeneral;       # try UmfPack for large model
system $systemTypeStatic
```

```
# TEST: # convergence test to
# Convergence TEST
(http://opensees.berkeley.edu/OpenSees/manuals/usermanual/360.htm)
#   -- Accept the current state of the domain as being on the converged
solution path
#   -- determine if convergence has been achieved at the end of an
iteration step
#          NormUnbalance -- Specifies a tolerance on the norm of the
unbalanced load at the current iteration
#          NormDispIncr -- Specifies a tolerance on the norm of the
displacement increments at the current iteration
#          EnergyIncr-- Specifies a tolerance on the inner product of the
unbalanced load and displacement increments at the current iteration
#          RelativeNormUnbalance --
#          RelativeNormDispIncr --
#          RelativeEnergyIncr --
variable TolStatic 1.e-5;          # Convergence Test: tolerance
variable maxNumIterStatic 100;     # Convergence Test: maximum number of
iterations that will be performed before "failure to converge" is returned
variable printFlagStatic 0;        # Convergence Test: flag used to print
information on convergence (optional)        # 1: print information on
each step;
variable testTypeStatic NormDispIncr;   # Convergence-test type
test $testTypeStatic $TolStatic $maxNumIterStatic $printFlagStatic;
# for improved-convergence procedure:
      variable maxNumIterConvergeStatic 2000;
      variable printFlagConvergeStatic 1;

# Solution ALGORITHM: -- Iterate from the last time step to the current
(http://opensees.berkeley.edu/OpenSees/manuals/usermanual/682.htm)
#          Linear -- Uses the solution at the first iteration and
continues
#          Newton -- Uses the tangent at the current iteration to iterate
to convergence
#          ModifiedNewton -- Uses the tangent at the first iteration to
iterate to convergence
#          NewtonLineSearch --
#          KrylovNewton --
#          BFGS --
#          Broyden --
variable algorithmTypeStatic Newton
algorithm $algorithmTypeStatic;

# Static INTEGRATOR: -- determine the next time step for an analysis
(http://opensees.berkeley.edu/OpenSees/manuals/usermanual/689.htm)
#          LoadControl -- Specifies the incremental load factor to be
applied to the loads in the domain
#          DisplacementControl -- Specifies the incremental displacement
at a specified DOF in the domain
#          Minimum Unbalanced Displacement Norm -- Specifies the
incremental load factor such that the residual displacement norm in
minimized
#          Arc Length -- Specifies the incremental arc-length of the load-
displacement path
```

```
# Transient INTEGRATOR: -- determine the next time step for an analysis
including inertial effects
#          Newmark -- The two parameter time-stepping method developed by
Newmark
#          HHT -- The three parameter Hilbert-Hughes-Taylor time-stepping
method
#          Central Difference -- Approximates velocity and acceleration by
centered finite differences of displacement
integrator DisplacementControl  $IDctrlNode   $IDctrlDOF $Dincr

# ANALYSIS  -- defines what type of analysis is to be performed
(http://opensees.berkeley.edu/OpenSees/manuals/usermanual/324.htm)
#          Static Analysis -- solves the KU=R problem, without the mass or
damping matrices.
#          Transient Analysis -- solves the time-dependent analysis. The
time step in this type of analysis is constant. The time step in the
output is also constant.
#          variableTransient Analysis -- performs the same analysis type
as the Transient Analysis object. The time step, however, is variable.
This method is used when
#                  there are convergence problems with the Transient
Analysis object at a peak or when the time step is too small. The time
step in the output is also variable.
set analysisTypeStatic Static
analysis $analysisTypeStatic
```

B.7 GENERATION OF DISPLACEMENT HISTORY

```
# ----------------------------------------------------
# File Name: LibAnalysisStaticParameters.tcl
# ----------------------------------------------------

# GeneratePeaks $Dmax $DincrStatic $CycleType $Fact
proc GeneratePeaks {Dmax {DincrStatic 0.01} {CycleType "Full"} {Fact 1} }
{;
# generate incremental disps for Dmax
# this proc creates a file which defines a vector then executes the file
to return the vector of disp. increments
# by Silvia Mazzoni, 2006
# input variables
#     $Dmax : peak displacement (can be + or negative)
#     $DincrStatic     : displacement increment (optional, default=0.01,
independently of units)
#     $CycleType  : Full (0->+peak), Half (0->+peak->0), Full (0->+peak->0-
>-peak->0)   (optional, def=Full)
#     $Fact : scaling factor (optional, default=1)
#     $iDstepFileName  : file name where displacement history is stored
temporarily, until next disp. peak
# output variable
#     $iDstep     : vector of displacement increments
      file mkdir data
      set outFileID [open data/tmpDsteps.tcl w]
      set Disp 0.
```

```
      puts $outFileID "set iDstep { ";puts $outFileID $Disp;puts
$outFileID $Disp;# open vector definition and some 0
      set Dmax [expr $Dmax*$Fact]; # scale value
      if {$Dmax<0} {;  # avoid the divide by zero
            set dx [expr -$DincrStatic]
      } else {
            set dx $DincrStatic;
      }
      set NstepsPeak [expr int(abs($Dmax)/$DincrStatic)]

      for {set i 1} {$i <= $NstepsPeak} {incr i 1} {; # zero to one
            set Disp [expr $Disp + $dx]
            puts $outFileID $Disp;                    # write to file
      }
      if {$CycleType !="Push"} {
            for {set i 1} {$i <= $NstepsPeak} {incr i 1} {; # one to zero
                  set Disp [expr $Disp - $dx]
                  puts $outFileID $Disp;                  # write to file
            }
            if {$CycleType !="Half"} {
                  for {set i 1} {$i <= $NstepsPeak} {incr i 1} {;
      # zero to minus one
                        set Disp [expr $Disp - $dx]
                        puts $outFileID $Disp;            # write to file
                  }
                  for {set i 1} {$i <= $NstepsPeak} {incr i 1} {;
      # minus one to zero
                        set Disp [expr $Disp + $dx]
                        puts $outFileID $Disp;            # write to file
                  }
            }
      }
      puts $outFileID " }";        # close vector definition
      close $outFileID
      source data/tmpDsteps.tcl;   # source tcl file to define entire
vector
      return $iDstep
```

Appendix C Input Files: Dynamic Analysis of Wall–Frame Building System

C.1 WALL–FRAME SYSTEM MODEL GENERATION

```
# ------------------------------------------------------------
# Example 3: Dynamic analysis of a wall-frame system using SFI-MVLEM
# File Name: 5storyWF_SFI.tcl
# ------------------------------------------------------------

# ********************************************************************
# * BUILD MODEL AND RUN GRAVITY ANALYSIS (Units: kips, inches, seconds)
# ********************************************************************

# Clear all memory
wipe all

# INPUT START ***************************************************************

# Set Up Directories -----------------------------------
# Define Model Name
set modelName "5story_WF_SFI";

# Set up output directory
set dataDir $modelName;           # name of output folder
file mkdir $dataDir;              # create output folder

# Building Geometry ------------------------------------

# Define model builder
model BasicBuilder -ndm 2 -ndf 3

# Define basic geometry ..............................
# Vertical geometry
set NumStories 5;
set NumFramesPerWall 1;
set HStory [expr 12.0*12.0];            # Story height, inches
set HTotal [expr $NumStories*$HStory];  # Total building height

# Horizontal geometry
set L1 [expr 20.0*12.0];          # Span L1, inches
set L2 [expr 20.0*12.0];          # Span L2, inches
```

```
# Wall geometry
set Lw [expr 20.0*12.0];          # Wall length, inches
set LengthBoundEl 30;             # Boundary Length
set Twall 12.0;                   # Wall thickness
set WallElPerStory 2;             # Number of wall elements per story (if
use other than 2 have to correct node 1xx coordinates input)

# Define beam geometry & parameters
set Dbeam 32.0;                   # Beam Depth
set Wbeam 18.0;                   # Beam Width
set Abeam [expr $Dbeam*$Wbeam];   # Cross-sectional area, full section
set Ibeam [expr 0.35*$Wbeam*pow($Dbeam,3.0)/12.0]; # Moment of inertia,
cracked section at 0.35EI
set Abeam [expr $NumFramesPerWall*$Abeam]; # Multiply Area of a single
beam with number of frames
set Ibeam [expr $NumFramesPerWall*$Ibeam]; # Multiply Moment of Inertia of
a single beam with number of frames
set MybeamTop 11232.0; # Yield moment at plastic hinge location, 7-#9 top
set MybeamBot 6624.0;  # Yield moment at plastic hinge location, 5-#8 bot.

# Define column geometry & parameters
set Dcol 28.0;                    # Beam Depth
set Wcol 28.0;                    # Beam Width
set Acol [expr $Dcol*$Wcol];      # Cross-sectional area, full section
set kcol {0.55 0.42 0.34 0.30 0.30};    # Array of column stiffness
modifiers {level_1 level_2 ...}
set Icol [expr $Wcol*pow($Dcol,3.0)/12.0];    # Moment of inertia,
uncracked
set Acol [expr $NumFramesPerWall*$Acol];      # Multiply Area of a single
column with number of frames
set Icol [expr $NumFramesPerWall*$Icol];      # Multiply Moment of Inertia
of a single column with number of frames
set Mycol 11250.0;                            # Average col yield moment
at plastic hinge location
#(taken as the average of col My at all levels), corresponding to what
axial load Pmin.

set BeamPHL [expr $Dcol/2.0];                 # Beam plastic hinge
location w.r.t. the joint node (@ face of column)
set ColumnPHL [expr $Dbeam/2.0];              # Column plastic hinge
location w.r.t. the joint node (@face of beam)

# Define rigid beam/column properties
set A_rigid 1.0e9;
set I_rigid 1.0e9;
set Econ_rigid 1.0e9;

# Calculate floor masses - nodal mass
set g 386.4;                # Acceleration due to gravity, in/(sec^2)
set pi 3.141593;            # pi
set WallWeight 360.0;                              # Wall weight, 0.15
ksf x tributary wall mass =0.15 ksf*60'*20'
set FrameWeight 270.0;                             # Frame weight, 0.15
ksf x tributary frame mass =0.15 ksf*60'*10'
```

```
set PDWeight 360;                                    # P-D column weight,
0.15 psf remaining floor mass  =0.15 ksf*60'*40'
set WallNodalMass      [expr $WallWeight/$g]; # Floor nodal mass
set FrameNodalMass     [expr $FrameWeight/$g];      # Floor nodal mass
set PDNodalMass  [expr $PDWeight/$g];   # Floor nodal mass
set Negligible 1.0e-9;                               # A very small number
to avoid problems with zero

# Define gravity loads on beams (line) and walls (nodal)
set wLineBeam_floor 0.133;   # DL + 0.25*LL = (0.15+0.25*0.04)*10.0ft =
1.6 k/ft = 0.133 k/in
set wNodalWall_floor 128;    # DL + 0.25*LL = (0.15+0.25*0.04)*20.0ft =
3.2 k/ft => nodalLoad = 3.2k/ft*40ft = 128 kips

# MODEL GENERATION ***********************************************************

# Nodes -----------------------------------------

# Command: node nodeID x-coord y-coord -mass mass_dof1 mass_dof2 mass_dof3
# Ground Floor Nodes - no mass
node 100    0.0   0.0;                          # Axis 1 (C.S. ORIGIN)
node 200    [expr $Lw/2.0 + $L1]   0.0;        # Axis 2
node 300    [expr $Lw/2.0 + $L1 + $L2]   0.0;  # Axis 3

for {set i 1} {$i <= $NumStories} {incr i} {
      node [expr 100 + (2*$i - 1)] 0.0
                  [expr (2*$i - 1)*$HStory/$WallElPerStory];    # 1xx -
Wall @ 1 - no mass at inter-story nodes
      node [expr 100 + 2*$i]             0.0
                        [expr $i*$HStory] -mass $WallNodalMass $Negligible
$Negligible;     # 1xx - Wall   @ 1 - mass
      node [expr 200 + $i]               [expr $Lw/2.0 + $L1]
            [expr $i*$HStory] -mass $FrameNodalMass $Negligible
$Negligible;     # 2xx - Column @ 2 - mass
      node [expr 300 + $i]               [expr $Lw/2.0 + $L1 + $L2]
            [expr $i*$HStory] -mass $FrameNodalMass $Negligible
$Negligible;     # 3xx - Column @ 3 - mass
      node [expr 700 + $i]               [expr $Lw/2.0 + $L1 + $BeamPHL]
            [expr $i*$HStory];                              # 7xx - Right
beam plastic hinge location @ 2
      node [expr 7000 + $i]              [expr $Lw/2.0 + $L1 + $BeamPHL]
            [expr $i*$HStory];                              # 7xxx - Right
beam plastic hinge location @ 2
      node [expr 800 + $i]               [expr $Lw/2.0 + $L1  + $L2 -
$BeamPHL]   [expr $i*$HStory];                              # 8xx - Left beam
plastic hinge location @ 3
      node [expr 8000 + $i]              [expr $Lw/2.0 + $L1  + $L2 -
$BeamPHL]   [expr $i*$HStory];                              # 8xxx - Left
beam plastic hinge location @ 3
      node [expr 2000 +(2*$i - 1)]       [expr $Lw/2.0 + $L1]
            [expr ($i - 1)*$HStory + $ColumnPHL];   # 2xxx - Column
plastic hinge location @ 2
      node [expr 2000 +2*$i]                    [expr $Lw/2.0 + $L1]
                  [expr $i*$HStory - $ColumnPHL];         # 2xxx - Column
plastic hinge location @ 2
```

```
      node [expr 20000 +(2*$i - 1)]      [expr $Lw/2.0 + $L1]
            [expr ($i - 1)*$HStory + $ColumnPHL];   # 2xxxx - Column
plastic hinge location @ 2
      node [expr 20000 +2*$i]            [expr $Lw/2.0 + $L1]
            [expr $i*$HStory - $ColumnPHL];         # 2xxxx - Column
plastic hinge location @ 2
      node [expr 3000 +(2*$i - 1)]       [expr $Lw/2.0 + $L1 + $L2]
            [expr ($i - 1)*$HStory + $ColumnPHL];   # 3xxx - Column
plastic hinge location @ 3
      node [expr 30000 +(2*$i - 1)]      [expr $Lw/2.0 + $L1 + $L2]
            [expr ($i - 1)*$HStory + $ColumnPHL];   # 3xxxx - Column
plastic hinge location @ 3
      node [expr 3000 +2*$i]                   [expr $Lw/2.0 + $L1 + $L2]
                  [expr $i*$HStory - $ColumnPHL];         # 3xxx - Column
plastic hinge location @ 3
      node [expr 30000 +2*$i]            [expr $Lw/2.0 + $L1 + $L2]
            [expr $i*$HStory - $ColumnPHL];         # 3xxxx - Column
plastic hinge location @ 3

}

# Define boundary conditions at ground nodes
fix 100 1 1 1;         # Fix node 1 in X, Y, Z-dir
fix 200 1 1 1;         # Fix node 2 in X, Y, Z-dir
fix 300 1 1 1;         # Fix node 2 in X, Y, Z-dir

# Apply rigid diaphragm, i.e. all nodes in a floor to have the same
lateral displacement
for {set i 1} {$i <= $NumStories} {incr i} {
      equalDOF [expr 100 + 2*$i] [expr 200 + $i] 1;
      equalDOF [expr 100 + 2*$i] [expr 300 + $i] 1;
}

# Set controlling parameters for displacement controlled analysis
set IDctrlNode [expr 100 + 2*$NumStories];    # Controlling node, Right-
side, roof node
set IDctrlDOF 1; # Controlling DOF, Constrain X-dir movements

puts "Nodes defined."

# Material / Element Tags -----------------------------------
# Material tags
set MatReinf 1;        # Steel
set MatUncConc 2;      # Unconfined concrete
set MatConConc 3;      # Confined conditions
set MatFSAM_Unc 4;     # Unconfined concrete(FSAM) - wall
set MatFSAM_Con 5;     # Confined concrete(FSAM) - wall
```

```
# Wall Section (SFI_MVLEM) ------------------------------------------
# Define steel material ..............................................
# Command: uniaxialMaterial Steel02 $tag $fy $Es $b $R0 $cR1 $cR2 $a1 $a2
$a3 $a4

# Define reinforcement in X(horiz.), Y(vertical) in both boundary and web
set fy 60.0;          # fy
set b 0.015;          # strain hardening

# Reinforcing steel parameters
set Es 29000.0;       # Young's modulus
set R0 20.0;          # Initial value of curvature parameter
set cR1 0.925;        # Curvature degradation parameter
set cR2 0.15;         # Curvature degradation parameter
set a1 0.0;           # Default isotropic hardening parameter
set a2 1.0;           # Default isotropic hardening parameter
set a3 0.0;           # Default isotropic hardening parameter
set a4 1.0;           # Default isotropic hardening parameter

# Build steel material
uniaxialMaterial Steel02 $MatReinf $fy $Es $b $R0 $cR1 $cR2 $a1 $a2 $a3
$a4

# Define concrete materials .........................................
# Command: uniaxialMaterial ConcreteCM $matTag $fpcc $epcc $Ec $rc $xcrn
$ft $et $rt $xcrp  <-GapClose $gap>

# Unconfined concrete
set fc_uc 5.0;        # peak compressive stress
set ec0_uc -0.0020;   # strain at peak compressive stress
set Ec_uc [expr 57.0*pow($fc_uc*1000.0,0.5)]; # Young's modulus
set r_uc 15.0;        # shape parameter - compression
set xcrn_uc 1.015;    # cracking strain - compression
set ft [expr 3.7334/1000*pow(abs($fc_uc)*1000,0.5)]; # peak tensile stress
set et 0.00008;       # strain at peak tensile stress
set rt 1.2;           # shape parameter - tension
set xcrp 10000.0;     # cracking strain - tension

# Confined concrete
set fc_con 7.705;     # peak compressive stress
set ec0_con -0.0050;  # strain at peak compressive stress
set Ec_con [expr 57.0*pow($fc_con*1000.0,0.5)];    # Young's modulus
set r_con 13;         # shape parameter - compression
set xcrn_con 1.03;    # cracking strain - compression

# Build concrete materials
uniaxialMaterial ConcreteCM $MatUncConc -$fc_uc  $ec0_uc  $Ec_uc  $r_uc
$xcrn_uc  $ft $et $rt $xcrp; # Unconfined concrete
uniaxialMaterial ConcreteCM $MatConConc -$fc_con $ec0_con $Ec_con $r_con
$xcrn_con $ft $et $rt $xcrp; # Confined concrete

# Define FSAM (Fixed-Strut Angle Model) ..............................
# Command: nDMaterial FSAM $matTag $rho $sX $sY $conc $rouX $rouY $nu
$alfadow
```

```
set rho   0.0;          # Density, use 0.0 (mass assigned at nodes)
set rouXw 0.0025;       # Reinforcing in X (horizontal) direction, web
set rouYw 0.0025;       # Reinforcing in Y (vertical) direction, web
set rouXb $rouXw;       # Reinforcing in X (horizontal) direction, boundary
set rouYb 0.0693;       # Reinforcing in Y (vertical) direction, boundary
(16-#11 @ each boundary)

set nu 1.0;             # Friction coefficient (0.0 < $nu < 1.0)
set alfadow 0.01;       # Stiffness coefficient of reinforcing dowel action
(0.0 < $alfadow < 0.1)

# Build FSAM RC panel materials
nDMaterial FSAM $MatFSAM_Unc $rho $MatReinf $MatReinf $MatUncConc $rouXw
$rouYw $nu $alfadow;          # Unconfined concrete, web
nDMaterial FSAM $MatFSAM_Con $rho $MatReinf $MatReinf $MatConConc $rouXb
$rouYb $nu $alfadow;          # Confined concrete, boundary

# Define SFI_MVLEM wall elements ....................................
set n_fibers 6;  # No. of macro fibers in wall (1 per each boundary, rest
for web)
set widthWebEl [expr ($Lw - 2*$LengthBoundEl)/($n_fibers-2)]; # Width of
web element
set c_rot 0.4; # Center of rotation with respect to iNode (0.4 recomm.)

# Command: element SFI_MVLEM eleTag iNode jNode m c -thick fiberThick -
width fiberWidth -mat matTags
for {set i 1} {$i <= [expr 2*$NumStories]} {incr i} {
      element SFI_MVLEM [expr 1000 + $i] [expr 100 + $i - 1] [expr 100 +
$i] $n_fibers $c_rot -thick $Twall $Twall $Twall $Twall $Twall $Twall -
width $LengthBoundEl $widthWebEl $widthWebEl $widthWebEl $widthWebEl
$LengthBoundEl -mat $MatFSAM_Con $MatFSAM_Unc $MatFSAM_Unc $MatFSAM_Unc
$MatFSAM_Unc $MatFSAM_Con;
}
puts "Wall elements defined."

# Beam Section ----------------------------------------
# Define section tags & geometric transformation for beam-column element
set BeamTransTag 1;

# Command: geomTransf Linear $transfTag <-jntOffset $dXi $dYi $dXj $dYj>
geomTransf Linear $BeamTransTag;

# Define beam elements
# Command: element elasticBeamColumn $eleID $iNode $jNode $A $E $I
$transfID
for {set i 1} {$i <= $NumStories} {incr i} {
      element elasticBeamColumn  [expr 3300 + $i] [expr 700 + $i]    [expr
800 + $i] $Abeam $Ec_uc $Ibeam $BeamTransTag; # 3xx - Beams 2-3
      element elasticBeamColumn  [expr 33300 + $i] [expr 200 + $i]   [expr
7000 + $i] $Abeam $Ec_uc $Ibeam $BeamTransTag;# 333xx - Joint Beams @ 2R
      element elasticBeamColumn  [expr 88800 + $i] [expr 8000 + $i]  [expr
300 + $i] $Abeam $Ec_uc $Ibeam $BeamTransTag; # 888xx - Joint Beams @ 3L
}
puts "Beam elements defined."
```

```
# Column Section ----------------------------------------
# Define section tags & geometric transformation for beam-column element
set ColTransTag 2;

# Command: geomTransf Linear $transfTag <-jntOffset $dXi $dYi $dXj $dYj>
geomTransf Linear $ColTransTag;

# Define column elements
# Command: element elasticBeamColumn $eleID $iNode $jNode $A $E $I
$transfID
for {set i 1} {$i <= $NumStories} {incr i} {

      set coeff [lindex $kcol [expr $i - 1]]
      set Icol_st [expr $coeff*$Icol];

      element elasticBeamColumn  [expr 2000 + $i] [expr 2000 + (2*$i - 1)]
[expr 2000 + 2*$i] $Acol $Ec_uc $Icol_st $ColTransTag; # 2xxx - Columns @
2
      element elasticBeamColumn  [expr 3000 + $i] [expr 3000 + (2*$i - 1)]
[expr 3000 + 2*$i] $Acol $Ec_uc $Icol_st $ColTransTag; # 3xxx - Columns @
3

      element elasticBeamColumn  [expr 20000 + (2*$i - 1)] [expr 20000 +
2*$i] [expr 200 + $i] $Acol $Ec_uc $Icol_st $ColTransTag; # 200xx - Joint
Column @ 2D - property?
      element elasticBeamColumn  [expr 30000 + (2*$i - 1)] [expr 30000 +
2*$i] [expr 300 + $i] $Acol $Ec_uc $Icol_st $ColTransTag; # 300xx - Joint
Column @ 3D - property?
}
      # exceptions - bottom column joint elements
      set coeff [lindex $kcol 0]
      set Icol_st [expr $coeff*$Icol];

      element elasticBeamColumn  [expr 20000] [expr 200]     [expr 20001]
$Acol $Ec_uc $Icol_st $ColTransTag; # 20000 - Joint Column @ 2U -
property?
      element elasticBeamColumn  [expr 30000] [expr 300]     [expr 30001]
$Acol $Ec_uc $Icol_st $ColTransTag; # 30000 - Joint Column @ 3U -
property?

for {set i 1} {$i <= [expr $NumStories - 1]} {incr i} {

      set coeff [lindex $kcol [expr $i]]
      set Icol_st [expr $coeff*$Icol];

      element elasticBeamColumn  [expr 20000 + 2*$i] [expr 200 + $i]
[expr 20000 + (2*$i + 1)]  $Acol $Ec_uc $Icol_st $ColTransTag; # 200xx -
Joint Column @ 2U - property?
      element elasticBeamColumn  [expr 30000 + 2*$i] [expr 300 + $i]
[expr 30000 + (2*$i + 1)]  $Acol $Ec_uc $Icol_st $ColTransTag; # 300xx -
Joint Column @ 3U - property?
}

puts "Column elements defined."
```

```
# BEAM Rotational Springs ------------------------------------
# Define rotational spring properties and create spring elements using
"rotSpring2DModIKModel" procedure

# rotSpring2DModIKModel creates a uniaxial material spring with a bilinear
response based on Modified Ibarra Krawinkler Deterioration Model
set K0 [expr $Ec_uc*$Ibeam];      # Elastic stiffness, k*in/rad
set as_Plus 0.01;                 # Strain hardening ratio for positive
loading direction
set as_Neg 0.01;                  # Strain hardening ratio for negative
loading direction
set Lamda_S 1.0;                  # Cyclic deterioration parameter for
strength deterioration [see definitions in Lignos and Krawinkler (2011)]
set Lamda_C 1.0;                  # Cyclic deterioration parameter for
post-capping strength deterioration [see definitions in Lignos and
Krawinkler (2011)]
set Lamda_A 1.0;                  # Cyclic deterioration parameter for
acceleration reloading stiffness deterioration [see definitions in Lignos
and Krawinkler (2011)]
set Lamda_K 1.0;                  # Cyclic deterioration parameter for
unloading stiffness deterioration [see definitions in Lignos and
Krawinkler (2011)]
set c_S    1.0;                   # Rate of strength deterioration. The
default value is 1.0.
set c_C    1.0;                   # Rate of post-capping strength
deterioration. The default value is 1.0.
set c_A    1.0;                   # Rate of accelerated reloading
deterioration. The default value is 1.0.
set c_K    1.0;                   # Rate of unloading stiffness
deterioration. The default value is 1.0.
set theta_p_Plus 0.05;            # Pre-capping rotation for positive
loading direction (often noted as plastic rotation capacity) !!! ASCE-41
set theta_p_Neg  0.05;            # Pre-capping rotation for negative
loading direction (often noted as plastic rotation capacity) (must be
defined as a positive value)
set theta_pc_Plus 0.03;           # Post-capping rotation for positive
loading direction
set theta_pc_Neg 0.03;            # Post-capping rotation for negative
loading direction (must be defined as a positive value)
set Res_Pos 0.2;                  # Residual strength ratio for positive
loading direction
set Res_Neg 0.2;                  # Residual strength ratio for negative
loading direction (must be defined as a positive value)
set theta_u_Plus 0.2;             # Ultimate rotation capacity for
positive loading direction
set theta_u_Neg  0.2;             # Ultimate rotation capacity for
negative loading direction (must be defined as a positive value)
set D_Plus 1.0;                   # Rate of cyclic deterioration in the
positive loading direction (this parameter is used to create assymetric
hysteretic behavior for the case of a composite beam). For symmetric
hysteretic response use 1.0.
set D_Neg 1.0;                    # Rate of cyclic deterioration in the
negative loading direction (this parameter is used to create assymetric
hysteretic behavior for the case of a composite beam). For symmetric
hysteretic response use 1.0.
```

```
# Command: uniaxialMaterial ModIMKPeakOriented $matTag $K0 $as_Plus
$as_Neg $My_Plus $My_Neg $Lamda_S $Lamda_C $Lamda_A $Lamda_K $c_S $c_C
$c_A $c_K $theta_p_Plus $theta_p_Neg $theta_pc_Plus $theta_pc_Neg $Res_Pos
$Res_Neg $theta_u_Plus $theta_u_Neg $D_Plus $D_Neg
uniaxialMaterial ModIMKPeakOriented 3002 $K0 $as_Plus $as_Neg $MybeamBot
[expr -$MybeamTop] $Lamda_S $Lamda_C $Lamda_A $Lamda_K $c_S $c_C $c_A $c_K
$theta_p_Plus $theta_p_Neg $theta_pc_Plus $theta_pc_Neg $Res_Pos $Res_Neg
$theta_u_Plus $theta_u_Neg $D_Plus $D_Neg

# Create zero-length elements for plastic hinge
# Command: element zeroLength $eleTag $iNode $jNode -mat $matTag1 $matTag2
... -dir $dir1 $dir2 ...<-doRayleigh $rFlag> <-orient $x1 $x2 $x3 $yp1
$yp2 $yp3>
# Direction 6 is rotation about local z-axis PH
for {set i 1} {$i <= $NumStories} {incr i} {

      # Zero Length elements - hinges
      element zeroLength [expr 700 + $i] [expr 7000 + $i] [expr 700 + $i]
-mat 3002 -dir 6;# @ 2R
      element zeroLength [expr 800 + $i] [expr 800 + $i] [expr 8000 + $i]
-mat 3002 -dir 6;# @ 3L

      # Constraint
      equalDOF [expr 700 + $i] [expr 7000 + $i] 1 2; # @ 2R
      equalDOF [expr 800 + $i] [expr 8000 + $i] 1 2; # @ 3L

}

puts "Beam plastic hinges defined."

# COLUMN Rotational Springs ----------------------------------
# Define rotational spring properties and create spring elements using
"rotSpring2DModIKModel" procedure

# rotSpring2DModIKModel creates a uniaxial material spring with a bilinear
response based on Modified Ibarra Krawinkler Deterioration Model
set K0_c [expr $Mycol/0.01];      # Elastic stiffness, k*in/rad
set as_Plus_c 0.01;               # Strain hardening ratio for positive
loading direction
set as_Neg_c 0.01;                # Strain hardening ratio for negative
loading direction
set Lamda_S_c    1.0;             # Cyclic deterioration parameter for
strength deterioration [see definitions in Lignos and Krawinkler (2011)]
set Lamda_C_c    1.0;             # Cyclic deterioration parameter for
post-capping strength deterioration [see definitions in Lignos and
Krawinkler (2011)]
set Lamda_A_c    1.0;             # Cyclic deterioration parameter for
acceleration reloading stiffness deterioration [see definitions in Lignos
and Krawinkler (2011)]
set Lamda_K_c    1.0;             # Cyclic deterioration parameter for
unloading stiffness deterioration [see definitions in Lignos and
Krawinkler (2011)]
set c_S_c  1.0;                   # Rate of strength deterioration. The
default value is 1.0.
```

```
set c_C_c  1.0;                    # Rate of post-capping strength
deterioration. The default value is 1.0.
set c_A_c  1.0;                    # Rate of accelerated reloading
deterioration. The default value is 1.0.
set c_K_c  1.0;                    # Rate of unloading stiffness
deterioration. The default value is 1.0.
set theta_p_Plus_c 0.05;           # Pre-capping rotation for positive
loading direction (often noted as plastic rotation capacity)
set theta_p_Neg_c0.05;             # Pre-capping rotation for negative
loading direction (often noted as plastic rotation capacity) (must be
defined as a positive value)
set theta_pc_Plus_c 0.03;          # Post-capping rotation for positive
loading direction
set theta_pc_Neg_c 0.03;           # Post-capping rotation for negative
loading direction (must be defined as a positive value)
set Res_Pos_c 0.3;                 # Residual strength ratio for positive
loading direction
set Res_Neg_c    0.3;              # Residual strength ratio for negative
loading direction (must be defined as a positive value)
set theta_u_Plus_c 0.2;            # Ultimate rotation capacity for
positive loading direction
set theta_u_Neg_c0.2;              # Ultimate rotation capacity for
negative loading direction (must be defined as a positive value)
set D_Plus_c 1.0;                  # Rate of cyclic deterioration in the
positive loading direction (this parameter is used to create assymetric
hysteretic behavior for the case of a composite beam). For symmetric
hysteretic response use 1.0.
set D_Neg_c 1.0;                   # Rate of cyclic deterioration in the
negative loading direction (this parameter is used to create assymetric
hysteretic behavior for the case of a composite beam). For symmetric
hysteretic response use 1.0.

# Command: uniaxialMaterial ModIMKPeakOriented $matTag $K0 $as_Plus
$as_Neg $My_Plus $My_Neg $Lamda_S $Lamda_C $Lamda_A $Lamda_K $c_S $c_C
$c_A $c_K $theta_p_Plus $theta_p_Neg $theta_pc_Plus $theta_pc_Neg $Res_Pos
$Res_Neg $theta_u_Plus $theta_u_Neg $D_Plus $D_Neg
uniaxialMaterial ModIMKPeakOriented 30002 $K0_c $as_Plus_c $as_Neg_c
$Mycol [expr -$Mycol] $Lamda_S_c $Lamda_C_c $Lamda_A_c $Lamda_K_c $c_S_c
$c_C_c $c_A_c $c_K_c $theta_p_Plus_c $theta_p_Neg_c $theta_pc_Plus_c
$theta_pc_Neg_c $Res_Pos_c $Res_Neg_c $theta_u_Plus_c $theta_u_Neg_c
$D_Plus_c $D_Neg_c

# Create zero-length elements for plastic hinge
# Command: element zeroLength $eleTag $iNode $jNode -mat $matTag1 $matTag2
... -dir $dir1 $dir2 ...<-doRayleigh $rFlag> <-orient $x1 $x2 $x3 $yp1
$yp2 $yp3>
# Direction 6 is rotation about local z-axis PH
# "2Down" - @ axis 2 below the beam-column joint

for {set i 1} {$i <= $NumStories} {incr i} {

      # Zero Length elements - hinges
      element zeroLength [expr 200000 + (2*$i)]           [expr 2000 +
(2*$i)]           [expr 20000 + (2*$i)]        -mat 30002 -dir 6;     # @
2Down
```

```
      element zeroLength [expr 200000 + (2*$i - 1)] [expr 20000 + (2*$i -
1)]   [expr 2000 + (2*$i - 1)]     -mat 30002 -dir 6;     # @ 2Up

      element zeroLength [expr 300000 + (2*$i)]           [expr 3000 +
(2*$i)]          [expr 30000 + (2*$i)]        -mat 30002 -dir 6;     # @
3Down
      element zeroLength [expr 300000 + (2*$i - 1)] [expr 30000 + (2*$i -
1)]   [expr 3000 + (2*$i - 1)]     -mat 30002 -dir 6;     # @ 3Up

      # Constraint
      equalDOF [expr 2000 + (2*$i)]           [expr 20000 + (2*$i)]
1 2;  # @ 2Down
      equalDOF [expr 20000 + (2*$i - 1)]      [expr 2000 + (2*$i - 1)]
1 2;  # @ 2Up

      equalDOF [expr 3000 + (2*$i)]           [expr 30000 + (2*$i)]
1 2;  # @ 3Down
      equalDOF [expr 30000 + (2*$i - 1)]      [expr 3000 + (2*$i - 1)]
1 2;  # @ 3Up

}

puts "Column plastic hinges defined."

# Define Recorders -----------------------------------

# Define Recorders
# Recorder Node <-file $fileName> <-precision $nSD> <-time> <-dT $deltaT>
<-closeOnWrite> <-node $node1 $node2...> <-nodeRange $startNode $endNode>
<-dof $dof1 $dof2> $respType
# Response Type: disp, vel, accel, incrDisp, "eigen i", reaction,
rayleighForces

# Node recorders
# Displacements
recorder Node -file $dataDir/NodeDisp1.out -time -nodeRange 100 110 -dof 1
2 disp; # Nodes @ 1
recorder Node -file $dataDir/NodeDisp2.out -time -nodeRange 200 205 -dof 1
2 disp; # Nodes @ 2
recorder Node -file $dataDir/NodeDisp3.out -time -nodeRange 300 305 -dof 1
2 disp; # Nodes @ 3

# Reactions
recorder Node -file $dataDir/NodeReactions.out -time -node 100 200 300 -
dof 1 2 3 reaction;

# Record drift histories
# Command: recorder Drift -file $filename -time -iNode $NodeI_ID -jNode
$NodeJ_ID -dof $dof -perpDirn
$Record.drift.perpendicular.to.this.direction
recorder Drift -file $dataDir/DriftRoof.out -time -iNode 100 -jNode 110 -
dof 1 -perpDirn 2; # Roof
recorder Drift -file $dataDir/DriftStory.out -time -iNode 100 102 104 106
108 -jNode 102 104 106 108 110 -dof 1 -perpDirn 2; # Story
```

```
# Record response history of ALL BEAM plastic hinge springs (one file for
moment, one for rotation)
# Axis 2Left
recorder Element -file $dataDir/PH_BeamMoment2R.out -time -ele 701 702 703
704 705 force;
recorder Element -file $dataDir/PH_BeamDeformation2R.out -time -ele 701
702 703 704 705 deformation;
# Axis 3Rigth
recorder Element -file $dataDir/PH_BeamMoment3L.out -time -ele 801 802 803
804 805 force;
recorder Element -file $dataDir/PH_BeamDeformation3L.out -time -ele 801
802 803 804 805 deformation;

# Record response history of ALL COLUMN plastic hinge springs (one file
for moment, one for rotation)
# Axis 2
recorder Element -file $dataDir/PH_ColMoment2.out -time -ele 200001 200002
200003 200004 200005 200006 200007 200008 200009 200010  force;
recorder Element -file $dataDir/PH_ColDeformation2.out -time -ele 200001
200002 200003 200004 200005 200006 200007 200008 200009 200010
deformation;
# Axis 3
recorder Element -file $dataDir/PH_ColMoment3.out -time -ele 300001 300002
300003 300004 300005 300006 300007 300008 300009 300010 force;
recorder Element -file $dataDir/PH_ColDeformation3.out -time -ele 300001
300002 300003 300004 300005 300006 300007 300008 300009 300010
deformation;

# Record responses for wall elements
recorder Element -file $dataDir/WallGlobalForces.out -time -ele 1001 1002
1003 1004 1005 1006 1007 1008 1009 1010 globalForce;
recorder Element -file $dataDir/WallCurvature.out -time -ele 1001 1002
1003 1004 1005 1006 1007 1008 1009 1010 Curvature;
recorder Element -file $dataDir/WallShearDef.out -time -ele 1001 1002 1003
1004 1005 1006 1007 1008 1009 1010 ShearDef;

# Record responses for wall fibers (one panel per recorder)
# Command: RCPanel $fibTag $Response
recorder Element -file $dataDir/WallFiberStrain_f1.out -time -ele 1001
1002 1003 1004 1005 1006 1007 1008 1009 1010 RCPanel 1 panel_strain
recorder Element -file $dataDir/WallFiberStrain_f6.out -time -ele 1001
1002 1003 1004 1005 1006 1007 1008 1009 1010 RCPanel 6 panel_strain
recorder Element -file $dataDir/WallPanelStrain.out -time -ele 1001
RCPanel 1 panel_strain
recorder Element -file $dataDir/WallPanelStress.out -time -ele 1001
RCPanel 1 panel_stress
recorder Element -file $dataDir/WallStressConcrete.out -time -ele 1001
RCPanel 1 panel_stress_concrete
recorder Element -file $dataDir/WallStressSteel.out -time -ele 1001
RCPanel 1 panel_stress_steel
recorder Element -file $dataDir/WallPanelSteel1.out -time -ele 1001
RCPanel 1 strain_stress_steelX
recorder Element -file $dataDir/WallPanelSteel2.out -time -ele 1001
RCPanel 1 strain_stress_steelY
```

```
recorder Element -file $dataDir/WallPanelConcrete1.out -time -ele 1001
RCPanel 1 strain_stress_concrete1
recorder Element -file $dataDir/WallPanelConcrete2.out -time -ele 1001
RCPanel 1 strain_stress_concrete2

# GRAVITY LOADS & GRAVITY ANALYSIS *************************************

# Apply gravity loads
# Construct a time series where load factor applied is linearly
proportional to the time domain
# Command: pattern PatternType $PatternID TimeSeriesType
pattern Plain 1 "Linear" { # Command for ndm=2 : eleLoad -ele $eleTag1
<$eleTag2...> -type -beamUniform $Wy <$Wx>
            # Line loads on all beams
      for {set i 1} {$i <= $NumStories} {incr i} {
            eleLoad -ele [expr 3300 + $i] -type -beamUniform -
$wLineBeam_floor;
            eleLoad -ele [expr 33300 + $i] -type -beamUniform -
$wLineBeam_floor;
            eleLoad -ele [expr 88800 + $i] -type -beamUniform -
$wLineBeam_floor;
      }
      # Nodal load on walls - command: load nodeID xForce yForce
      for {set i 1} {$i <= $NumStories} {incr i} {

            load [expr 100 + 2*$i]  0.0 -$wNodalWall_floor 0.0;
      }
}

# Gravity-analysis: load-controlled static analysis
set Tol 1.0e-6;                  # convergence tolerance for test
set NstepGravity 10;             # apply gravity in 10 steps
set DGravity [expr 1.0/$NstepGravity];  # load increment
constraints Plain;               # how it handles boundary conditions
numberer RCM;                    # renumber dof's to minimize band-width
(optimization)
system BandGeneral;              # how to store and solve the system of
equations in the analysis (large model: try UmfPack)
test NormDispIncr $Tol 6;        # determine if convergence has been
achieved at the end of an iteration step
algorithm Newton;                # use Newton's solution algorithm:
updates tangent stiffness at every iteration
integrator LoadControl $DGravity; # determine the next time step for an
analysis
analysis Static;                 # define type of analysis: static or
transient
analyze $NstepGravity;           # apply gravity

puts "Model built & gravity analysis completed."
```

C.2 MODAL ANALAYSIS

```
# ----------------------------------------------------
# Modal Analysis
# File Name: Modal.tcl
# ----------------------------------------------------

# Generate the model and run gravity analysis
source 5storyWF_SFI.tcl

# Rayleigh Damping ----------------------------------
# Apply Rayleigh damping from $xDamp:
(http://opensees.berkeley.edu/OpenSees/manuals/usermanual/1099.htm)
# D=$alphaM*M + $betaKcurr*Kcurrent + $betaKcomm*KlastCommit +
$betaKinit*$Kinitial
      set xDamp 0.02;
      # Damping ratio
      set MpropSwitch 1.0;   # Type 1.0 for each M and K matrix you want
damping matrix to be proportional to.
      set KcurrSwitch 1.0;   # Use this: tangent stiffness changes per
time series in dynamic nonlinear analysis
      set KcommSwitch 0.0;
      set KinitSwitch 0.0;
      set nEigenI 1;
      # Mode i: 1
      set nEigenJ 3;
      # Mode j: 3
      set lambdaN [eigen $nEigenJ]
      set lambdaI [lindex $lambdaN [expr $nEigenI-1]]; # Eigenvalue mode i
      set lambdaJ [lindex $lambdaN [expr $nEigenJ-1]]; # Eigenvalue mode j
      set omegaI [expr pow($lambdaI,0.5)];
      set omegaJ [expr pow($lambdaJ,0.5)];
      set alphaM [expr
$MpropSwitch*$xDamp*(2*$omegaI*$omegaJ)/($omegaI+$omegaJ)];    # M-prop.
damping; D = alphaM*M
      set betaKcurr [expr $KcurrSwitch*2.0*$xDamp/($omegaI+$omegaJ)];
            # Current-K + betaKcurr*KCurrent
      set betaKcomm [expr $KcommSwitch*2.0*$xDamp/($omegaI+$omegaJ)];
                  # Last-committed K + betaKcomm*KlastCommitt
      set betaKinit [expr $KinitSwitch*2.0*$xDamp/($omegaI+$omegaJ)];
            # initial- K + betaKinit*Kini

# Eigen analysis - for period
      set T {};
      foreach lam $lambdaN {
            lappend Tperiod [expr (2.0*$pi)/sqrt($lam)];
      }
      puts "T1 = [lindex $Tperiod 0] s"
      puts "T2 = [lindex $Tperiod 1] s"

# Apply reyleigh damping
rayleigh $alphaM $betaKcurr $betaKinit $betaKcomm;
```

C.3 DYNAMIC TIME-HISTORY ANALYSIS

```
# ------------------------------------------------------------------
# Dynamic Time-History Analysis
# File Name: Dynamic.tcl
# ------------------------------------------------------------------

# Perform modal analysis
source Modal.tcl

# First, set gravity loads acting constant and time in domain to 0.0
      loadConst -time 0.0

# Define ground motion parameters
      set GMfile "MCEScaledEQ1X.acc";    # Ground motion filename (g units)
      set DtSeries 0.04;     # time-step Dt for definition of time series
      set NSteps  2201.0;    # Number of steps in ground motion

# Define ground motion parameters
      set patternID 2;       # Load pattern ID
      set GMdirection 1;     # Ground motion direction (1 = x)
      set Scalefactor [expr 1*$g]; # Ground motion scaling factor

      set DtAnalysis   0.04; # time-step Dt for lateral analysis
      set TmaxAnalysis [expr $DtSeries*$NSteps]; # duration of GM analysis

# Define the acceleration series for the ground motion
      # Command: "Series -dt $timestep_of_record -filePath
$filename_with_acc_history -factor $scale_record_by_this_amount"
      set accelSeries "Series -dt $DtSeries -filePath $GMfile -factor
$Scalefactor";

# Create load pattern: apply acceleration to all fixed nodes with
UniformExcitation
      # Command: pattern UniformExcitation $patternID $GMdir -accel
$timeSeriesID
      pattern UniformExcitation $patternID $GMdirection -accel
$accelSeries;

      puts "GM parameters and acceleration series defined."

      set start [clock seconds]

      # Convergence Test
      set Tol 1.e-3;         # tolerance
      set maxNumIter 1000;   # maximum number of iterations
      set printFlag 0;       # print convergence information flag
      set TestType NormDispIncr;   # test type

      # Algorithm
      set algorithmType ModifiedNewton

      # Newmark-integrator parameters
      set NewmarkGamma 0.5;                    # gamma
      set NewmarkBeta 0.25;                    # beta
```

```
      constraints Transformation;
      numberer RCM;
      system BandGeneral;
      test $TestType $Tol $maxNumIter; # $printFlag;
      algorithm $algorithmType;
      integrator Newmark $NewmarkGamma $NewmarkBeta;
      analysis Transient;

      set Nsteps [expr int($TmaxAnalysis/$DtAnalysis)];
      # Perform analysis: ok=0 (successful)
      set ok [analyze $Nsteps $DtAnalysis];

if {$ok != 0} { ;
      # If analysis was not successful change
      # analysis parameters to achieve convergence.
      set ok 0;
      set controlTime [getTime];
      while {$controlTime < $TmaxAnalysis && $ok == 0} {
            set ok [analyze 1 $DtAnalysis]
            set controlTime [getTime]
            set ok [analyze 1 $DtAnalysis]
            if {$ok != 0} {
                  puts "Trying Newton with Initial Tangent .."
                  test NormDispIncr   $Tol 1000  0
                  algorithm Newton -initial
                  set ok [analyze 1 $DtAnalysis]
                  test $TestType $Tol $maxNumIter  0
                  algorithm $algorithmType
            }
            if {$ok != 0} {
                  puts "Trying Broyden .."
                  algorithm Broyden 8
                  set ok [analyze 1 $DtAnalysis]
                  algorithm $algorithmType
            }
            if {$ok != 0} {
                  puts "Trying NewtonWithLineSearch .."
                  algorithm NewtonLineSearch .8
                  set ok [analyze 1 $DtAnalysis]
                  algorithm $algorithmType
            }
            if {$ok != 0} {
                  puts "Trying BFGS.."
                  algorithm BFGS
                  set ok [analyze 1 $DtAnalysis]
                  algorithm $algorithmType
            }
      }
};      # end if ok !0

puts "Ground Motion Done."
      set currentTime [getTime];   # get current analysis time
      puts "The current time is: $currentTime";
      # Print the state at control node
      print node $IDctrlNode
```

PEER REPORTS

PEER reports are available as a free PDF download from http://peer.berkeley.edu/publications/peer_reports_complete.html. Printed hard copies of PEER reports can be ordered directly from our printer by following the instructions at http://peer.berkeley.edu/publications/peer_reports.html. For other related questions about the PEER Report Series, contact the Pacific Earthquake Engineering Research Center, 325 Davis Hall mail code 1792, Berkeley, CA 94720. Tel.: (510) 642-3437; Fax: (510) 665-1655; Email: peer_editor@berkeley.edu

PEER 2015/12 *Shear-Flexure Interaction Modeling for Reinforced Concrete Structural Walls and Columns under Reversed Cyclic Loading.* Kristijan Kolozvari, Kutay Orakcal, and John Wallace. December 2015.

PEER 2015/11 *Selection and Scaling of Ground Motions for Nonlinear Response History Analysis of Buildings in Performance-Based Earthquake Engineering.* N. Simon Kwong and Anil K. Chopra. December 2015.

PEER 2015/10 *Structural Behavior of Column-Bent Cap Beam-Box Girder Systems in Reinforced Concrete Bridges Subjected to Gravity and Seismic Loads. Part II: Hybrid Simulation and Post-Test Analysis.* Mohamed A. Moustafa and Khalid M. Mosalam. November 2015.

PEER 2015/09 *Structural Behavior of Column-Bent Cap Beam-Box Girder Systems in Reinforced Concrete Bridges Subjected to Gravity and Seismic Loads. Part I: Pre-Test Analysis and Quasi-Static Experiments.* Mohamed A. Moustafa and Khalid M. Mosalam. September 2015.

PEER 2015/08 *NGA-East: Adjustments to Median Ground-Motion Models for Center and Eastern North America.* August 2015.

PEER 2015/07 *NGA-East: Ground-Motion Standard-Deviation Models for Central and Eastern North America.* Linda Al Atik. June 2015.

PEER 2015/06 *Adjusting Ground-Motion Intensity Measures to a Reference Site for which V_{S30} = 3000 m/sec.* David M. Boore. May 2015.

PEER 2015/05 *Hybrid Simulation of Seismic Isolation Systems Applied to an APR-1400 Nuclear Power Plant.* Andreas H. Schellenberg, Alireza Sarebanha, Matthew J. Schoettler, Gilberto Mosqueda, Gianmario Benzoni, and Stephen A. Mahin. April 2015.

PEER 2015/04 *NGA-East: Median Ground-Motion Models for the Central and Eastern North America Region.* April 2015.

PEER 2015/03 *Single Series Solution for the Rectangular Fiber-Reinforced Elastomeric Isolator Compression Modulus.* James M. Kelly and Niel C. Van Engelen. March 2015.

PEER 2015/02 *A Full-Scale, Single-Column Bridge Bent Tested by Shake-Table Excitation.* Matthew J. Schoettler, José I. Restrepo, Gabriele Guerrini, David E. Duck, and Francesco Carrea. March 2015.

PEER 2015/01 *Concrete Column Blind Prediction Contest 2010: Outcomes and Observations.* Vesna Terzic, Matthew J. Schoettler, José I. Restrepo, and Stephen A Mahin. March 2015.

PEER 2014/20 *Stochastic Modeling and Simulation of Near-Fault Ground Motions for Performance-Based Earthquake Engineering.* Mayssa Dabaghi and Armen Der Kiureghian. December 2014.

PEER 2014/19 *Seismic Response of a Hybrid Fiber-Reinforced Concrete Bridge Column Detailed for Accelerated Bridge Construction.* Wilson Nguyen, William Trono, Marios Panagiotou, and Claudia P. Ostertag. December 2014.

PEER 2014/18 *Three-Dimensional Beam-Truss Model for Reinforced Concrete Walls and Slabs Subjected to Cyclic Static or Dynamic Loading.* Yuan Lu, Marios Panagiotou, and Ioannis Koutromanos. December 2014.

PEER 2014/17 *PEER NGA-East Database.* Christine A. Goulet, Tadahiro Kishida, Timothy D. Ancheta, Chris H. Cramer, Robert B. Darragh, Walter J. Silva, Youssef M.A. Hashash, Joseph Harmon, Jonathan P. Stewart, Katie E. Wooddell, and Robert R. Youngs. October 2014.

PEER 2014/16 *Guidelines for Performing Hazard-Consistent One-Dimensional Ground Response Analysis for Ground Motion Prediction.* Jonathan P. Stewart, Kioumars Afshari, and Youssef M.A. Hashash. October 2014.

PEER 2014/15 *NGA-East Regionalization Report: Comparison of Four Crustal Regions within Central and Eastern North America using Waveform Modeling and 5%-Damped Pseudo-Spectral Acceleration Response.* Jennifer Dreiling, Marius P. Isken, Walter D. Mooney, Martin C. Chapman, and Richard W. Godbee. October 2014.

PEER 2014/14 *Scaling Relations between Seismic Moment and Rupture Area of Earthquakes in Stable Continental Regions*. Paul Somerville. August 2014.

PEER 2014/13 *PEER Preliminary Notes and Observations on the August 24, 2014, South Napa Earthquake*. Grace S. Kang (Editor), Stephen A. Mahin (Editors). September 2014.

PEER 2014/12 *Reference-Rock Site Conditions for Central and Eastern North America: Part II – Attenuation (Kappa) Definition*. Kenneth W. Campbell, Youssef M.A. Hashash, Byungmin Kim, Albert R. Kottke, Ellen M. Rathje, Walter J. Silva, and Jonathan P. Stewart. August 2014.

PEER 2014/11 *Reference-Rock Site Conditions for Central and Eastern North America: Part I - Velocity Definition*. Youssef M.A. Hashash, Albert R. Kottke, Jonathan P. Stewart, Kenneth W. Campbell, Byungmin Kim, Ellen M. Rathje, Walter J. Silva, Sissy Nikolaou, and Cheryl Moss. August 2014.

PEER 2014/10 *Evaluation of Collapse and Non-Collapse of Parallel Bridges Affected by Liquefaction and Lateral Spreading*. Benjamin Turner, Scott J. Brandenberg, and Jonathan P. Stewart. August 2014.

PEER 2014/09 *PEER Arizona Strong-Motion Database and GMPEs Evaluation*. Tadahiro Kishida, Robert E. Kayen, Olga-Joan Ktenidou, Walter J. Silva, Robert B. Darragh, and Jennie Watson-Lamprey. June 2014.

PEER 2014/08 *Unbonded Pretensioned Bridge Columns with Rocking Detail*. Jeffrey A. Schaefer, Bryan Kennedy, Marc O. Eberhard, John F. Stanton. June 2014.

PEER 2014/07 *Northridge 20 Symposium Summary Report: Impacts, Outcomes, and Next Steps*. May 2014.

PEER 2014/06 *Report of the Tenth Planning Meeting of NEES/E-Defense Collaborative Research on Earthquake Engineering*. December 2013.

PEER 2014/05 *Seismic Velocity Site Characterization of Thirty-One Chilean Seismometer Stations by Spectral Analysis of Surface Wave Dispersion.* Robert Kayen, Brad D. Carkin, Skye Corbet, Camilo Pinilla, Allan Ng, Edward Gorbis, and Christine Truong. April 2014.

PEER 2014/04 *Effect of Vertical Acceleration on Shear Strength of Reinforced Concrete Columns.* Hyerin Lee and Khalid M. Mosalam. April 2014.

PEER 2014/03 *Retest of Thirty-Year-Old Neoprene Isolation Bearings.* James M. Kelly and Niel C. Van Engelen. March 2014.

PEER 2014/02 *Theoretical Development of Hybrid Simulation Applied to Plate Structures.* Ahmed A. Bakhaty, Khalid M. Mosalam, and Sanjay Govindjee. January 2014.

PEER 2014/01 *Performance-Based Seismic Assessment of Skewed Bridges.* Peyman Kaviani, Farzin Zareian, and Ertugrul Taciroglu. January 2014.

PEER 2013/26 *Urban Earthquake Engineering. Proceedings of the U.S.-Iran Seismic Workshop.* December 2013.

PEER 2013/25 *Earthquake Engineering for Resilient Communities: 2013 PEER Internship Program Research Report Collection.* Heidi Tremayne (Editor), Stephen A. Mahin (Editor), Jorge Archbold Monterossa, Matt Brosman, Shelly Dean, Katherine deLaveaga, Curtis Fong, Donovan Holder, Rakeeb Khan, Elizabeth Jachens, David Lam, Daniela Martinez Lopez, Mara Minner, Geffen Oren, Julia Pavicic, Melissa Quinonez, Lorena Rodriguez, Sean Salazar, Kelli Slaven, Vivian Steyert, Jenny Taing, and Salvador Tena. December 2013.

PEER 2013/24 *NGA-West2 Ground Motion Prediction Equations for Vertical Ground Motions.* September 2013.

PEER 2013/23 *Coordinated Planning and Preparedness for Fire Following Major Earthquakes.* Charles Scawthorn. November 2013.

PEER 2013/22 *GEM-PEER Task 3 Project: Selection of a Global Set of Ground Motion Prediction Equations.* Jonathan P. Stewart, John Douglas, Mohammad B. Javanbarg, Carola Di Alessandro, Yousef Bozorgnia, Norman A. Abrahamson, David M. Boore, Kenneth W. Campbell, Elise Delavaud, Mustafa Erdik and Peter J. Stafford. December 2013.

PEER 2013/21 *Seismic Design and Performance of Bridges with Columns on Rocking Foundations.* Grigorios Antonellis and Marios Panagiotou. September 2013.

PEER 2013/20 *Experimental and Analytical Studies on the Seismic Behavior of Conventional and Hybrid Braced Frames.* Jiun-Wei Lai and Stephen A. Mahin. September 2013.

PEER 2013/19 *Toward Resilient Communities: A Performance-Based Engineering Framework for Design and Evaluation of the Built Environment.* Michael William Mieler, Bozidar Stojadinovic, Robert J. Budnitz, Stephen A. Mahin and Mary C. Comerio. September 2013.

PEER 2013/18 *Identification of Site Parameters that Improve Predictions of Site Amplification.* Ellen M. Rathje and Sara Navidi. July 2013.

PEER 2013/17 *Response Spectrum Analysis of Concrete Gravity Dams Including Dam-Water-Foundation Interaction.* Arnkjell Løkke and Anil K. Chopra. July 2013.

PEER 2013/16 *Effect of hoop reinforcement spacing on the cyclic response of large reinforced concrete special moment frame beams.* Marios Panagiotou, Tea Visnjic, Grigorios Antonellis, Panagiotis Galanis, and Jack P. Moehle. June 2013.

PEER 2013/15 *A Probabilistic Framework to Include the Effects of Near-Fault Directivity in Seismic Hazard Assessment.* Shrey Kumar Shahi, Jack W. Baker. October 2013.

PEER 2013/14 *Hanging-Wall Scaling using Finite-Fault Simulations.* Jennifer L. Donahue and Norman A. Abrahamson. September 2013.

PEER 2013/13 *Semi-Empirical Nonlinear Site Amplification and its Application in NEHRP Site Factors.* Jonathan P. Stewart and Emel Seyhan. November 2013.

PEER 2013/12 *Nonlinear Horizontal Site Response for the NGA-West2 Project.* Ronnie Kamai, Norman A. Abramson, Walter J. Silva. May 2013.

PEER 2013/11 *Epistemic Uncertainty for NGA-West2 Models.* Linda Al Atik and Robert R. Youngs. May 2013.

PEER 2013/10 *NGA-West 2 Models for Ground-Motion Directionality.* Shrey K. Shahi and Jack W. Baker. May 2013.

PEER 2013/09 *Final Report of the NGA-West2 Directivity Working Group.* Paul Spudich, Jeffrey R. Bayless, Jack W. Baker, Brian S.J. Chiou, Badie Rowshandel, Shrey Shahi, and Paul Somerville. May 2013.

PEER 2013/08 *NGA-West2 Model for Estimating Average Horizontal Values of Pseudo-Absolute Spectral Accelerations Generated by Crustal Earthquakes.* I. M. Idriss. May 2013.

PEER 2013/07 *Update of the Chiou and Youngs NGA Ground Motion Model for Average Horizontal Component of Peak Ground Motion and Response Spectra.* Brian Chiou and Robert Youngs. May 2013.

PEER 2013/06 *NGA-West2 Campbell-Bozorgnia Ground Motion Model for the Horizontal Components of PGA, PGV, and 5%-Damped Elastic Pseudo-Acceleration Response Spectra for Periods Ranging from 0.01 to 10 sec.* Kenneth W. Campbell and Yousef Bozorgnia. May 2013.

PEER 2013/05 *NGA-West 2 Equations for Predicting Response Spectral Accelerations for Shallow Crustal Earthquakes.* David M. Boore, Jonathan P. Stewart, Emel Seyhan, Gail M. Atkinson. May 2013.

PEER 2013/04 *Update of the AS08 Ground-Motion Prediction Equations Based on the NGA-West2 Data Set.* Norman Abrahamson, Walter Silva, and Ronnie Kamai. May 2013.

PEER 2013/03 *PEER NGA-West2 Database.* Timothy D. Ancheta, Robert B. Darragh, Jonathan P. Stewart, Emel Seyhan, Walter J. Silva, Brian S.J. Chiou, Katie E. Wooddell, Robert W. Graves, Albert R. Kottke, David M. Boore, Tadahiro Kishida, and Jennifer L. Donahue. May 2013.

PEER 2013/02 *Hybrid Simulation of the Seismic Response of Squat Reinforced Concrete Shear Walls.* Catherine A. Whyte and Bozidar Stojadinovic. May 2013.

PEER 2013/01 *Housing Recovery in Chile: A Qualitative Mid-program Review.* Mary C. Comerio. February 2013.

PEER 2012/08 *Guidelines for Estimation of Shear Wave Velocity.* Bernard R. Wair, Jason T. DeJong, and Thomas Shantz. December 2012.

PEER 2012/07 *Earthquake Engineering for Resilient Communities: 2012 PEER Internship Program Research Report Collection.* Heidi Tremayne (Editor), Stephen A. Mahin (Editor), Collin Anderson, Dustin Cook, Michael Erceg, Carlos Esparza, Jose Jimenez, Dorian Krausz, Andrew Lo, Stephanie Lopez, Nicole McCurdy, Paul Shipman, Alexander Strum, Eduardo Vega. December 2012.

PEER 2012/06 *Fragilities for Precarious Rocks at Yucca Mountain.* Matthew D. Purvance, Rasool Anooshehpoor, and James N. Brune. December 2012.

PEER 2012/05 *Development of Simplified Analysis Procedure for Piles in Laterally Spreading Layered Soils.* Christopher R. McGann, Pedro Arduino, and Peter Mackenzie–Helnwein. December 2012.

PEER 2012/04 *Unbonded Pre-Tensioned Columns for Bridges in Seismic Regions.* Phillip M. Davis, Todd M. Janes, Marc O. Eberhard, and John F. Stanton. December 2012.

PEER 2012/03 *Experimental and Analytical Studies on Reinforced Concrete Buildings with Seismically Vulnerable Beam-Column Joints.* Sangjoon Park and Khalid M. Mosalam. October 2012.

PEER 2012/02 *Seismic Performance of Reinforced Concrete Bridges Allowed to Uplift during Multi-Directional Excitation.* Andres Oscar Espinoza and Stephen A. Mahin. July 2012.

PEER 2012/01 *Spectral Damping Scaling Factors for Shallow Crustal Earthquakes in Active Tectonic Regions.* Sanaz Rezaeian, Yousef Bozorgnia, I. M. Idriss, Kenneth Campbell, Norman Abrahamson, and Walter Silva. July 2012.

PEER 2011/10 *Earthquake Engineering for Resilient Communities: 2011 PEER Internship Program Research Report Collection.* Eds. Heidi Faison and Stephen A. Mahin. December 2011.

PEER 2011/09 *Calibration of Semi-Stochastic Procedure for Simulating High-Frequency Ground Motions.* Jonathan P. Stewart, Emel Seyhan, and Robert W. Graves. December 2011.

PEER 2011/08 *Water Supply in regard to Fire Following Earthquake.* Charles Scawthorn. November 2011.

PEER 2011/07 *Seismic Risk Management in Urban Areas. Proceedings of a U.S.-Iran-Turkey Seismic Workshop.* September 2011.

PEER 2011/06 *The Use of Base Isolation Systems to Achieve Complex Seismic Performance Objectives.* Troy A. Morgan and Stephen A. Mahin. July 2011.

PEER 2011/05 *Case Studies of the Seismic Performance of Tall Buildings Designed by Alternative Means.* Task 12 Report for the Tall Buildings Initiative. Jack Moehle, Yousef Bozorgnia, Nirmal Jayaram, Pierson Jones, Mohsen Rahnama, Nilesh Shome, Zeynep Tuna, John Wallace, Tony Yang, and Farzin Zareian. July 2011.

PEER 2011/04 *Recommended Design Practice for Pile Foundations in Laterally Spreading Ground.* Scott A. Ashford, Ross W. Boulanger, and Scott J. Brandenberg. June 2011.

PEER 2011/03 *New Ground Motion Selection Procedures and Selected Motions for the PEER Transportation Research Program.* Jack W. Baker, Ting Lin, Shrey K. Shahi, and Nirmal Jayaram. March 2011.

PEER 2011/02 *A Bayesian Network Methodology for Infrastructure Seismic Risk Assessment and Decision Support.* Michelle T. Bensi, Armen Der Kiureghian, and Daniel Straub. March 2011.

PEER 2011/01 *Demand Fragility Surfaces for Bridges in Liquefied and Laterally Spreading Ground.* Scott J. Brandenberg, Jian Zhang, Pirooz Kashighandi, Yili Huo, and Minxing Zhao. March 2011.

PEER 2010/05 *Guidelines for Performance-Based Seismic Design of Tall Buildings.* Developed by the Tall Buildings Initiative. November 2010.

PEER 2010/04 *Application Guide for the Design of Flexible and Rigid Bus Connections between Substation Equipment Subjected to Earthquakes.* Jean-Bernard Dastous and Armen Der Kiureghian. September 2010.

PEER 2010/03 *Shear Wave Velocity as a Statistical Function of Standard Penetration Test Resistance and Vertical Effective Stress at Caltrans Bridge Sites.* Scott J. Brandenberg, Naresh Bellana, and Thomas Shantz. June 2010.

PEER 2010/02 *Stochastic Modeling and Simulation of Ground Motions for Performance-Based Earthquake Engineering.* Sanaz Rezaeian and Armen Der Kiureghian. June 2010.

PEER 2010/01 *Structural Response and Cost Characterization of Bridge Construction Using Seismic Performance Enhancement Strategies.* Ady Aviram, Božidar Stojadinović, Gustavo J. Parra-Montesinos, and Kevin R. Mackie. March 2010.

PEER 2009/03 *The Integration of Experimental and Simulation Data in the Study of Reinforced Concrete Bridge Systems Including Soil-Foundation-Structure Interaction.* Matthew Dryden and Gregory L. Fenves. November 2009.

PEER 2009/02 *Improving Earthquake Mitigation through Innovations and Applications in Seismic Science, Engineering, Communication, and Response. Proceedings of a U.S.-Iran Seismic Workshop.* October 2009.

PEER 2009/01 *Evaluation of Ground Motion Selection and Modification Methods: Predicting Median Interstory Drift Response of Buildings.* Curt B. Haselton, Ed. June 2009.

PEER 2008/10 *Technical Manual for Strata.* Albert R. Kottke and Ellen M. Rathje. February 2009.

PEER 2008/09 *NGA Model for Average Horizontal Component of Peak Ground Motion and Response Spectra.* Brian S.-J. Chiou and Robert R. Youngs. November 2008.

PEER 2008/08 *Toward Earthquake-Resistant Design of Concentrically Braced Steel Structures.* Patxi Uriz and Stephen A. Mahin. November 2008.

PEER 2008/07 *Using OpenSees for Performance-Based Evaluation of Bridges on Liquefiable Soils.* Stephen L. Kramer, Pedro Arduino, and HyungSuk Shin. November 2008.

PEER 2008/06 *Shaking Table Tests and Numerical Investigation of Self-Centering Reinforced Concrete Bridge Columns.* Hyung IL Jeong, Junichi Sakai, and Stephen A. Mahin. September 2008.

PEER 2008/05 *Performance-Based Earthquake Engineering Design Evaluation Procedure for Bridge Foundations Undergoing Liquefaction-Induced Lateral Ground Displacement.* Christian A. Ledezma and Jonathan D. Bray. August 2008.

PEER 2008/04 *Benchmarking of Nonlinear Geotechnical Ground Response Analysis Procedures.* Jonathan P. Stewart, Annie On-Lei Kwok, Yousseff M. A. Hashash, Neven Matasovic, Robert Pyke, Zhiliang Wang, and Zhaohui Yang. August 2008.

PEER 2008/03 *Guidelines for Nonlinear Analysis of Bridge Structures in California.* Ady Aviram, Kevin R. Mackie, and Božidar Stojadinović. August 2008.

PEER 2008/02 *Treatment of Uncertainties in Seismic-Risk Analysis of Transportation Systems.* Evangelos Stergiou and Anne S. Kiremidjian. July 2008.

PEER 2008/01 *Seismic Performance Objectives for Tall Buildings.* William T. Holmes, Charles Kircher, William Petak, and Nabih Youssef. August 2008.

PEER 2007/12 *An Assessment to Benchmark the Seismic Performance of a Code-Conforming Reinforced Concrete Moment-Frame Building.* Curt Haselton, Christine A. Goulet, Judith Mitrani-Reiser, James L. Beck, Gregory G. Deierlein, Keith A. Porter, Jonathan P. Stewart, and Ertugrul Taciroglu. August 2008.

PEER 2007/11 *Bar Buckling in Reinforced Concrete Bridge Columns.* Wayne A. Brown, Dawn E. Lehman, and John F. Stanton. February 2008.

PEER 2007/10 *Computational Modeling of Progressive Collapse in Reinforced Concrete Frame Structures.* Mohamed M. Talaat and Khalid M. Mosalam. May 2008.

PEER 2007/09 *Integrated Probabilistic Performance-Based Evaluation of Benchmark Reinforced Concrete Bridges.* Kevin R. Mackie, John-Michael Wong, and Božidar Stojadinović. January 2008.

PEER 2007/08 *Assessing Seismic Collapse Safety of Modern Reinforced Concrete Moment-Frame Buildings.* Curt B. Haselton and Gregory G. Deierlein. February 2008.

PEER 2007/07 *Performance Modeling Strategies for Modern Reinforced Concrete Bridge Columns.* Michael P. Berry and Marc O. Eberhard. April 2008.

PEER 2007/06 *Development of Improved Procedures for Seismic Design of Buried and Partially Buried Structures.* Linda Al Atik and Nicholas Sitar. June 2007.

PEER 2007/05 *Uncertainty and Correlation in Seismic Risk Assessment of Transportation Systems.* Renee G. Lee and Anne S. Kiremidjian. July 2007.

PEER 2007/04 *Numerical Models for Analysis and Performance-Based Design of Shallow Foundations Subjected to Seismic Loading.* Sivapalan Gajan, Tara C. Hutchinson, Bruce L. Kutter, Prishati Raychowdhury, José A. Ugalde, and Jonathan P. Stewart. May 2008.

PEER 2007/03 *Beam-Column Element Model Calibrated for Predicting Flexural Response Leading to Global Collapse of RC Frame Buildings.* Curt B. Haselton, Abbie B. Liel, Sarah Taylor Lange, and Gregory G. Deierlein. May 2008.

PEER 2007/02 *Campbell-Bozorgnia NGA Ground Motion Relations for the Geometric Mean Horizontal Component of Peak and Spectral Ground Motion Parameters.* Kenneth W. Campbell and Yousef Bozorgnia. May 2007.

PEER 2007/01 *Boore-Atkinson NGA Ground Motion Relations for the Geometric Mean Horizontal Component of Peak and Spectral Ground Motion Parameters.* David M. Boore and Gail M. Atkinson. May. May 2007.

PEER 2006/12 *Societal Implications of Performance-Based Earthquake Engineering.* Peter J. May. May 2007.

PEER 2006/11 *Probabilistic Seismic Demand Analysis Using Advanced Ground Motion Intensity Measures, Attenuation Relationships, and Near-Fault Effects.* Polsak Tothong and C. Allin Cornell. March 2007.

PEER 2006/10 *Application of the PEER PBEE Methodology to the I-880 Viaduct.* Sashi Kunnath. February 2007.

PEER 2006/09 *Quantifying Economic Losses from Travel Forgone Following a Large Metropolitan Earthquake.* James Moore, Sungbin Cho, Yue Yue Fan, and Stuart Werner. November 2006.

PEER 2006/08 *Vector-Valued Ground Motion Intensity Measures for Probabilistic Seismic Demand Analysis*. Jack W. Baker and C. Allin Cornell. October 2006.

PEER 2006/07 *Analytical Modeling of Reinforced Concrete Walls for Predicting Flexural and Coupled–Shear-Flexural Responses*. Kutay Orakcal, Leonardo M. Massone, and John W. Wallace. October 2006.

PEER 2006/06 *Nonlinear Analysis of a Soil-Drilled Pier System under Static and Dynamic Axial Loading.* Gang Wang and Nicholas Sitar. November 2006.

PEER 2006/05 *Advanced Seismic Assessment Guidelines.* Paolo Bazzurro, C. Allin Cornell, Charles Menun, Maziar Motahari, and Nicolas Luco. September 2006.

PEER 2006/04 *Probabilistic Seismic Evaluation of Reinforced Concrete Structural Components and Systems.* Tae Hyung Lee and Khalid M. Mosalam. August 2006.

PEER 2006/03 *Performance of Lifelines Subjected to Lateral Spreading.* Scott A. Ashford and Teerawut Juirnarongrit. July 2006.

PEER 2006/02 *Pacific Earthquake Engineering Research Center Highway Demonstration Project.* Anne Kiremidjian, James Moore, Yue Yue Fan, Nesrin Basoz, Ozgur Yazali, and Meredith Williams. April 2006.

PEER 2006/01 *Bracing Berkeley. A Guide to Seismic Safety on the UC Berkeley Campus.* Mary C. Comerio, Stephen Tobriner, and Ariane Fehrenkamp. January 2006.

PEER 2005/16 *Seismic Response and Reliability of Electrical Substation Equipment and Systems.* Junho Song, Armen Der Kiureghian, and Jerome L. Sackman. April 2006.

PEER 2005/15 *CPT-Based Probabilistic Assessment of Seismic Soil Liquefaction Initiation.* R. E. S. Moss, R. B. Seed, R. E. Kayen, J. P. Stewart, and A. Der Kiureghian. April 2006.

PEER 2005/14 *Workshop on Modeling of Nonlinear Cyclic Load-Deformation Behavior of Shallow Foundations.* Bruce L. Kutter, Geoffrey Martin, Tara Hutchinson, Chad Harden, Sivapalan Gajan, and Justin Phalen. March 2006.

PEER 2005/13 *Stochastic Characterization and Decision Bases under Time-Dependent Aftershock Risk in Performance-Based Earthquake Engineering.* Gee Liek Yeo and C. Allin Cornell. July 2005.

PEER 2005/12 *PEER Testbed Study on a Laboratory Building: Exercising Seismic Performance Assessment.* Mary C. Comerio, editor. November 2005.

PEER 2005/11 *Van Nuys Hotel Building Testbed Report: Exercising Seismic Performance Assessment.* Helmut Krawinkler, editor. October 2005.

PEER 2005/10 *First NEES/E-Defense Workshop on Collapse Simulation of Reinforced Concrete Building Structures.* September 2005.

PEER 2005/09 *Test Applications of Advanced Seismic Assessment Guidelines.* Joe Maffei, Karl Telleen, Danya Mohr, William Holmes, and Yuki Nakayama. August 2006.

PEER 2005/08 *Damage Accumulation in Lightly Confined Reinforced Concrete Bridge Columns.* R. Tyler Ranf, Jared M. Nelson, Zach Price, Marc O. Eberhard, and John F. Stanton. April 2006.

PEER 2005/07 *Experimental and Analytical Studies on the Seismic Response of Freestanding and Anchored Laboratory Equipment.* Dimitrios Konstantinidis and Nicos Makris. January 2005.

PEER 2005/06 *Global Collapse of Frame Structures under Seismic Excitations*. Luis F. Ibarra and Helmut Krawinkler. September 2005.

PEER 2005//05 *Performance Characterization of Bench- and Shelf-Mounted Equipment.* Samit Ray Chaudhuri and Tara C. Hutchinson. May 2006.

PEER 2005/04 *Numerical Modeling of the Nonlinear Cyclic Response of Shallow Foundations.* Chad Harden, Tara Hutchinson, Geoffrey R. Martin, and Bruce L. Kutter. August 2005.

PEER 2005/03 *A Taxonomy of Building Components for Performance-Based Earthquake Engineering.* Keith A. Porter. September 2005.

PEER 2005/02 *Fragility Basis for California Highway Overpass Bridge Seismic Decision Making*. Kevin R. Mackie and Božidar Stojadinović. June 2005.

PEER 2005/01 *Empirical Characterization of Site Conditions on Strong Ground Motion.* Jonathan P. Stewart, Yoojoong Choi, and Robert W. Graves. June 2005.

PEER 2004/09 *Electrical Substation Equipment Interaction: Experimental Rigid Conductor Studies.* Christopher Stearns and André Filiatrault. February 2005.

PEER 2004/08 *Seismic Qualification and Fragility Testing of Line Break 550-kV Disconnect Switches.* Shakhzod M. Takhirov, Gregory L. Fenves, and Eric Fujisaki. January 2005.

PEER 2004/07 *Ground Motions for Earthquake Simulator Qualification of Electrical Substation Equipment.* Shakhzod M. Takhirov, Gregory L. Fenves, Eric Fujisaki, and Don Clyde. January 2005.

PEER 2004/06 *Performance-Based Regulation and Regulatory Regimes.* Peter J. May and Chris Koski. September 2004.

PEER 2004/05 *Performance-Based Seismic Design Concepts and Implementation: Proceedings of an International Workshop.* Peter Fajfar and Helmut Krawinkler, editors. September 2004.

PEER 2004/04 *Seismic Performance of an Instrumented Tilt-up Wall Building*. James C. Anderson and Vitelmo V. Bertero. July 2004.

PEER 2004/03 *Evaluation and Application of Concrete Tilt-up Assessment Methodologies.* Timothy Graf and James O. Malley. October 2004.

PEER 2004/02 *Analytical Investigations of New Methods for Reducing Residual Displacements of Reinforced Concrete Bridge Columns.* Junichi Sakai and Stephen A. Mahin. August 2004.

PEER 2004/01 *Seismic Performance of Masonry Buildings and Design Implications.* Kerri Anne Taeko Tokoro, James C. Anderson, and Vitelmo V. Bertero. February 2004.

PEER 2003/18 *Performance Models for Flexural Damage in Reinforced Concrete Columns.* Michael Berry and Marc Eberhard. August 2003.

PEER 2003/17 *Predicting Earthquake Damage in Older Reinforced Concrete Beam-Column Joints.* Catherine Pagni and Laura Lowes. October 2004.

PEER 2003/16 *Seismic Demands for Performance-Based Design of Bridges.* Kevin Mackie and Božidar Stojadinović. August 2003.

PEER 2003/15 *Seismic Demands for Nondeteriorating Frame Structures and Their Dependence on Ground Motions.* Ricardo Antonio Medina and Helmut Krawinkler. May 2004.

PEER 2003/14 *Finite Element Reliability and Sensitivity Methods for Performance-Based Earthquake Engineering.* Terje Haukaas and Armen Der Kiureghian. April 2004.

PEER 2003/13 *Effects of Connection Hysteretic Degradation on the Seismic Behavior of Steel Moment-Resisting Frames.* Janise E. Rodgers and Stephen A. Mahin. March 2004.

PEER 2003/12 *Implementation Manual for the Seismic Protection of Laboratory Contents: Format and Case Studies.* William T. Holmes and Mary C. Comerio. October 2003.

PEER 2003/11 *Fifth U.S.-Japan Workshop on Performance-Based Earthquake Engineering Methodology for Reinforced Concrete Building Structures.* February 2004.

PEER 2003/10 *A Beam-Column Joint Model for Simulating the Earthquake Response of Reinforced Concrete Frames.* Laura N. Lowes, Nilanjan Mitra, and Arash Altoontash. February 2004.

PEER 2003/09 *Sequencing Repairs after an Earthquake: An Economic Approach.* Marco Casari and Simon J. Wilkie. April 2004.

PEER 2003/08 *A Technical Framework for Probability-Based Demand and Capacity Factor Design (DCFD) Seismic Formats.* Fatemeh Jalayer and C. Allin Cornell. November 2003.

PEER 2003/07 *Uncertainty Specification and Propagation for Loss Estimation Using FOSM Methods.* Jack W. Baker and C. Allin Cornell. September 2003.

PEER 2003/06 *Performance of Circular Reinforced Concrete Bridge Columns under Bidirectional Earthquake Loading.* Mahmoud M. Hachem, Stephen A. Mahin, and Jack P. Moehle. February 2003.

PEER 2003/05 *Response Assessment for Building-Specific Loss Estimation.* Eduardo Miranda and Shahram Taghavi. September 2003.

PEER 2003/04 *Experimental Assessment of Columns with Short Lap Splices Subjected to Cyclic Loads.* Murat Melek, John W. Wallace, and Joel Conte. April 2003.

PEER 2003/03 *Probabilistic Response Assessment for Building-Specific Loss Estimation.* Eduardo Miranda and Hesameddin Aslani. September 2003.

PEER 2003/02 *Software Framework for Collaborative Development of Nonlinear Dynamic Analysis Program.* Jun Peng and Kincho H. Law. September 2003.

PEER 2003/01 *Shake Table Tests and Analytical Studies on the Gravity Load Collapse of Reinforced Concrete Frames.* Kenneth John Elwood and Jack P. Moehle. November 2003.

PEER 2002/24 *Performance of Beam to Column Bridge Joints Subjected to a Large Velocity Pulse.* Natalie Gibson, André Filiatrault, and Scott A. Ashford. April 2002.

PEER 2002/23 *Effects of Large Velocity Pulses on Reinforced Concrete Bridge Columns.* Greg L. Orozco and Scott A. Ashford. April 2002.

PEER 2002/22 *Characterization of Large Velocity Pulses for Laboratory Testing.* Kenneth E. Cox and Scott A. Ashford. April 2002.

PEER 2002/21 *Fourth U.S.-Japan Workshop on Performance-Based Earthquake Engineering Methodology for Reinforced Concrete Building Structures*. December 2002.

PEER 2002/20 *Barriers to Adoption and Implementation of PBEE Innovations.* Peter J. May. August 2002.

PEER 2002/19 *Economic-Engineered Integrated Models for Earthquakes: Socioeconomic Impacts.* Peter Gordon, James E. Moore II, and Harry W. Richardson. July 2002.

PEER 2002/18 *Assessment of Reinforced Concrete Building Exterior Joints with Substandard Details.* Chris P. Pantelides, Jon Hansen, Justin Nadauld, and Lawrence D. Reaveley. May 2002.

PEER 2002/17 *Structural Characterization and Seismic Response Analysis of a Highway Overcrossing Equipped with Elastomeric Bearings and Fluid Dampers: A Case Study.* Nicos Makris and Jian Zhang. November 2002.

PEER 2002/16 *Estimation of Uncertainty in Geotechnical Properties for Performance-Based Earthquake Engineering.* Allen L. Jones, Steven L. Kramer, and Pedro Arduino. December 2002.

PEER 2002/15 *Seismic Behavior of Bridge Columns Subjected to Various Loading Patterns.* Asadollah Esmaeily-Gh. and Yan Xiao. December 2002.

PEER 2002/14 *Inelastic Seismic Response of Extended Pile Shaft Supported Bridge Structures.* T.C. Hutchinson, R.W. Boulanger, Y.H. Chai, and I.M. Idriss. December 2002.

PEER 2002/13 *Probabilistic Models and Fragility Estimates for Bridge Components and Systems.* Paolo Gardoni, Armen Der Kiureghian, and Khalid M. Mosalam. June 2002.

PEER 2002/12 *Effects of Fault Dip and Slip Rake on Near-Source Ground Motions: Why Chi-Chi Was a Relatively Mild M7.6 Earthquake.* Brad T. Aagaard, John F. Hall, and Thomas H. Heaton. December 2002.

PEER 2002/11 *Analytical and Experimental Study of Fiber-Reinforced Strip Isolators*. James M. Kelly and Shakhzod M. Takhirov. September 2002.

PEER 2002/10 *Centrifuge Modeling of Settlement and Lateral Spreading with Comparisons to Numerical Analyses***.** Sivapalan Gajan and Bruce L. Kutter. January 2003.

PEER 2002/09 *Documentation and Analysis of Field Case Histories of Seismic Compression during the 1994 Northridge, California, Earthquake.* Jonathan P. Stewart, Patrick M. Smith, Daniel H. Whang, and Jonathan D. Bray. October 2002.

PEER 2002/08 *Component Testing, Stability Analysis and Characterization of Buckling-Restrained Unbonded Braces™.* Cameron Black, Nicos Makris, and Ian Aiken. September 2002.

PEER 2002/07 *Seismic Performance of Pile-Wharf Connections.* Charles W. Roeder, Robert Graff, Jennifer Soderstrom, and Jun Han Yoo. December 2001.

PEER 2002/06 *The Use of Benefit-Cost Analysis for Evaluation of Performance-Based Earthquake Engineering Decisions*. Richard O. Zerbe and Anthony Falit-Baiamonte. September 2001.

PEER 2002/05 *Guidelines, Specifications, and Seismic Performance Characterization of Nonstructural Building Components and Equipment*. André Filiatrault, Constantin Christopoulos, and Christopher Stearns. September 2001.

PEER 2002/04 *Consortium of Organizations for Strong-Motion Observation Systems and the Pacific Earthquake Engineering Research Center Lifelines Program: Invited Workshop on Archiving and Web Dissemination of Geotechnical Data, 4–5 October 2001*. September 2002.

PEER 2002/03 *Investigation of Sensitivity of Building Loss Estimates to Major Uncertain Variables for the Van Nuys Testbed.* Keith A. Porter, James L. Beck, and Rustem V. Shaikhutdinov. August 2002.

PEER 2002/02 *The Third U.S.-Japan Workshop on Performance-Based Earthquake Engineering Methodology for Reinforced Concrete Building Structures*. July 2002.

PEER 2002/01 *Nonstructural Loss Estimation: The UC Berkeley Case Study.* Mary C. Comerio and John C. Stallmeyer. December 2001.

PEER 2001/16 *Statistics of SDF-System Estimate of Roof Displacement for Pushover Analysis of Buildings.* Anil K. Chopra, Rakesh K. Goel, and Chatpan Chintanapakdee. December 2001.

PEER 2001/15 *Damage to Bridges during the 2001 Nisqually Earthquake.* R. Tyler Ranf, Marc O. Eberhard, and Michael P. Berry. November 2001.

PEER 2001/14 *Rocking Response of Equipment Anchored to a Base Foundation.* Nicos Makris and Cameron J. Black. September 2001.

PEER 2001/13 *Modeling Soil Liquefaction Hazards for Performance-Based Earthquake Engineering.* Steven L. Kramer and Ahmed-W. Elgamal. February 2001.

PEER 2001/12 *Development of Geotechnical Capabilities in OpenSees.* Boris Jeremić. September 2001.

PEER 2001/11 *Analytical and Experimental Study of Fiber-Reinforced Elastomeric Isolators*. James M. Kelly and Shakhzod M. Takhirov. September 2001.

PEER 2001/10 *Amplification Factors for Spectral Acceleration in Active Regions.* Jonathan P. Stewart, Andrew H. Liu, Yoojoong Choi, and Mehmet B. Baturay. December 2001.

PEER 2001/09 *Ground Motion Evaluation Procedures for Performance-Based Design.* Jonathan P. Stewart, Shyh-Jeng Chiou, Jonathan D. Bray, Robert W. Graves, Paul G. Somerville, and Norman A. Abrahamson. September 2001.

PEER 2001/08 *Experimental and Computational Evaluation of Reinforced Concrete Bridge Beam-Column Connections for Seismic Performance*. Clay J. Naito, Jack P. Moehle, and Khalid M. Mosalam. November 2001.

PEER 2001/07 *The Rocking Spectrum and the Shortcomings of Design Guidelines.* Nicos Makris and Dimitrios Konstantinidis. August 2001.

PEER 2001/06 *Development of an Electrical Substation Equipment Performance Database for Evaluation of Equipment Fragilities*. Thalia Agnanos. April 1999.

PEER 2001/05 *Stiffness Analysis of Fiber-Reinforced Elastomeric Isolators.* Hsiang-Chuan Tsai and James M. Kelly. May 2001.

PEER 2001/04 *Organizational and Societal Considerations for Performance-Based Earthquake Engineering.* Peter J. May. April 2001.

PEER 2001/03 *A Modal Pushover Analysis Procedure to Estimate Seismic Demands for Buildings: Theory and Preliminary Evaluation.* Anil K. Chopra and Rakesh K. Goel. January 2001.

PEER 2001/02 *Seismic Response Analysis of Highway Overcrossings Including Soil-Structure Interaction.* Jian Zhang and Nicos Makris. March 2001.

PEER 2001/01 *Experimental Study of Large Seismic Steel Beam-to-Column Connections.* Egor P. Popov and Shakhzod M. Takhirov. November 2000.

PEER 2000/10 *The Second U.S.-Japan Workshop on Performance-Based Earthquake Engineering Methodology for Reinforced Concrete Building Structures.* March 2000.

PEER 2000/09 *Structural Engineering Reconnaissance of the August 17, 1999 Earthquake: Kocaeli (Izmit), Turkey.* Halil Sezen, Kenneth J. Elwood, Andrew S. Whittaker, Khalid Mosalam, John J. Wallace, and John F. Stanton. December 2000.

PEER 2000/08 *Behavior of Reinforced Concrete Bridge Columns Having Varying Aspect Ratios and Varying Lengths of Confinement.* Anthony J. Calderone, Dawn E. Lehman, and Jack P. Moehle. January 2001.

PEER 2000/07 *Cover-Plate and Flange-Plate Reinforced Steel Moment-Resisting Connections.* Taejin Kim, Andrew S. Whittaker, Amir S. Gilani, Vitelmo V. Bertero, and Shakhzod M. Takhirov. September 2000.

PEER 2000/06 *Seismic Evaluation and Analysis of 230-kV Disconnect Switches.* Amir S. J. Gilani, Andrew S. Whittaker, Gregory L. Fenves, Chun-Hao Chen, Henry Ho, and Eric Fujisaki. July 2000.

PEER 2000/05 *Performance-Based Evaluation of Exterior Reinforced Concrete Building Joints for Seismic Excitation.* Chandra Clyde, Chris P. Pantelides, and Lawrence D. Reaveley. July 2000.

PEER 2000/04 *An Evaluation of Seismic Energy Demand: An Attenuation Approach.* Chung-Che Chou and Chia-Ming Uang. July 1999.

PEER 2000/03 *Framing Earthquake Retrofitting Decisions: The Case of Hillside Homes in Los Angeles.* Detlof von Winterfeldt, Nels Roselund, and Alicia Kitsuse. March 2000.

PEER 2000/02 *U.S.-Japan Workshop on the Effects of Near-Field Earthquake Shaking.* Andrew Whittaker, ed. July 2000.

PEER 2000/01 *Further Studies on Seismic Interaction in Interconnected Electrical Substation Equipment.* Armen Der Kiureghian, Kee-Jeung Hong, and Jerome L. Sackman. November 1999.

PEER 1999/14 *Seismic Evaluation and Retrofit of 230-kV Porcelain Transformer Bushings*. Amir S. Gilani, Andrew S. Whittaker, Gregory L. Fenves, and Eric Fujisaki. December 1999.

PEER 1999/13 *Building Vulnerability Studies: Modeling and Evaluation of Tilt-up and Steel Reinforced Concrete Buildings.* John W. Wallace, Jonathan P. Stewart, and Andrew S. Whittaker, editors. December 1999.

PEER 1999/12 *Rehabilitation of Nonductile RC Frame Building Using Encasement Plates and Energy-Dissipating Devices.* Mehrdad Sasani, Vitelmo V. Bertero, James C. Anderson. December 1999.

PEER 1999/11 *Performance Evaluation Database for Concrete Bridge Components and Systems under Simulated Seismic Loads.* Yael D. Hose and Frieder Seible. November 1999.

PEER 1999/10 *U.S.-Japan Workshop on Performance-Based Earthquake Engineering Methodology for Reinforced Concrete Building Structures.* December 1999.

PEER 1999/09 *Performance Improvement of Long Period Building Structures Subjected to Severe Pulse-Type Ground Motions*. James C. Anderson, Vitelmo V. Bertero, and Raul Bertero. October 1999.

PEER 1999/08 *Envelopes for Seismic Response Vectors.* Charles Menun and Armen Der Kiureghian. July 1999.

PEER 1999/07 *Documentation of Strengths and Weaknesses of Current Computer Analysis Methods for Seismic Performance of Reinforced Concrete Members.* William F. Cofer. November 1999.

PEER 1999/06 *Rocking Response and Overturning of Anchored Equipment under Seismic Excitations.* Nicos Makris and Jian Zhang. November 1999.

PEER 1999/05 *Seismic Evaluation of 550 kV Porcelain Transformer Bushings.* Amir S. Gilani, Andrew S. Whittaker, Gregory L. Fenves, and Eric Fujisaki. October 1999.

PEER 1999/04 *Adoption and Enforcement of Earthquake Risk-Reduction Measures.* Peter J. May, Raymond J. Burby, T. Jens Feeley, and Robert Wood.

PEER 1999/03 *Task 3 Characterization of Site Response General Site Categories.* Adrian Rodriguez-Marek, Jonathan D. Bray, and Norman Abrahamson. February 1999.

PEER 1999/02 *Capacity-Demand-Diagram Methods for Estimating Seismic Deformation of Inelastic Structures: SDF Systems*. Anil K. Chopra and Rakesh Goel. April 1999.

PEER 1999/01 *Interaction in Interconnected Electrical Substation Equipment Subjected to Earthquake Ground Motions.* Armen Der Kiureghian, Jerome L. Sackman, and Kee-Jeung Hong. February 1999.

PEER 1998/08 *Behavior and Failure Analysis of a Multiple-Frame Highway Bridge in the 1994 Northridge Earthquake.* Gregory L. Fenves and Michael Ellery. December 1998.

PEER 1998/07 *Empirical Evaluation of Inertial Soil-Structure Interaction Effects.* Jonathan P. Stewart, Raymond B. Seed, and Gregory L. Fenves. November 1998.

PEER 1998/06 *Effect of Damping Mechanisms on the Response of Seismic Isolated Structures.* Nicos Makris and Shih-Po Chang. November 1998.

PEER 1998/05 *Rocking Response and Overturning of Equipment under Horizontal Pulse-Type Motions.* Nicos Makris and Yiannis Roussos. October 1998.

PEER 1998/04 *Pacific Earthquake Engineering Research Invitational Workshop Proceedings, May 14–15, 1998: Defining the Links between Planning, Policy Analysis, Economics and Earthquake Engineering.* Mary Comerio and Peter Gordon. September 1998.

PEER 1998/03 *Repair/Upgrade Procedures for Welded Beam to Column Connections.* James C. Anderson and Xiaojing Duan. May 1998.

PEER 1998/02 *Seismic Evaluation of 196 kV Porcelain Transformer Bushings.* Amir S. Gilani, Juan W. Chavez, Gregory L. Fenves, and Andrew S. Whittaker. May 1998.

PEER 1998/01 *Seismic Performance of Well-Confined Concrete Bridge Columns.* Dawn E. Lehman and Jack P. Moehle. December 2000.

ONLINE PEER REPORTS

The following PEER reports are available by Internet only at http://peer.berkeley.edu/publications/peer_reports_complete.html.

PEER 2012/103 *Performance-Based Seismic Demand Assessment of Concentrically Braced Steel Frame Buildings.* Chui-Hsin Chen and Stephen A. Mahin. December 2012.

PEER 2012/102 *Procedure to Restart an Interrupted Hybrid Simulation: Addendum to PEER Report 2010/103.* Vesna Terzic and Bozidar Stojadinovic. October 2012.

PEER 2012/101 *Mechanics of Fiber Reinforced Bearings.* James M. Kelly and Andrea Calabrese. February 2012.

PEER 2011/107 *Nonlinear Site Response and Seismic Compression at Vertical Array Strongly Shaken by 2007 Niigata-ken Chuetsu-oki Earthquake.* Eric Yee, Jonathan P. Stewart, and Kohji Tokimatsu. December 2011.

PEER 2011/106 *Self Compacting Hybrid Fiber Reinforced Concrete Composites for Bridge Columns.* Pardeep Kumar, Gabriel Jen, William Trono, Marios Panagiotou, and Claudia Ostertag. September 2011.

PEER 2011/105 *Stochastic Dynamic Analysis of Bridges Subjected to Spacially Varying Ground Motions.* Katerina Konakli and Armen Der Kiureghian. August 2011.

PEER 2011/104 *Design and Instrumentation of the 2010 E-Defense Four-Story Reinforced Concrete and Post-Tensioned Concrete Buildings.* Takuya Nagae, Kenichi Tahara, Taizo Matsumori, Hitoshi Shiohara, Toshimi Kabeyasawa, Susumu Kono, Minehiro Nishiyama (Japanese Research Team) and John Wallace, Wassim Ghannoum, Jack Moehle, Richard Sause, Wesley Keller, Zeynep Tuna (U.S. Research Team). June 2011.

PEER 2011/103 *In-Situ Monitoring of the Force Output of Fluid Dampers: Experimental Investigation.* Dimitrios Konstantinidis, James M. Kelly, and Nicos Makris. April 2011.

PEER 2011/102 *Ground-motion prediction equations 1964 - 2010.* John Douglas. April 2011.

PEER 2011/101 *Report of the Eighth Planning Meeting of NEES/E-Defense Collaborative Research on Earthquake Engineering.* Convened by the Hyogo Earthquake Engineering Research Center (NIED), NEES Consortium, Inc. February 2011.

PEER 2010/111 *Modeling and Acceptance Criteria for Seismic Design and Analysis of Tall Buildings.* Task 7 Report for the Tall Buildings Initiative - Published jointly by the Applied Technology Council. October 2010.

PEER 2010/110 *Seismic Performance Assessment and Probabilistic Repair Cost Analysis of Precast Concrete Cladding Systems for Multistory Buildlings.* Jeffrey P. Hunt and Božidar Stojadinovic. November 2010.

PEER 2010/109 *Report of the Seventh Joint Planning Meeting of NEES/E-Defense Collaboration on Earthquake Engineering. Held at the E-Defense, Miki, and Shin-Kobe, Japan, September 18–19, 2009.* August 2010.

PEER 2010/108 *Probabilistic Tsunami Hazard in California.* Hong Kie Thio, Paul Somerville, and Jascha Polet, preparers. October 2010.

PEER 2010/107 *Performance and Reliability of Exposed Column Base Plate Connections for Steel Moment-Resisting Frames.* Ady Aviram, Božidar Stojadinovic, and Armen Der Kiureghian. August 2010.

PEER 2010/106 *Verification of Probabilistic Seismic Hazard Analysis Computer Programs.* Patricia Thomas, Ivan Wong, and Norman Abrahamson. May 2010.

PEER 2010/105 *Structural Engineering Reconnaissance of the April 6, 2009, Abruzzo, Italy, Earthquake, and Lessons Learned.* M. Selim Günay and Khalid M. Mosalam. April 2010.

PEER 2010/104 *Simulating the Inelastic Seismic Behavior of Steel Braced Frames, Including the Effects of Low-Cycle Fatigue.* Yuli Huang and Stephen A. Mahin. April 2010.

PEER 2010/103 *Post-Earthquake Traffic Capacity of Modern Bridges in California.* Vesna Terzic and Božidar Stojadinović. March 2010.

PEER 2010/102 *Analysis of Cumulative Absolute Velocity (CAV) and JMA Instrumental Seismic Intensity (I_{JMA}) Using the PEER–NGA Strong Motion Database.* Kenneth W. Campbell and Yousef Bozorgnia. February 2010.

PEER 2010/101 *Rocking Response of Bridges on Shallow Foundations.* Jose A. Ugalde, Bruce L. Kutter, and Boris Jeremic. April 2010.

PEER 2009/109 *Simulation and Performance-Based Earthquake Engineering Assessment of Self-Centering Post-Tensioned Concrete Bridge Systems.* Won K. Lee and Sarah L. Billington. December 2009.

PEER 2009/108 *PEER Lifelines Geotechnical Virtual Data Center.* J. Carl Stepp, Daniel J. Ponti, Loren L. Turner, Jennifer N. Swift, Sean Devlin, Yang Zhu, Jean Benoit, and John Bobbitt. September 2009.

PEER 2009/107 *Experimental and Computational Evaluation of Current and Innovative In-Span Hinge Details in Reinforced Concrete Box-Girder Bridges: Part 2: Post-Test Analysis and Design Recommendations.* Matias A. Hube and Khalid M. Mosalam. December 2009.

PEER 2009/106 *Shear Strength Models of Exterior Beam-Column Joints without Transverse Reinforcement.* Sangjoon Park and Khalid M. Mosalam. November 2009.

PEER 2009/105 *Reduced Uncertainty of Ground Motion Prediction Equations through Bayesian Variance Analysis.* Robb Eric S. Moss. November 2009.

PEER 2009/104 *Advanced Implementation of Hybrid Simulation.* Andreas H. Schellenberg, Stephen A. Mahin, Gregory L. Fenves. November 2009.

PEER 2009/103 *Performance Evaluation of Innovative Steel Braced Frames.* T. Y. Yang, Jack P. Moehle, and Božidar Stojadinovic. August 2009.

PEER 2009/102 *Reinvestigation of Liquefaction and Nonliquefaction Case Histories from the 1976 Tangshan Earthquake.* Robb Eric Moss, Robert E. Kayen, Liyuan Tong, Songyu Liu, Guojun Cai, and Jiaer Wu. August 2009.

PEER 2009/101 *Report of the First Joint Planning Meeting for the Second Phase of NEES/E-Defense Collaborative Research on Earthquake Engineering.* Stephen A. Mahin et al. July 2009.

PEER 2008/104 *Experimental and Analytical Study of the Seismic Performance of Retaining Structures.* Linda Al Atik and Nicholas Sitar. January 2009.

PEER 2008/103 *Experimental and Computational Evaluation of Current and Innovative In-Span Hinge Details in Reinforced Concrete Box-Girder Bridges. Part 1: Experimental Findings and Pre-Test Analysis.* Matias A. Hube and Khalid M. Mosalam. January 2009.

PEER 2008/102 *Modeling of Unreinforced Masonry Infill Walls Considering In-Plane and Out-of-Plane Interaction.* Stephen Kadysiewski and Khalid M. Mosalam. January 2009.

PEER 2008/101 *Seismic Performance Objectives for Tall Buildings.* William T. Holmes, Charles Kircher, William Petak, and Nabih Youssef. August 2008.

PEER 2007/101 *Generalized Hybrid Simulation Framework for Structural Systems Subjected to Seismic Loading.* Tarek Elkhoraibi and Khalid M. Mosalam. July 2007.

PEER 2007/100 *Seismic Evaluation of Reinforced Concrete Buildings Including Effects of Masonry Infill Walls.* Alidad Hashemi and Khalid M. Mosalam. July 2007.

Disclaimer

The opinions, findings, and conclusions or recommendations expressed in this publication are those of the author(s) and do not necessarily reflect the views of the study sponsor(s) or the Pacific Earthquake Engineering Research Center.

The Pacific Earthquake Engineering Research Center (PEER) is a multi-institutional research and education center with headquarters at the University of California, Berkeley. Investigators from over 20 universities, several consulting companies, and researchers at various state and federal government agencies contribute to research programs focused on performance-based earthquake engineering.

These research programs aim to identify and reduce the risks from major earthquakes to life safety and to the economy by including research in a wide variety of disciplines including structural and geotechnical engineering, geology/seismology, lifelines, transportation, architecture, economics, risk management, and public policy.

PEER is supported by federal, state, local, and regional agencies, together with industry partners.

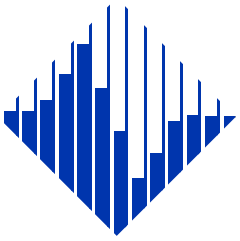

PEER Core Institutions:
University of California, Berkeley (Lead Institution)
California Institute of Technology
Oregon State University
Stanford University
University of California, Davis
University of California, Irvine
University of California, Los Angeles
University of California, San Diego
University of Southern California
University of Washington

PEER reports can be ordered at http://peer.berkeley.edu/publications/peer_reports.html or by contacting

Pacific Earthquake Engineering Research Center
University of California, Berkeley
325 Davis Hall, mail code 1792
Berkeley, CA 94720-1792
Tel: 510-642-3437
Fax: 510-642-1655
Email: peer_editor@berkeley.edu

ISSN 1547-0587X